

**OFFICE OF CIVILIAN RADIOACTIVE WASTE MANAGEMENT
ANALYSIS/MODEL COVER SHEET**

1. QA: QA
Page: 1 of 104

Complete Only Applicable Items

2. Analysis Check all that apply

Type of Analysis	<input type="checkbox"/> Engineering <input type="checkbox"/> Performance Assessment <input checked="" type="checkbox"/> Scientific
Intended Use of Analysis	<input type="checkbox"/> Input to Calculation <input type="checkbox"/> Input to another Analysis or Model <input checked="" type="checkbox"/> Input to Technical Document
Describe use:	
Evaluated impact of thermal load on temperature, saturation, liquid and gas flux, for use in the UZ PMR	

3. Model Check all that apply

Type of Model	<input type="checkbox"/> Conceptual Model <input type="checkbox"/> Mathematical Model <input checked="" type="checkbox"/> Process Model	<input type="checkbox"/> Abstraction Model <input type="checkbox"/> System Model
Intended Use of Model	<input type="checkbox"/> Input to Calculation <input type="checkbox"/> Input to another Model or Analysis <input checked="" type="checkbox"/> Input to Technical Document	
Describe use:		
Provide Mountain Scale TH Model for UZ PMR and for evaluating impact of thermal load on mountain scale flow and transport		

4. Title:
Mountain-Scale Coupled Processes (TH) Models

5. Document Identifier (including Rev. No. and Change No., if applicable):
MDL-NBS-HS-000007 REV 00

6. Total Attachments: 2	7. Attachment Numbers - No. of Pages in Each: I- 34 II-1
----------------------------	--

	Printed Name	Signature	Date
8. Originator	Charles Haukwa		3/12/2000
9. Checker	Richard Stover		3/12/00
10. Lead/Supervisor	G.S. Bodvarsson		3/12/00
11. Responsible Manager	Dwight Hoxie G.S. Bodvarsson		3/12/00

12. Remarks: GSB 3/12/00

**OFFICE OF CIVILIAN RADIOACTIVE WASTE MANAGEMENT
ANALYSIS/MODEL REVISION RECORD**

Complete Only Applicable Items

1. Page: 2 of 104

2. Analysis or Model Title:

Mountain-Scale Coupled Processes (TH) Model

3. Document Identifier (including Rev. No. and Change No., if applicable):

MDL-NBS-HS-000007 REV 00

4. Revision/Change No.

5. Description of Revision/Change

00

Initial Issue

CONTENTS

	Page
ACRONYMS	11
1. PURPOSE	13
2. QUALITY ASSURANCE	15
3. COMPUTER SOFTWARE AND MODEL USAGE	17
4. INPUTS	19
4.1 DATA AND PARAMETERS	19
4.2 CRITERIA	21
4.3 CODES AND STANDARDS	21
5. ASSUMPTIONS	23
5.1 ASSUMPTIONS REGARDING BOUNDARY CONDITIONS MODEL AND THERMAL LOADING	23
5.2 ASSUMPTIONS REGARDING EFFECTS OF THERMAL LOAD ON FLOW PROPERTIES	24
5.3 ASSUMPTION REGARDING EFFECT OF PERCHED WATER ON TH PROCESSES	25
6. ANALYSIS/MODEL	27
6.1 CONCEPTUAL MODEL	27
6.1.1 Numerical Methods for Modeling Fluid and Heat Flow	28
6.1.2 Continuum Approach and Fracture-Matrix Interactions	28
6.2 NUMERICAL GRIDS	29
6.2.1 3-D Numerical Grid for Potential Repository Submodel	31
6.2.2 2-D North-South Grids	31
6.3 POTENTIAL REPOSITORY THERMAL LOAD	33
6.3.1 Base-Case Mountain-Scale Thermal Load	33
6.3.2 Thermal Load with Repository Ventilation	33
6.3.3 Heat Distribution at the Repository	33
6.4 BOUNDARY AND INITIAL CONDITIONS	37
6.4.1 Top Boundary	37
6.4.2 Bottom Boundary	37
6.4.3 Initial Conditions	38
6.5 THERMAL PROPERTIES	40
6.6 INFILTRATION	42
6.7 TH MODELS	43
6.8 3-D UNSATURATED-ZONE REPOSITORY TH SUBMODEL	44
6.8.1 Modeling Approach	44
6.8.2 Results of the 3-D TH Simulations	44

6.9	2-D UNSATURATED ZONE TH SIMULATIONS	57
6.9.1	Modeling Approach.....	57
6.9.2	2-D Ambient Conditions	57
6.10	RESULTS OF THE 2-D TH SIMULATIONS AT CROSS SECTION NS#1	59
6.10.1	Model 3, NS#1 Case 1.....	59
6.10.2	Model 4, NS#1 Case 2.....	64
6.11	RESULTS OF THE 2-D TH SIMULATIONS AT CROSS SECTION NS#2	71
6.11.1	Model 5, NS#2 Case 1.....	71
6.11.2	Model 6, NS#2 Case 2.....	80
6.12	MODEL VALIDATION	90
7.	DISCUSSION AND CONCLUSIONS.....	93
8.	INPUTS AND REFERENCES	96
8.1	CITED DOCUMENTS.....	96
8.2	CODES, STANDARDS, REGULATIONS, AND PROCEDURES.....	101
8.3	SOURCE DATA, LISTED BY DATA TRACKING NUMBER	102
8.4	OUTPUT DATA, LISTED BY DATA TRACKING NUMBER	103
9.	ATTACHMENTS	104
	ATTACHMENT I – DOCUMENT INPUT REFERENCE SYSTEM	
	ATTACHMENT II – LIST OF MODEL INPUT AND OUTPUT FILES	

FIGURES

	Page
1. Plan View of the 1999 UZ TSPA Grid, Showing the Locations of Potential Repository Submodel Domain	30
2. Lateral and Vertical Discretization at the NS# Cross Section Based on the 1999 UZ TSPA Numerical Grid.....	32
3. Lateral and Vertical Discretization at the NS#2 Cross Section Based on the Refined Numerical Grid.....	32
4. Representation of Drifts at the Potential Repository in Grid NS#1.....	35
5. Representation of Drifts at the Potential Repository in Refined Grid NS#2.....	36
6. Model Ambient Temperature Distribution (Deg C) at the Water Table, ECM Model, Mean Present Day Infiltration.....	39
7. Temperature Distribution along NS#1 Cross Section at 500 Years, Model 1.....	46
8. Temperature Distribution along NS#1 Cross Section at 1,000 Years, Model 1.....	46
9. Temperature at Location #1, Model 1.....	47
10. Temperature along the Potential Repository at Cross Section NS#1, Model 1.....	47
11. Matrix Liquid Saturation (SL), along Cross Section NS#1, 500 Years, Model 1.....	48
12. Matrix Liquid Saturation (SL), along Cross Section NS#1, 1,000 Years, Model 1.....	48
13. Matrix Liquid Saturation at Location #1, Model 1.....	49
14. Matrix Liquid Saturation along the Potential Repository, at Cross Section NS#1, Model 1.....	49
15. Fracture Liquid Flux, at 1,000 Years, at the Potential Repository (mm/year), Model 1.....	51
16. Fracture Liquid Flux, at 1,000 Years, at the Top of the CHn (mm/year), Model 1.....	52
17. Fracture Liquid Flux, at Location #1, Model 1.....	53
18. Fracture Liquid Flux along the Potential Repository at Cross Section NS#1, Model 1.....	53
19. Temperature Distribution along NS#1 Cross Section at 1,000 Years, Model 2.....	55

FIGURES (CONTINUED)

	Page
20. Temperature at Location #1, Model 2.....	55
21. Temperature along the Potential Repository Horizon at Cross Section NS#1, Model 2.	56
22. Matrix Liquid Saturation along Cross Section NS#1, 1,000 Years, Model 2.....	56
23. Ambient Matrix Liquid Saturation along Cross Section NS#2.....	58
24. Ambient Temperature (deg C) along Cross Section NS#2.	58
25. Temperature Distribution along NS#1 Cross Section of Grid at 1,000 Years, Model 3.	60
26. Temperature at Location #1, Model 3.....	61
27. Temperature along the Potential Repository Horizon, Model 3.	61
28. Matrix Liquid Saturation along NS#1 Grid at 1,000 Years, Model 3.....	62
29. Matrix Liquid Saturation at Location #1, Model 3.	62
30. Matrix Liquid Saturation along the Potential Repository, Model 3.....	63
31. Fracture Liquid Flux, at Location #1, Model 3.....	63
32. Fracture Liquid Flux along the Potential Repository, Model 3.....	64
33. Temperature Distribution along NS#1 Grid at 500 Years, Model 4.	66
34. Temperature Distribution along NS#1 Grid at 1,000 Years, Model 4.	66
35. Temperature at Location #1, Model 4.....	67
36. Temperature along the Potential Repository Horizon, Model 4.	67
37. Matrix Liquid Saturation (SL) along NS#1 Grid at 500 Years, Model 4.....	68
38. Matrix Liquid Saturation (SL) along NS#1 Grid at 1,000 Years, Model 4.....	68
39. Matrix Liquid Saturation at Location #1, Model 4.	69
40. Matrix Liquid Saturation along the Potential Repository Horizon, Model 4.....	69
41. Fracture Liquid Flux at Location #1, Model 4.....	69

FIGURES (CONTINUED)

	Page
42. Fracture Liquid Flux along the Potential Repository Horizon, Model 4.	70
43. Matrix Liquid Flux along the Potential Repository Horizon, Model 4.	71
44. Temperature Distribution along NS#2 Grid at 500 Years, Model 5.	73
45. Temperature Distribution along NS#2 Grid at 1,000 Years, Model 5.	74
46. Temperature at Location #1, NS#2 Grid, Model 5.	74
47. Temperature at Location #2, NS#2 Grid, Model 5.	75
48. Temperature along the Potential Repository Horizon NS#2 Grid, Model 5.	75
49. Matrix Liquid Saturation (SL) along NS#2 Grid at 500 Years, Model 5.	76
50. Matrix Liquid Saturation (SL) along NS#2 Grid at 1,000 Years, Model 5.	76
51. Matrix Liquid Saturation Location #1, Model 5.	77
52. Matrix Liquid Saturation along the Potential Repository Horizon, NS#2 Grid, Model 5.	77
53. Fracture Liquid Flux at Location #1, NS#2 Grid, Model 5.	78
54. Fracture Liquid Flux along the Potential Repository Horizon NS#2 Grid, Model 5.	78
55. Repository Fracture Liquid Flux along the Potential Repository Horizon NS#2 Grid, Model 5 (detail plot).	79
56. Matrix Liquid Flux along the Potential Repository Horizon NS#2 Grid, Model 5.	79
57. Fracture Liquid Flux along the Potential Repository Horizon NS#2 Grid, Model 5 (detail Plot).	80
58. Temperature Distribution along NS#2 Grid at 500 Years, Model 6.	82
59. Temperature Distribution along NS#2 Grid at 1,000 Years, Model 6.	82
60. Temperature at Location #1, NS#2 Grid, Model 6.	83
61. Temperature at Location #2, NS#2 Grid, Model 6.	83

FIGURES (CONTINUED)

	Page
62. Temperature along the Potential Repository Horizon NS#2 Grid, Model 6.	84
63. Matrix Liquid Saturation (SL) along NS#2 Grid at 500 Years, Model 6.....	84
64. Matrix Liquid Saturation (SL) along NS#2 Grid at 1,000 Years, Model 6.....	85
65. Matrix Liquid Saturation at Location #1, Model 6.	85
66. Matrix Liquid Saturation along the Potential Repository NS#2 Grid, Model 6.	86
67. Fracture Liquid Flux at Location #1, Model 6.	86
68. Fracture Liquid Flux along the Potential Repository Horizon NS#2 Grid, Model 6.	87
69. Fracture Liquid Flux along the Potential Repository NS#2 Grid, Model 6 (detail plot).	87
70. Matrix Liquid Flux along the Potential Repository Horizon NS#2 Grid, Model 6.	88
71. Matrix Liquid Flux along the Potential Repository Horizon NS#2 Grid, Model 6 (detail plot).	88
72. Fracture Gas Flux along the NS#2 Cross Section at 500 Years, Model 6.	89
73. Fracture Gas Flux along the NS#2 Cross Section at 1,000 Years, Model 6.	89

TABLES

	Page
1. Computer Software	17
2. Input Data Source and Data Tracking Numbers	20
3. Scientific Notebooks	27
4. Thermal Properties for UZ Thermal Hydrology Modeling.....	40
5. Summary of Numerical Models for Mountain-Scale TH.....	43

INTENTIONALLY LEFT BLANK

ACRONYMS

2-D	two-dimensional, two dimensions
3-D	three-dimensional, three dimensions
ACC	Accession Number
AMR	Analysis/Model Report
AP	Administrative Procedure
CFR	Code of Federal Regulations
CHn	Calico Hills nonwelded hydrogeologic unit
DIRS	Document Input Reference System
DOE	Department of Energy
DTN	Data Tracking Number
ECM	Effective Continuum Model
ECRB	Enhanced Characterization of Repository Block
ESE	East South East
ESF	Exploratory Studies Facility
FY	Fiscal Year
GFM	Geological Framework Model
HLW	High Level Waste
IFDM	Integral Finite Difference Method
LBNL	Lawrence Berkeley National Laboratory
M&O	Management and Operating Contractor
masl	meters above sea level
NS	North South
OCRWM	Office of Civilian Radioactive Waste Management
PA	Performance Assessment
PTn	Paintbrush nonwelded hydrogeologic unit
Q	Qualified
QA	Quality Assurance
QAP	Quality Administrative Procedure (M&O)
QARD	Quality Assurance Requirements and Description
QIP	Quality Implementing Procedure

ACRONYMS (Continued)

SN	Scientific Notebook
SRR	Software Routine Report
STN	Software Tracking Number
TBD	To Be Determined
TBV	To Be Verified
TDMS	Technical Data Management System
TH	Thermal-Hydrological
THC	Thermal-Hydrologic-Chemical
THM	Thermal-Hydrologic-Mechanical
TM	Thermal Mechanical
TSw	Topopah Spring welded hydrogeologic unit
TSPA	Total System Performance Assessment
UZ	Unsaturated Zone
YMP	Yucca Mountain Site Characterization Project
WNW	West North West
WP	Waste Package
WPO	Waste Package Operations

1. PURPOSE

The purpose of this Analysis/Model Report (AMR) is to document the development of the Mountain-Scale Thermal-Hydrologic (TH) Model and evaluate the effects of coupled TH processes on mountain-scale conditions at Yucca Mountain, Nevada. This is in accordance with the *AMR Development Plan for U0105, Mountain-Scale Coupled Processes (TH) Models* (CRWMS M&O 1999a). This model and its submodels provides the necessary framework to test conceptual hypotheses of heat and fluid flow and predict flow behavior in response to radioactive decay heat release from a potential nuclear waste repository at the Yucca Mountain site. This AMR provides input for Performance Assessment (PA) and the unsaturated zone (UZ) Flow and Transport Process Model Report (PMR). In this AMR any reference to "repository" means the potential nuclear waste repository at Yucca Mountain and any reference to "drifts" means the potential emplacement drifts at the repository horizon.

The Mountain-Scale TH Model numerically simulates the impact of nuclear waste heat release on the natural hydrogeological system, including a representation of heat-driven processes occurring in the far field. The simulations provide predictions for thermally affected liquid saturation, gas- and liquid-phase flux, and water and rock temperature (together referred to as flow fields). Of particular interest is the impact of thermal loading imposed by waste emplacement on percolation at and near the repository host rock and the potential flow barrier effects in the basal vitrophyre underlying the repository horizon.

The mountain-scale TH flow fields are developed using the UZ Flow and Transport Model (UZ Model) with input parameters based on the calibrated property set (DTN: LB997141233129.001). The flow fields are developed with a spatially varying mean infiltration rate and also with varying climates during the thermal-loading period. The simulations were performed using the average thermal load of 72.7 kW/acre and a ventilation efficiency of 70% for 50 years (DTN: SN9907T0872799.001). The flow fields have been submitted to the Technical Data Management System (TDMS) for input to Total System Performance Assessment (TSPA) activities.

Predictions of thermal-loading effects in such models in turn require establishment and acceptance of mathematical models that accurately represent the physics of heat and fluid transport in the UZ. In this AMR the mathematical formulation employed in the TOUGH2 family of codes (Pruess 1987, pp. 2-11, 1991), the continuum models, and the van Genuchten capillary pressure and relative permeability relationships are relied upon to adequately describe the behavior of the UZ under thermal-loading conditions. This formulation is based on the traditional energy and mass conservation relationships, together with appropriate constitutive equations.

Model validation is documented within this AMR. During the development of the UZ TH flow submodels, the accuracy and validity of the model results were evaluated based on scientific principles and current understanding of fracture-matrix interactions, heat transport, and two-phase flow in unsaturated subsurface systems. Calibration of model temperature provides a basis for assessing the effectiveness of the model to capture mountain-scale processes. The analyses conducted in this AMR are intended to evaluate the mountain-scale response to thermal load under the proposed design conditions. The numerical models are used to determine the effect of

thermal loading on mountain-scale liquid and gas flux, temperature, and moisture distribution in the UZ.

2. QUALITY ASSURANCE

The activities documented in this AMR were evaluated with other related activities in accordance with QAP-2-0 Rev.5, *Conduct of Activities*, and were determined to be quality affecting and subject to the requirements of the U.S. DOE Office of Civilian Radioactive Waste Management (OCRWM) *Quality Assurance Requirements and Description (QARD)* (DOE 1998). This evaluation is documented in *Activity Evaluation of M&O Site Investigations* (CRWMS M&O 1999b, 1999c; and Wemheuer 1999). Accordingly, the modeling activities documented in this AMR have been conducted in accordance with the CRWMS M&O quality assurance program, using OCRWM Administrative Procedures (APs) and YMP-LBNL Quality Implementing Procedures (QIPs) identified in the *AMR Development Plan for U0105, Mountain-Scale Coupled Processes (TH) Models* (CRWMS M&O 1999a). This AMR has been developed in accordance with procedure AP-3.10Q, Rev. 1, ICN 1, *Analyses and Models*.

INTENTIONALLY LEFT BLANK

3. COMPUTER SOFTWARE AND MODEL USAGE

The software codes and routines used in this study are listed in Table 1. These were appropriate for the intended application, were used only within the range of their software validation, and were obtained from configuration management in accordance with AP-SI.1Q, Rev. 2, ICN2, *Software Management*.

Table 1. Computer Software

Software Name	Version	Software Tracking Number (STN):	Computer Platform
TOUGH2 V1.4	1.4	10007-1.4-01	Sun or DEC Workstation w/ Unix OS
EXT V1.0	1.0	10047-1.0-00	Sun Workstation w/ Unix OS
Infil2grid V1.6	1.6	10077-1.6-00	Sun Workstation w/ Unix OS
Wingridder	1.0	10024-1.0-00	PC
Routines:			
thbcgen-v0.f	1.0	10219-1.0-00	Sun Workstation w/ Unix OS
gen-incon-v0.f	1.0	10220-1.0-00	Sun Workstation w/ Unix OS
get_a_layer_v0.f	1.0	10221-1.0-00	Sun Workstation w/ Unix OS
get_temp_v0.f	1.0	10222-1.0-00	Sun Workstation w/ Unix OS
add_rep_v0.f	1.0	10223-1.0-00	Sun Workstation w/ Unix OS
toptemp_v0.f	1.0	10224-1.0-00	Sun Workstation w/ Unix OS
hsource_v0.f	1.0	10225-1.0-00	Sun Workstation w/ Unix OS
dk2ecm_mat_v0.f	1.0	10226-1.0-00	Sun Workstation w/ Unix OS

To model the nonisothermal effects of thermal loading on the UZ, we used the program TOUGH2 V1.4 with equation of state module EOS3. This program has been qualified under AP-SI.1Q. The use of TOUGH2 V1.4 prior to obtaining it from configuration management is being evaluated under AP-3.17Q, *Impact Reviews*, but no impact is anticipated. To process the TOUGH2 output for plotting, we use the code EXT V1.0 a postprocessor for TOUGH2 codes that was reverified under AP-SI.1Q. Infil2grid V1.6 is used to map the infiltration flux from the infiltration maps onto the numerical grid. This code is being qualified under AP-SI.1Q, Rev. 2, ICN 4, and a Software Activity Plan for use of unqualified software and copy of the code have been submitted to configuration management per AP-SI.1Q. The code Wingridder V1.0 was used to generate numerical grids used here and is documented in a separate AMR. We used this code to develop an additional refined North-South for detailed evaluation of thermal-loading effects. The code is also being qualified under AP-SI 1Q, Rev. 2, ICN 4, Software Activity Plan for use of unqualified software and copy of the code have been submitted to configuration management per AP-SI.1Q.

The documentation for the routines is provided in the Software Routine Reports (SRR) submitted under the STN in Table 1. These were used for pre- and post-processing of files for TOUGH2 V1.4.

Standard spreadsheet and graphics software programs (TecPLOT V7.0 and EXCEL 97 SR-1) were also used but are not subject to software quality assurance requirements, because these are commercially available software products.

This AMR documents the Mountain-Scale TH Model. Input and output files for the model simulations documented in this AMR are listed and discussed under each modeled scenario in Section 6.

4. INPUTS

4.1 DATA AND PARAMETERS

Key input data used in the TH model development are listed in Table 2 and include the following:

- Fracture properties (frequency, permeability, van Genuchten parameters, and aperture, porosity, and interface area) for each UZ model layer.
- Matrix properties (porosity, permeability, van Genuchten α and m) for each UZ model layer.
- Thermal properties (grain density, wet and dry thermal conductivity, grain specific heat, and tortuosity coefficients) for each model layer.
- Fault properties (matrix and fracture) for each hydrogeologic unit.
- Repository thermal-load and ventilation efficiency.
- Infiltration rates and changes with climate

The calibrated parameter sets also include estimates of active-fracture parameters, γ , (Liu et al. 1998) for each model layer that accounts for the reduction in interaction between matrix and fracture flow resulting from flow fingering and channeling. Specific input data sets, associated Data Tracking Numbers (DTNs) and Input Tracking Numbers (ITN) are provided in Table 2. The QA status of these data is provided in the Document Input Reference System (DIRS) included as Attachment I. Complete References are also presented in Section 8.3.

Table 2. Input Data Source and Data Tracking Numbers

Data Description	DTN or ITN
Current climate infiltration maps – average, low and high	GS000399991221.002
Future climate (monsoon) infiltration maps– average, low and high	GS000399991221.002
Future climate (glacial transition) infiltration maps – average, low and high	GS000399991221.002
3-D UZ Model Grid, properties calibration	LB990501233129.004
3-D UZ Model Grid	LB990701233129.001
Repository thermal load and decay data	SN9907T0872799.001
Thermal properties for model layers	LB991091233129.006
Calibrated fracture and matrix properties sets (base case)	LB997141233129.001
<i>In situ</i> gas pressure and temperature data– UZ#4, UZ#5, NRG-6, NRG-7a, SD-12, UZ-7a	GS960308312232.001
<i>In situ</i> gas pressure and temperature data– NRG-6, NRG-7a	GS950208312232.003
<i>In situ</i> gas pressure and temperature data UZ#4 and UZ#4	GS951108312232.008
<i>In situ</i> borehole instrumentation and monitoring NRG-7a, NRG-6, UZ#4, UZ#5, UZ-7a and SD-12 – temperature, pressure, and water potential	GS970108312232.002
<i>In situ</i> borehole instrumentation and monitoring–NRG-7a, UZ#4, UZ#5, UZ-7a, SD-12 – temperature, pressure, and water potential	GS970808312232.005
<i>In situ</i> borehole instrumentation and monitoring NRG-7a, UZ#4, UZ#5, UZ-7a and SD-12–temperature, pressure, and water potential	GS971108312232.007
<i>In situ</i> borehole instrumentation and monitoring NRG-6, NRG-7a, UZ#4, UZ#5, UZ-7a and SD-12–temperature, pressure, and water potential	GS980408312232.001
Geologic Framework Model, GFM 3.1 or borehole logs -list	MO9901MWDGFM31.000
Matrix hydrologic property data	GS960908312231.004

^aInput transmittal per AP-3.14Q, (CRWMS M&O, 1999d)

4.2 CRITERIA

This AMR complies with the DOE interim guidance (Dyer 1999). Subparts of the interim guidance that apply to this analysis or modeling activity are those pertaining to the characterization of the Yucca Mountain site (Subpart B, Section 15). The compilation of information regarding geology of the site is in support of the License Application (Subpart B, Section 21(c)(1)(ii)) and the definition of geologic parameters and conceptual models used in performance assessment (Subpart E, Section 114(a)). The compilation of information regarding hydrology of the site is in support of the License Application (Subpart B, Section 21(c)(1)(ii)) and the definition of hydrologic parameters and conceptual models used in performance assessment (Subpart E, Section 114(a)).

4.3 CODES AND STANDARDS

No specific formally established standards have been identified as applying to this modeling activity.

INTENTIONALLY LEFT BLANK

5. ASSUMPTIONS

The assumptions documented below are required to develop the UZ Mountain-Scale TH Model discussed in this AMR. This section presents the rationale and justification for using these assumptions and references the sections in the AMR where these assumptions are used. The assumptions are in the numerical representation of thermal load conditions at the repository, the model boundary conditions, the effect of TH process on flow properties, and the influence of perched water on TH processes. The assumptions below apply to all the TH models discussed in Sections 6.7–6.11. Further confirmation of these assumptions is not required for the intended use of these model results. Detailed discussion of the implementation of these assumptions in the TH models is presented in Sections 6.1–6.6.

5.1 ASSUMPTIONS REGARDING BOUNDARY CONDITIONS MODEL AND THERMAL LOADING

Treatment of boundary conditions can be directly incorporated in the numerical grid generation scheme, since model boundaries can coincide with numerical grid boundaries. In TOUGH2, boundary conditions are generally specified by means of appropriately chosen volume elements and flow connections. Boundary conditions can be of two basic types. Dirichlet conditions prescribe thermodynamic conditions, such as pressure or temperature on the boundary, while Neumann conditions prescribe fluxes of mass or heat crossing boundary surfaces (Pruess 1991, p. 33-37). A special case of Neumann boundary conditions is the no-flux boundary. In the Integral Finite Difference Method (IFDM) used in TOUGH2, this case is handled by not specifying any flow conditions across the boundary. Dirichlet-type boundary conditions, such as constant pressures or temperatures, can be specified by introducing appropriate boundary elements and connections. Specific assumptions under this category are as follows:

1. Thermal conditions at the top and bottom boundaries are represented using fixed temperatures. This is equivalent to using an infinite heat sink/source term. In addition, top and bottom model boundaries are also subject to constant pressure and saturation conditions.

The use of constant temperature, pressure, and saturation boundaries has been discussed extensively (e.g., Wu et al. 1999a). The fixed temperature condition at the top and bottom boundaries is a simplified representation of the heat exchange on the boundary “surfaces” between the model domain and the atmosphere or the water table. The top boundary of the model, made up of the land surface and tuff-alluvial contact, is controlled mainly by the atmosphere, while temperatures at the water table are determined by the ambient geothermal gradients and infiltration flux. The two boundaries are both far away from the potential repository horizon; therefore, the effects of specified temperatures on thermal behavior at or near the repository are expected to be small. As a result, constant temperatures, estimated from field-measured values along these boundaries, will provide a good approximation of the TH system to be simulated.

2. An equivalent heat load is evenly distributed within potential emplacement drifts and released from time zero after waste emplacement, according to the predicted heat load history (thermal decay curve).

Actual thermal load at the repository will be discretely distributed in both space and time. The assumption of an evenly distributed thermal source over all the drifts will have little effect on far-field TH processes on the mountain-scale model, because detailed thermal load distributions affect only drift-scale processes and are limited to the first few years of thermal load.

3. Potential waste emplacement drifts are assigned matrix and fracture properties of the hydrogeological unit in which they are located.

Excavation and backfill of the drifts will substantially affect only the near-field environment. Mountain-scale TH models are designed to evaluate the TH processes primarily on the large scale of the UZ system as well as averaged behavior near the drifts over tens of thousands of years. Over this period, the material used in drifts will have little impact on mountain-scale TH processes.

4. Ventilation removes thermal energy only. The amount of water vapor and air removed by ventilation can be ignored.

When ventilation is used to remove some of the heat generated earlier by the emplaced waste, it is assumed that 70% of the heat generated is removed by ventilation for the first 50 years. In the model, ventilation is assumed to remove the heat only, and the effects of ventilation and associated air circulation on water vapor and air at the repository are ignored. Although ventilation may remove some water vapor from the drifts, the amount removed is negligible because for most of the ventilated period, the drift walls will be completely dry.

5.2 ASSUMPTIONS REGARDING EFFECTS OF THERMAL LOAD ON FLOW PROPERTIES

Flow and transport properties can be affected by changes in temperature through thermal-mechanical (TM) effects. Similarly, dissolution, precipitation, adsorption as well as other geochemical reactions resulting from thermal-hydrologic-chemical (THC) coupling can alter flow and transport properties. Many of the temperature-dependent properties, such as fluid density, viscosity, and specific enthalpy, are incorporated in the formulation of the TOUGH2 V1.4 (STN: 10007-1.4 01, V1.4) code. However, the effects of TM and THC on rock properties, such as permeability, relative permeability and the relationship between capillary pressure and liquid saturation, have not been implemented in TOUGH2, V1.4 as used in this study. In this AMR, we assume:

1. Effects of TM and THC on rock properties as a result of thermal load can be ignored.

THC and TM effects may have a significant impact on TH processes only at or near drifts during the first few years of the thermal-loading period. On the mountain-scale domain and long-term analyses, the effects of TM and THC on flow and transport properties are expected to be small.

2. Hysteresis effects are negligible.

In addition to TM and THC effects, the thermal load will create significant dry-out and rewetting phenomena in the nearby regions of tuffs. Hysteresis effects will accompany these drying (drainage) and rewetting (imbibition) processes. This leads to different curves of relative permeability and capillary pressures for describing drainage and imbibing processes, respectively. In this work, we ignore hysteresis effects because they are small compared to the uncertainty inherent to the development of the capillary pressure and relative permeability relationships.

Use of the two assumptions regarding TM/THC coupling and hysteresis effects results partially from the limitations of available field data and constitutive relations to describe these phenomena. However, these effects are considered negligible when compared with the uncertainty of the rock properties existing in the collected data.

5.3 ASSUMPTION REGARDING EFFECT OF PERCHED WATER ON TH PROCESSES

Perched water effects are ignored.

The occurrence of perched water and its effects on the UZ flow fields are discussed in a separate AMR. Perched water conditions are confined mainly to the lower units of the Topopah Springs welded (TSw) hydrogeological unit and on top of the Calico Hills nonwelded unit (CHn). Over the repository domain, perched water locations are typically 100-150 m below the repository horizon (Wu et al 1999b). Because the dominant heat-transfer mechanism at these locations is heat conduction (boiling conditions not attained), the effect of repository thermal load on perched water bodies is ignored.

INTENTIONALLY LEFT BLANK

6. ANALYSIS/MODEL

As discussed in Section 1, this AMR documents the development and the results of the Mountain-Scale TH Model. This section describes the conceptual model of UZ flow at Yucca Mountain, the numerical models developed, the numerical grids used, and the modeling parameters used in the TH submodels. It consists of the following sections:

- Conceptual model
- Numerical grids
- Thermal load
- Boundary and ambient conditions
- Thermal properties
- Infiltration
- Results of the TH models, submodels, and simulations

Key scientific notebooks used to document modeling activities described in this AMR are listed in Table 3.

Table 3. Scientific Notebooks

LBL Scientific Notebook ID	M&O Scientific Notebook ID	Page Numbers	Accession Numbers (ACC)
YMP-LBNL-GSB-1.6.3	SN-LBNL-SI-085-VI.	pp. 81-135	MOL.19991217.0514
YMP-LBNL-YSW-2	SN-LBNL-SI-120-VI	pp. 168-172	MOL19991217.0515
YMP-LBNL-GSB-LP-2	SN-LBNL-SI-103-VI	pp. 79-81	MOL19991217.0516
YMP-LBNL-GSB-1.1.2	SN-LBNL-SI-003-VI	pp. 148-151	MOL.19991223.0175

6.1 CONCEPTUAL MODEL

To model unsaturated flow under thermal loading, the selected conceptual model for UZ flow must be consistent with field observations. Detailed discussion of the conceptual models of UZ flow at Yucca Mountain and the validity of the numerical methods are documented in separate AMRs.

These conceptual models are based on the current understanding of the Yucca Mountain geology and the UZ hydrology and incorporate previous models of UZ flow (Montazer and Wilson 1984). Field studies, lithological evaluation of boreholes, and detailed evaluation of the exposed subsurface within the recently completed Exploratory Studies Facility (ESF) drift and the east-west cross drift (ECRB) were used to validate the flow and transport conceptual models. These findings are further supported by conceptual experiments of flow in exposed rocks, in the ESF and ECRB, as well as by laboratory measurements. The major elements of the conceptual models also include numerical approaches of the volume averaged, continuum concept for modeling fluid and heat flow and fracture-matrix interactions. Note that in the TH submodels of this AMR, we ignore thermal-mechanical (TM) and thermal-hydrologic-chemical (THC) coupling. Therefore, the input flow properties are treated as constants for the modeled period.

6.1.1 Numerical Methods for Modeling Fluid and Heat Flow

The physical laws and empirical relationships that govern the flow of heat and fluids through porous media lead to equations that describe the balances of mass, momentum, and energy. The partial differential equations describe the variation of fluid phase saturation and composition as well as pressure and temperature as functions of continuous space and time coordinates in the subsurface. The relevant numerical formulation for multicomponent mass and heat transport are applied (Pruess 1987, pp. 2–11) to the equations of flow.

The TOUGH2 V1.4 (STN: 10007-1.4-0.1, Version 1.4) code implements the Integral Finite Difference Method (IFDM) numerical method to model multiphase, multicomponent flow of mass (liquid, vapor and air) and heat. The validity and accuracy of the numerical methods used have been extensively investigated particularly for the limitations and assumptions in mathematical formulations of the discretized form (Pruess, et. al., 1987, pp. 2–11, 1991 pp. 5–52). The equation-of-state (EOS3; water, air and heat) module of the TOUGH2 V1.4 code, providing the thermophysical properties for two-phase fluid mixtures of water and gas phases, is used in this study.

In this AMR, the relationships between saturation and relative permeability and between saturation and capillary pressure for unsaturated rock are estimated using documented equations from Brooks and Corey (1966), and van Genuchten (1980). The base-case properties set (DTN: LB997141233129.001) used in this AMR was developed by calibration of moisture potential data using these relationships. In developing these properties, a modified Brooks and Corey relationship (implemented in TOUGH2 v1.4) is used to estimate the gas relative permeability. The van Genuchten relationship is used to estimate the relationship between liquid saturation and relative permeability and the capillary pressure.

6.1.2 Continuum Approach and Fracture-Matrix Interactions

Numerical models generally use large computational gridblocks to represent a hydrogeological system. For example, the UZ site-scale model consists of gridblocks with a dimension range of 5 to 300 m. In the physical domain, these large-size blocks may contain tens to hundreds of fractures. For modeling flow in fractured porous media, the key issue is how to evaluate fluid and heat exchange between fractures and matrix. Several conceptual formulations of the dual-continua approaches can be used to model flow in such media. These include (1) the explicit discrete fracture and matrix treatment; (2) the effective-continuum method (ECM); (3) the double-porosity method; (4) the dual-permeability (dual-k) method; and (5) the multiple-interacting-continua (MINC) method (Pruess and Narasimhan 1985). A discussion of these different model concepts is presented in Doughty (1999, pp. 69–106). In this AMR, we use the following continuum approaches:

1. The ambient heat and fluid flow is modeled by both the ECM (Klavetter and Peters 1986) and dual-k numerical models. The generalized form of the ECM method has been implemented into the TOUGH2 V1.4 code, as described in detail by Wu (1996).

2. The dual-k formulation, with a single fracture continuum and single matrix continuum representing each discrete block, is used for thermal-loading studies. This model allows matrix-to-matrix and fracture-to-fracture flow as well as fracture-matrix interactions.
3. The active fracture concept (Liu et al. 1998) is used to modify liquid flow between fractures and matrix.

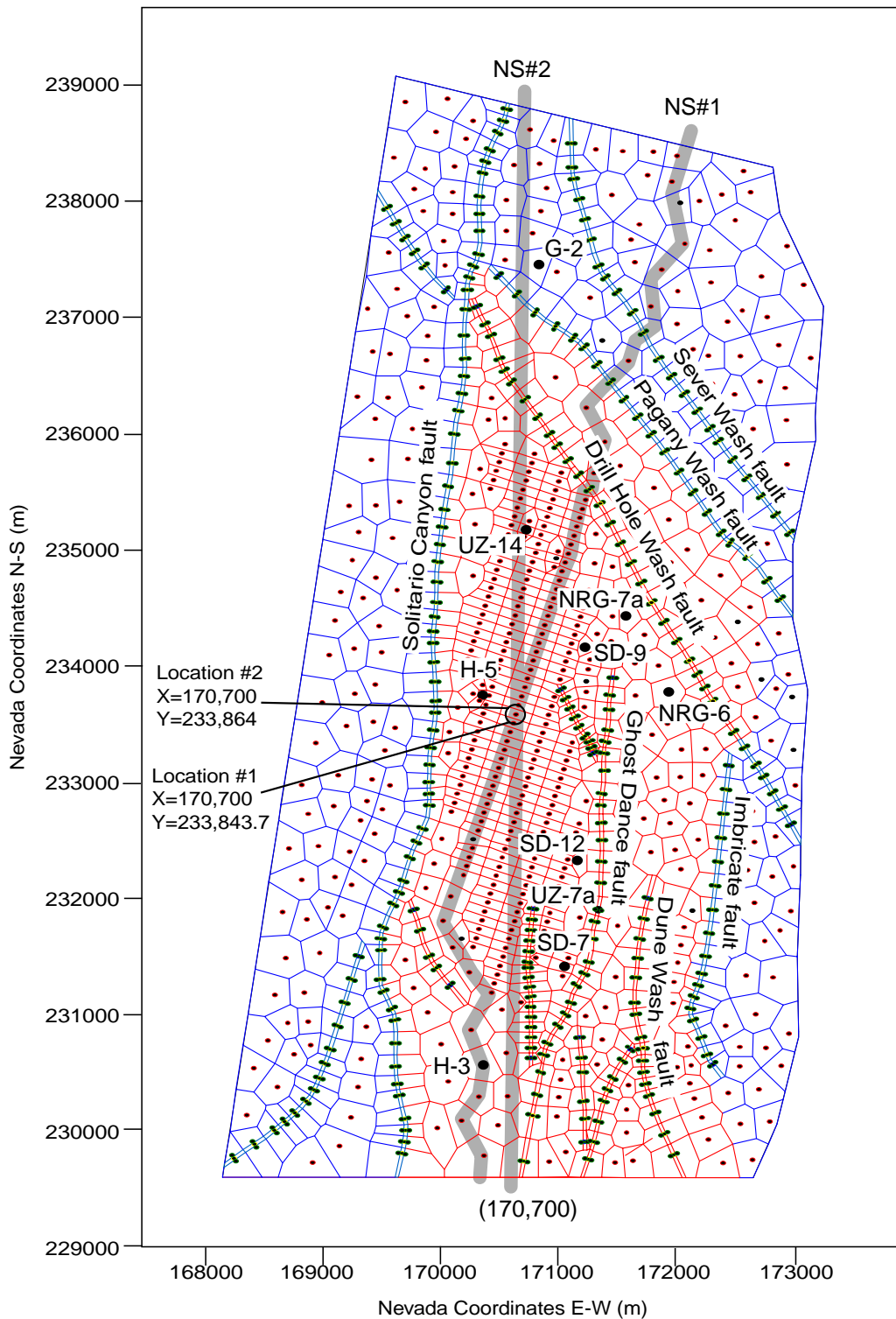
6.2 NUMERICAL GRIDS

The numerical model grids used for simulating the effects of heat are: (1) a 3-D submodel grid of the UZ 3-D model grid and (2) two 2-D cross section model grids (NS#1 and NS#2). The first 2-D grid (NS#1) is directly extracted from the UZ 3-D grid. The second grid (NS#2) is a refined north-south cross section also based on the Geological Framework Model, GFM 3.1 (DTN: MO9901MWDGFM31.000). The grids were generated using Wingridder V1.0. Figure 1 shows a plan view of the UZ 3-D model and the location of the submodel domain and the 2-D cross sections.

In all the grids, a 5 m thick grid layer is used to represent the repository horizon. This repository layer is bounded immediately above and below also by 5 m thick layers. In the 3-D grid, the lateral spacing over the repository domain is equal to the spacing between the drifts (81 m), and about 270 m along the drifts. This coarse grid is used in a separate AMR to generate the UZ flow fields for TSPA.

Because both the 3-D submodel grid and the 2-D NS#1 grid are directly extracted from the 3-D UZ grid, the lateral spacing over the potential repository is the same as the drift spacing (i.e., 81 m). This type of grid, although sufficient to resolve mountain-scale UZ flux, may not provide enough resolution for detailed evaluation of flow around and between drifts. Because liquid flux in the UZ at Yucca Mountain is predominantly vertical, and drifts are widely spaced, the potential exists for flow between the drifts. Modifications of the numerical grids to allow for drift-by-drift models are documented in Scientific Notebook YMP-LBNL-GSB-1.6.3 (pp. 109-113). There may also be significant differences in temperature and saturation laterally between the heated drift and the middle portion of the rock between the drifts, particularly during earlier times of thermal load. Such processes cannot be modeled by the UZ 3-D grid or any submodel extracted from it, because there are no numerical grid nodes between the drifts. In this AMR, we use the following approaches to model near-drift UZ TH processes:

1. Use local refinement at the repository to resolve temperature, saturation, and flux changes only at and near this horizon.
2. Use local refinement at the repository together with lateral refinement over the entire grid so that both the ambient infiltration and the repository TH processes can be resolved.



Based on modeling results submitted with this AMR under DTN: LB991201233129.001

Figure 1. Plan View of the 1999 UZ TSPA Grid, Showing the Locations of Potential Repository Submodel Domain (in red). The Cross Sections, NS#1 and NS#2, and Locations #1 and #2 are used for detailed plots. Large solid circles refer to boreholes. Small circles refer to centers of grid columns.

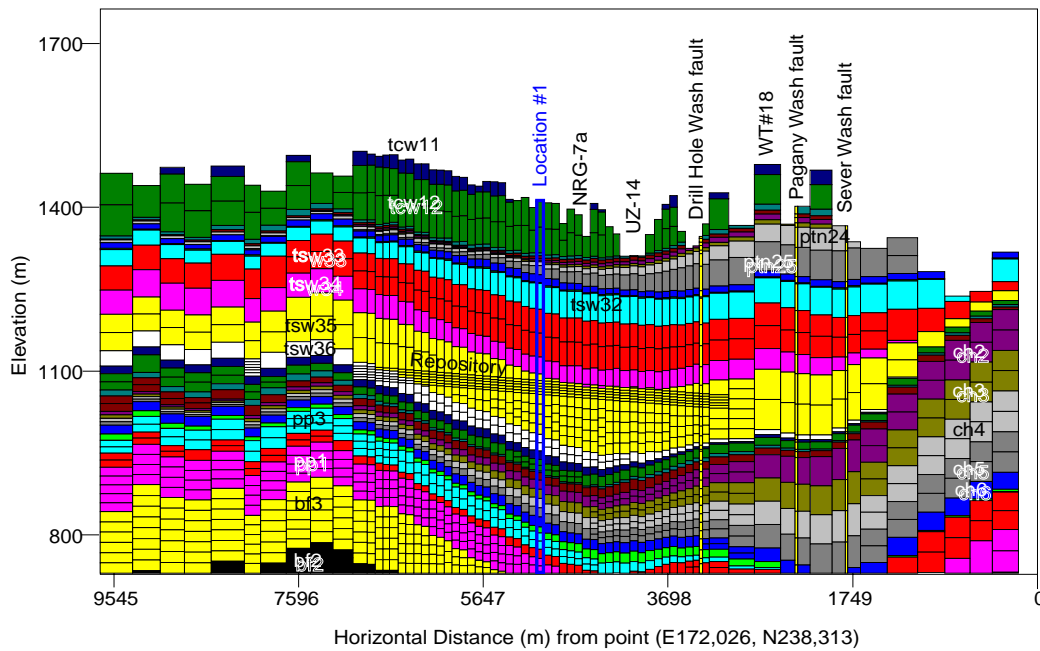
6.2.1 3-D Numerical Grid for Potential Repository Submodel

The repository submodel domain is bounded by the Solitario Canyon fault to the west, the Pagany Wash fault to the north, the Imbricate fault to the east, and the 3-D UZ model boundary to the south. It consists of 62,884 elements and 249,813 connections in a dual-k formulation. The 3-D repository submodel was extracted from the 3-D UZ numerical grid (DTN: LB990701233129.001). This grid does not include perched water zones, which are assumed to have little impact on TH processes (see Section 5.3). The development of the 3-D UZ numerical grid is described in a separate AMR. A 3-D repository submodel is used to reduce the computational intensity required in terms of memory and CPU time for the TH simulations. In addition, we are primarily interested in the TH processes in the immediate vicinity of the repository. The predominantly vertical percolation fluxes in the UZ system also makes it unnecessary to use a larger modeling domain, such as the entire UZ Model grid.

6.2.2 2-D North-South Grids

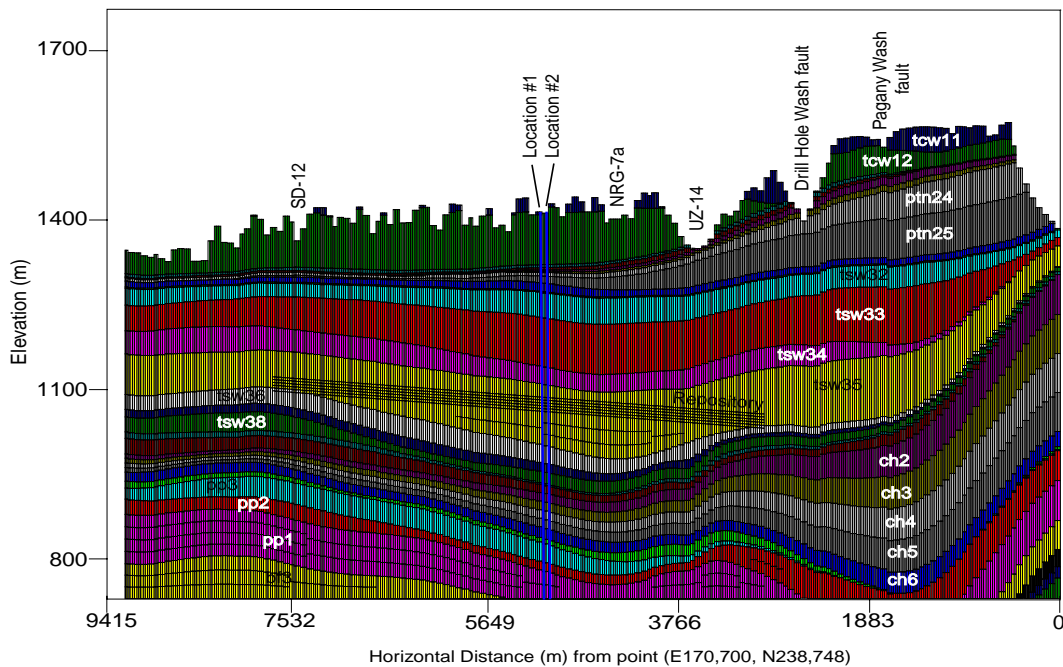
Two north-south 2-D grids of the UZ Model are used in this AMR, with the locations shown in Figure 1. The first cross section (NS#1, Figure 2) is directly extracted from the UZ 3-D grid for TSPA (DTN: LB990701233129.001), which excludes formulations for perched water. The second cross section (NS#2, Figure 3) is a refined north-south grid located at 170,700 east, in which the lateral grid spacing is equal to 1/4 of the drift spacing. This grid was specifically developed for detailed study of TH processes and is also based on the GFM 3.1 geological model. We use WinGridder V1.0 (STN:10024-1.0-00), Version 1.0. WinGridder Version 1.0, and its development is documented in Scientific Notebook YMP-LBNL-GSB-LP-2 (pp. 79-81). This refined NS#2 grid also ignores the effects of perched water.

The refined NS#2 numerical grid provides a better resolution than NS#1 for the heat distribution and detailed evaluation of the effect drift scale processes on mountain-scale TH. It also provides a method of estimating the TH conditions and flow within the pillars. Evaluation of the extent of this bypass flow is important for TSPA because the fluid displaced by heat at the drifts may condense and drain between the drifts.



Based on modeling results submitted with this AMR under DTN: LB991201233129.001

Figure 2. Lateral and Vertical Discretization at the NS# Cross Section Based on the 1999 UZ TSPA Numerical Grid. The plot shows projected locations of UZ boreholes and the potential repository. Labels show hydrogeologic unit names (Table 4).



Based on modeling results submitted with this AMR under DTN: LB991201233129.001

Figure 3. Lateral and Vertical Discretization at the NS#2 Cross Section Based on the Refined Numerical Grid. Plot shows location of potential repository and hydrogeologic units layering.

6.3 POTENTIAL REPOSITORY THERMAL LOAD

For the TH submodels, we use mountain-scale thermal-loading data obtained from the TDMS (DTN: SN9907T0872799.001). The data were developed by Waste Package Operations (WPO) using a QAP-3-12 *Transmittal of Design Input*, request (PA-WP-99184.Ta) and documented under the QAP-3-15 *Calculations*.

The thermal load and the resulting temperature field may have a large influence on many TH related processes. These processes can directly impact the performance of the potential repository. For example, emplacement of heat-generating high level waste (HLW) will elevate the temperature and cause the redistribution of the *in situ* moisture at the repository as well as in the unsaturated zone. As heat is released from the waste unit and transferred to the surrounding host rock, the temperature near the waste packages will approach or exceed the boiling point of water (approximately 97°C at ambient pressure). Boiling of formation water will then take place, with the associated increase in vapor pressure and overall gas-phase pressure. This will result in forced convection of the gas phase, with a redistribution of water, accompanied by large latent heat effects. With favorable conditions, this may result in "heat-pipe" conditions, the steady counter-current flow of liquid towards the repository and vapor-phase away from the repository. The liquid-phase and gas-phase flow will perturb the *in situ* fluid saturation in both fractures and matrix, and may result in a large two-phase zone above the repository and may increase the potential for changes in the flow properties within the condensation zones. The impact of heat on the TH processes will depend on the thermal load and its distribution at the repository.

6.3.1 Base-Case Mountain-Scale Thermal Load

The total thermal load for the "base-case" TSPA-SR Rev0 scenario is 72.72 kW/acre, based on a repository area of 1,050 acres. This thermal load is used in all the thermal load modeling studies. The thermal load was input as a tabulated lookup of time versus thermal load data, following the decay curve, using the heat GENER card incorporated into the input file for TOUGH2 V1.4. The "GENER" block in the TOUGH2 V1.4 input is used to specify mass or heat sources/sinks in individual elements of the model (Pruess 1987, p. 29).

6.3.2 Thermal Load with Repository Ventilation

Information on the effective mountain-scale thermal load under ventilation is also given in DTN: SN9909T0872799.001. The base-case repository thermal-load design with ventilation provides that 70% of the generated heat can be removed by ventilation for the preclosure period of 50 years. After 50 years, the thermal load reverts to the "no-ventilation" rate. To account for heat removal by ventilation during the first 50 years, we multiply the "no-ventilation" thermal load, heat source term, by the ventilation factor (30%) for the 50-year period.

6.3.3 Heat Distribution at the Repository

In all models, each repository drift is represented by a single element (with both matrix and fracture continua for a dual-k formulation) and is modeled with the properties of the UZ Model layer in which the element is located. Thermal load is applied directly only to the matrix continuum of the repository node, because it forms more than 99% of continua and the thermal

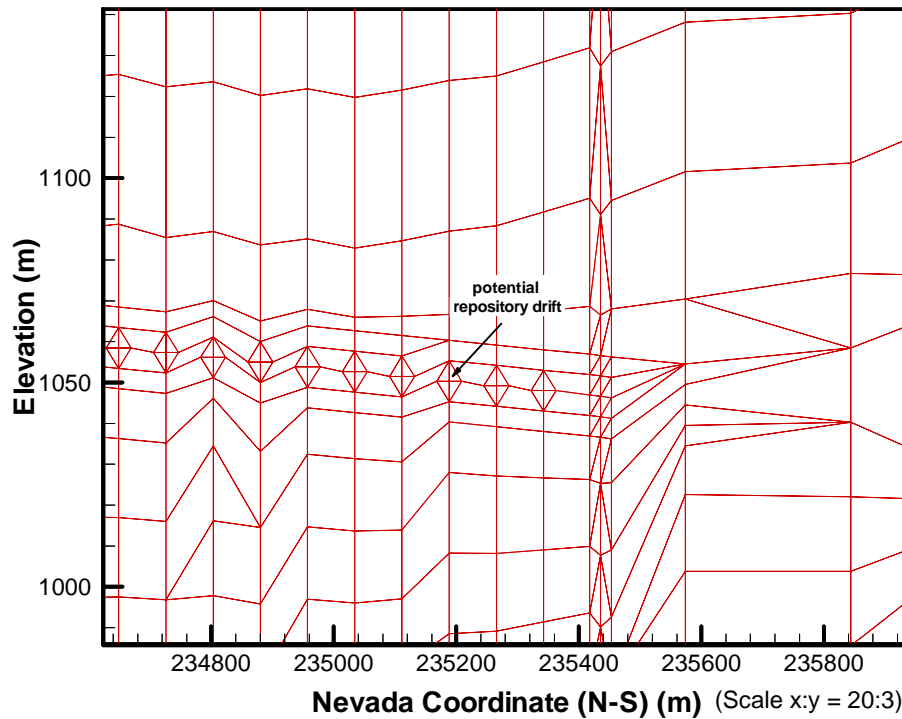
load is computed using the column areas (combined matrix and fracture continua). The distribution of the heat source at the potential repository horizon depends on the discrete representation of the drifts within the repository nodes and the grid spacing.

6.3.3.1 Continuous Heat Source

If the grid spacing within the repository is equal to the drift spacing, then the entire repository node is used to represent the drift. This results in a continuous and smeared heat source across the repository laterally. This approach cannot provide detailed resolution to studies of TH processes in terms of temperature, saturation, and flux for the intervening space between the drifts. While not allowing these phenomena to be modeled near the drifts, this coarse-grid model allows for simple and fast estimation of the long-term, average response to thermal load (after 500 years, according to this AMR). Beyond this time, heat distribution is sufficiently diffused at the repository that such a model presents a good approximation of the heat-source distribution. This type of modeling approach is only used in the repository submodel and the NS#1 numerical grids, which are directly extracted from the 3-D TSPA grid. The major advantage of this modeling approach is that it allows for direct comparison of fluid, temperature, and flux distribution between the 3-D ambient TSPA flow field models and the TH model over the repository domain. The impact of TH on flow and transport can then be directly estimated using flow-fields extracted from the TH model.

6.3.3.2 Discrete Heat Source

Although the repository thermal load is computed based on the total acreage of the repository, the heat-generating radioactive waste will be stored in the drifts within the repository at a discrete spacing. The current repository design has drifts of 5.5 m diameter, spaced 81 m apart in a WNW-ESE direction (Figure 1). Because of the large spacing between the drifts and the disparity in infiltration across the model, a potential for large differences or gradients in temperature, saturation, and flux exists between the heated drifts. The discrete (drift-by-drift) model attempts to provide a refined-grid model that accounts for such phenomena to investigate their importance and effect on mountain-scale TH processes.



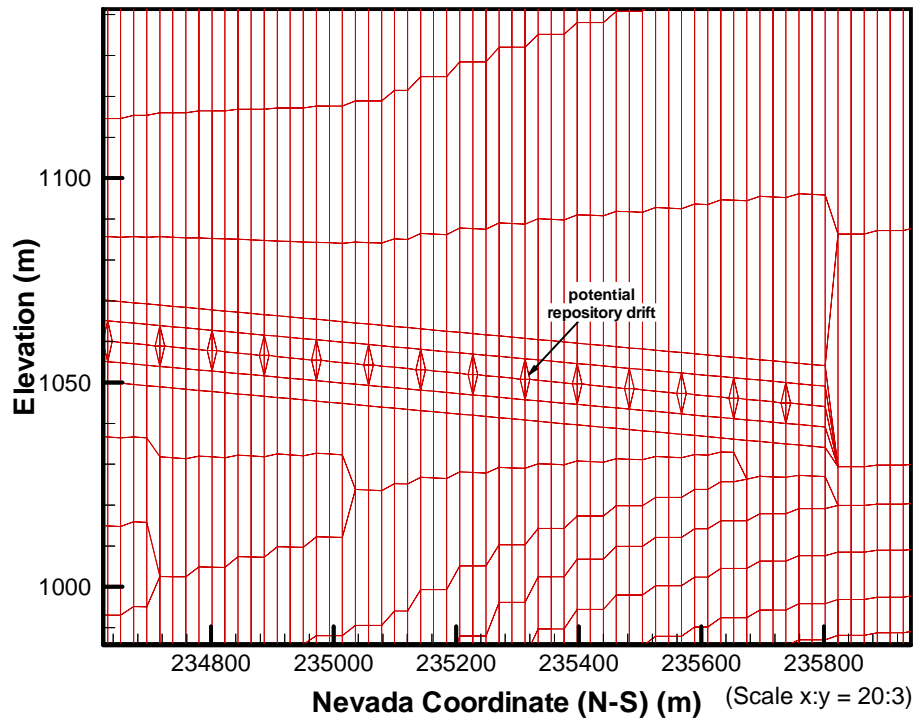
Based on modeling results submitted with this AMR under DTN: LB991201233129.001

Figure 4. Representation of Drifts at the Potential Repository in Grid NS#1.

If the lateral grid spacing is several times smaller than the drift spacing, then a drift-by-drift distribution of the heat source can be simulated. We can also subdivide the repository nodes in such a grid to explicitly include an element that approximates the dimensions of the drift. To model a more physically accurate heat distribution at the repository horizon, we performed local refinement on the NS#1 grid by inserting a 5.0 m drift element for every 81 m lateral spacing along the repository. We use a 5.0 m drift element (close to the 5.5 m drift diameter), because 5.0 m layers are used in the numerical grid. This drift element is bordered laterally by two equal subelements of the original repository element. Figure 4 shows the connections between elements in the modified grid. In this cross section, the drifts are separated by two 38.0 m wide elements. Above and below the repository, the three elements in each repository element are connected to the overlying and underlying elements within the same column and laterally between themselves and the laterally adjacent elements. This locally refined grid allows for flow between drifts. However, since the refinement is limited to the potential repository level, the applied surface infiltration is based on the original, coarse grid spacing of 81 meters between the drifts. The thermal loads computed based on the lateral spacing between the drifts is then applied only to the matrix continua of the discrete drift elements.

We also used local refinement on the refined north-south NS#2 grid. In this case there are three elements over a lateral grid spacing of 85.6 m between two drifts, each 21.39 m wide (owing to the difference in the orientation of the drifts relative to the orientation of this cross section). Within each drift element at the repository level, we again insert a 5.0 m wide locally refined

element to represent the drift and two equal subelements each 8.145 m wide, and use the grid connection scheme described above. In this refined grid, each drift element is laterally separated by five elements between the drifts. Figure 5 shows the resulting connections in the modified grid. The thermal load is again computed using the drift spacing (thermal load for drift column multiplied by four) and applied to the matrix continuum of the drift element.



Based on modeling results submitted with this AMR under DTN: LB991201233129.001

Figure 5. Representation of Drifts at the Potential Repository in Refined Grid NS#2.

6.4 BOUNDARY AND INITIAL CONDITIONS

For TH studies, the steady-state, ambient mountain-scale temperature and saturation conditions serve as initial conditions for the various thermal-load and infiltration scenarios. Liquid saturation, water potential, and pneumatic pressure data are used to calibrate the flow and transport properties, while temperature data, which are not directly used in parameter calibration for flow and transport properties, are required to describe the geothermal conditions of the UZ model. A steady-state ambient moisture, pressure, and temperature distribution in the mountain can be obtained using the TOUGH2 V1.4 simulation under fixed top and bottom temperature, pressure, and saturation boundary conditions.

6.4.1 Top Boundary

The top of the Mountain-Scale TH Model is the ground surface, except in areas with thick alluvium cover, where the top of the model is the alluvium-Tiva Canyon (TCw) contact. The top boundary provides for heat, liquid and gas exchange between the modeled domain and the atmosphere. At this boundary, the gas saturation is fixed at 0.99 (to ensure two-phase conditions and avoid switching of primary variables), and the gas pressure is determined by the gas-static conditions based on the fixed pressure at the bottom boundary. This is obtained directly using the TOUGH2 simulation results at the equilibrium state with a fixed bottom pressure. The surface temperature T_s at any elevation Z is computed as constant according to the following equation (Wu et al. 1999a, p. 195–196):

$$T_s = T_{ref} - \lambda(Z - Z_{ref}) \quad (\text{Eq. 1})$$

where T_{ref} is the mean surface temperature at reference elevation Z_{ref} and λ is the dry adiabatic atmospheric lapse rate in °C/m. This lapse is 0.01°C/m (Driscoll 1986, pp. 49–51). In this model, the reference temperature is 18.23°C at an elevation of 1231.0 m. This surface temperature is determined from the mean surface temperature in boreholes NRG-6 and NRG-7a (DTN: GS950208312232.003), which had several years of continuous temperature monitoring.

6.4.2 Bottom Boundary

The water table is used as the flow boundary (in some of the submodels, it is also used as the temperature boundary). In the numerical models, elements with the first two characters “BT” represent the conditions at the water table. To specify fixed conditions at this level, these elements are assigned a very large volume and thermal capacity so that their assigned initial conditions are invariant throughout the simulations. To allow for sufficient gas mobility across the water-table boundary, we assign a fixed liquid saturation of 0.99 (to ensure two-phase conditions) to the elements representing the water table. The gas pressure is fixed at 0.92 bar, representing estimated gas pressure at the water table, derived from the reference barometric pressure at Yucca Mountain.

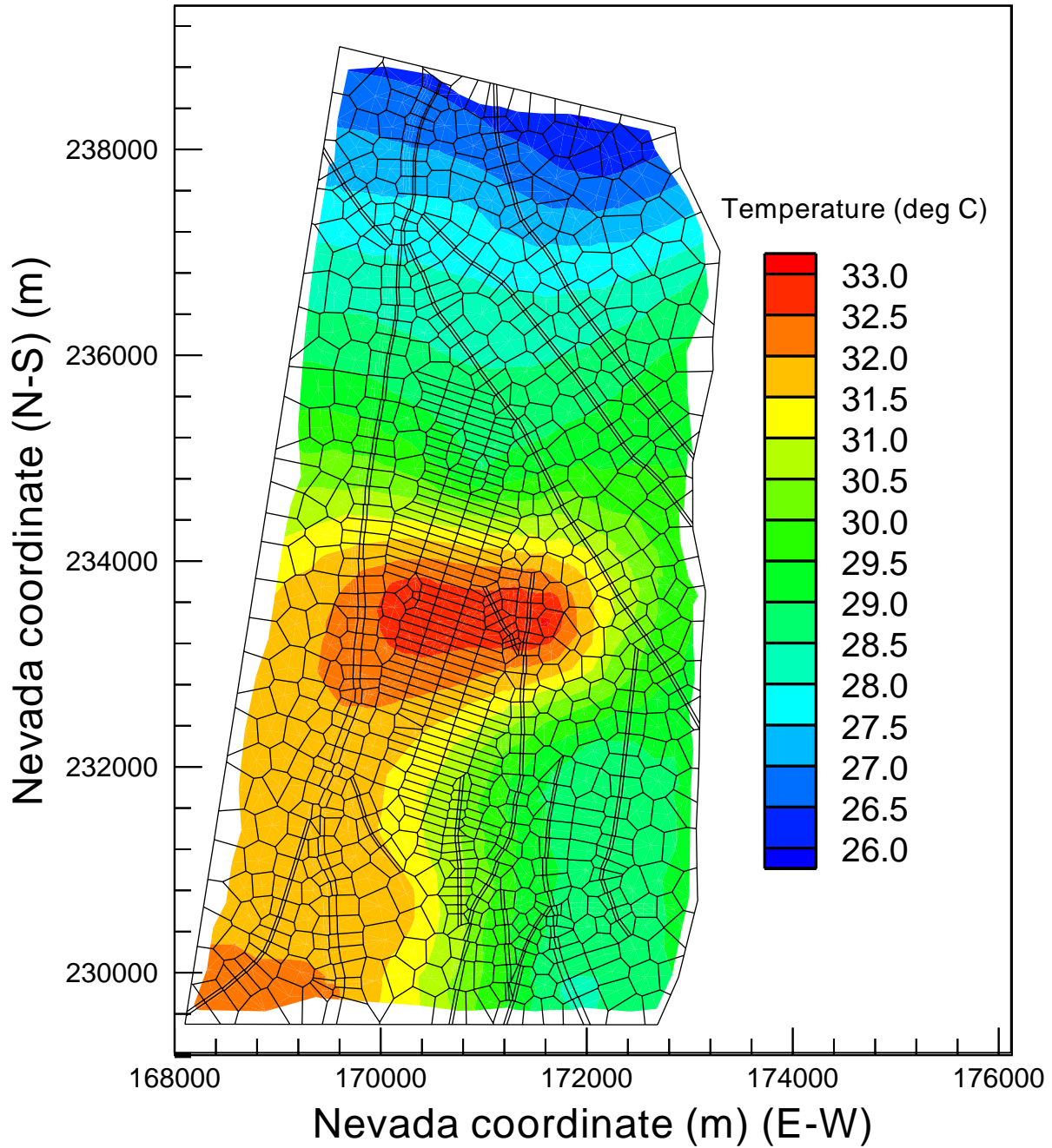
Calibrated temperature, described in a separate AMR, was used to specify the temperature at the water table boundary. This is sufficient if temperature changes at the water table resulting from

thermal load are not significant. This boundary temperature is used in the 3-D TH model (Section 6.8, Case #1). To model changes in temperature at the water table arising from thermal load, the boundary must be located away from it. In this AMR, we model temperature changes at the water table by extending the bottom temperature boundary to 1,000 m below the water table. The extended temperature boundary is used in the 3-D model case 2 (Section 6.8) and in all the 2-D TH models (Section 6.9–6.11). For the extended boundary, thermal conductivity of the boundary elements at the water table was set to zero to cut off conductive heat flow into these large-volume elements. The temperature at the extended boundary was fixed at 65°C by specifying a large volume and thermal capacity for the bottom elements in the extended boundary. This in effect nullifies any predetermined temperatures at the water table because the only fixed temperature conditions are at the top and the extended bottom boundaries. The permeability of the extended domain is set to zero, and therefore the entire fluid mass exchange is limited to the water-table boundary. Below the water table, only heat conduction is modeled.

Extending the model bottom boundary to a fixed temperature of 65°C at -270 masl (1,000 m below water table) is based on an average geothermal gradient of 35°C/km at the water table. We use this uniform temperature at this boundary and allow the re-estimation of the water-table temperatures using the prescribed boundary conditions. Steady-state simulations using extended temperature boundary conditions show that the temperature distribution at the water table is within $\pm 2^\circ\text{C}$ of the calibrated temperature distribution and is primarily controlled by the ambient infiltration and geothermal gradients. Figure 6 shows the contour plot of model temperature at the water table. This temperature distribution was used in all the simulations in which the model temperature boundary is fixed at the water table. Over the repository domain, average temperature at the water table (730 masl) is between 30 and 33°C.

6.4.3 Initial Conditions

The calibrated temperature boundary distributions, together with the specified pressure and saturation boundary conditions, were used to obtain steady-state initial conditions in each of the numerical models used. The initial conditions developed will be further discussed for the relevant models.



Based on modeling results submitted with this AMR under DTN: LB991201233129.001

Figure 6. Model Ambient Temperature Distribution (Deg C) at the Water Table, ECM Model, Mean Present-Day Infiltration.

6.5 THERMAL PROPERTIES

The thermal properties used for the different formation units for the UZ were obtained from the TDMS (DTN: LB991091233129.006) (Francis et al. 1997; Ho and Francis 1997). Table 4 summarizes the properties used in all the numerical models described in this AMR. The processes used to obtain layer-specific properties for the UZ Model grids are documented in the DTN.

Table 4. Thermal Properties for UZ Thermal Hydrology Modeling

Stratigraphic Unit		Grain density Kg/m ³	Thermal conductivity		Heat capacity J/kgK
Dual-k	ECM		Kwet W/mK	Kdry W/mK	
tcwM1	tcw11	2550.0	2.000	1.600	823.06
tcwM2	tcw12	2512.5	1.806	1.239	850.88
tcwM3	tcw13	2470.0	0.980	0.540	857.00
ptnM1	ptn21	2380.0	1.070	0.500	1037.0
ptnM2	ptn22	2340.0	0.500	0.350	1077.0
ptnM3	ptn23	2400.0	0.970	0.440	849.00
ptnM4	ptn24	2370.0	1.020	0.460	1016.0
ptnM5	ptn25	2260.0	0.820	0.350	1330.0
ptnM6	ptn 26	2370.0	0.670	0.230	1224.0
tswM1	tsw31	2510.0	1.000	0.370	834.00
tswM2	tsw32	2550.0	1.620	1.060	866.00
tswM3	tsw33	2510.0	1.683	0.790	882.50
tswM4	tsw34	2530.0	2.330	1.560	948.00
tswM5	tsw35	2540.0	2.020	1.200	900.00
tswM6	tsw36	2560.0	1.840	1.420	865.00
tswM7	tsw37	2560.0	1.840	1.420	865.00
tswM8	tsw38	2360.0	2.080	1.690	984.00
tswM9	tsw39	2360.0	2.080	1.690	984.00
ch1Mv	ch1	2310.0	1.310	0.700	1057.0
ch1Mz	ch1	2310.0	1.310	0.700	1057.0
ch1Mt	ch1	2310.0	1.310	0.700	1057.0
ch[2345]Mv	ch[2345]	2240.0	1.170	0.580	1201.0
ch[2345]Mz	ch[2345]	2350.0	1.200	0.610	1154.0
ch[2345]Mt	ch[2345]	2295.0	1.185	0.595	1177.0
ch6Mv	ch6	2440.0	1.350	0.730	1174.0

DTN: LB991091233129.006

Table 4. Thermal Properties for UZ Thermal Hydrology Modeling (Cont.)

Stratigraphic Unit		Grain density Kg/m ³	Thermal conductivity		Heat capacity J/kgK
Dual-k	ECM		Kwet W/mK	Kdry W/mK	
ch6Mz	ch6	2440.0	1.350	0.730	1174.0
ch6Mt	ch6	2440.0	1.350	0.730	1174.0
pp4Mz	pp4	2410.0	1.210	0.620	577.00
pp3Mv	pp3	2580.0	1.260	0.660	841.00
pp2Mv	pp2	2580.0	1.260	0.660	841.00
pp1Mz	pp1	2465.0	1.330	0.719	634.85
bf3Mv	bf3	2570.0	1.830	1.410	763.00
bf2Mz	bf2	2410.0	1.360	0.740	633.00
tcwMf ¹	tcwf ¹	2510.8	1.446	0.914	843.47
ptnMf ¹	ptnf ¹	2353.3	0.783	0.363	1086.4
tswMf ¹	tswf ¹	2497.8	1.736	1.002	901.89
chnMf ¹	chnf ¹	2321.7	1.230	0.630	1156.9

DTN: LB991091233129.006

Note:

¹ Thermal properties used for faults are slightly different from those submitted under the DTN. Simulations were run to confirm that these differences do not impact the TH results. This is because faults are treated as boundaries in the 3-D submodel or are defined as small thickness and are far from the potential repository. These simulations are documented in SN YMP-LBNL-GSB-1.6.3, p. 117.

The thermal properties initially assigned to the bottom boundary elements are also applied to the extended boundary zone below the water table. The thermal conductivity of the water table boundary elements is then set to zero to turn off heat conduction into this boundary. For the fracture continuum, we use a very small thermal conductivity (four orders of magnitude smaller than matrix thermal conductivity) to turn off the fracture-matrix thermal conduction. This is because the large fracture-matrix interface areas specified in the dual-k grids are for fluid flow and do not apply to heat conduction. In addition, heat conduction in global fracture-fracture connections is much smaller than matrix-matrix connections or advection through fractures in the same domain, because of the small areas of fracture-to-fracture connections in the UZ system.

6.6 INFILTRATION

The infiltration maps used for calculation of the input water recharge are documented in Scientific Notebook (DTN: GS000399991221.002) YMP-LBNL-GSB-1.1.2 (pp. 148–150). For TH modeling, we use the following climate types, which give infiltration in mm/year on Nevada State Coordinates (CRWMS M&O 1999d):

Present Day: Present-day climate, mean; This is used in the 3-D and 2-D NS#1 models, and for 0-600 years in the refined NS#2 cross section models.

Monsoon: Monsoon climate, mean; for 600-2000 years in the NS#2 cross section models.

Glacial Transition: Glacial transition climate, mean, for 2000+ years in the NS#2 cross section models.

Infiltration maps corresponding to these climates are used, together with the Infil2grid V1.6 code and the input MESH files for each numerical grid, to compute the mass source terms in “GENER,” block of the TOUGH2 V1.4 input files. The mapping of the infiltration flux onto the numerical grids is documented in Scientific Notebook YMP-LBNL-GSB-1.6.3 (p.121-122)

The infiltration flux in all these GENER files is applied as a constant mass injection of water to the fracture continuum at the top boundary of the models. For the nonisothermal numerical simulations performed here, we use a constant enthalpy of 75.6 kJ/kg corresponding to pure water at 15°C (EOS.3 Module, TOUGH2 V1.4, STN: 10007-1.4-01, Version 1.4). Note that because of proximity of the infiltration nodes to the top boundary at which temperature is held constant, the temperature in the infiltration nodes is controlled by the boundary temperature and not by temperature of the infiltrating fluid.

The accuracy with which the infiltration data is mapped onto the numerical grid depends on the grid resolution at the top boundary. The higher grid resolution used in the 2-D NS#2 grid better resolves the infiltration patterns than the coarse 3-D and 2-D NS#1 grids.

6.7 TH MODELS

Table 5 summarizes the numerical simulation scenarios performed to characterize the TH processes of mountain-scale UZ flow fields under thermal loading. The simulations employ numerical concepts, boundary conditions, and properties described in the previous sections, to model nonisothermal heat and mass transport in the UZ. In the following sections, we discuss the modeling approaches used and briefly discuss the results of each case.

Table 5. Summary of Numerical Models for Mountain-Scale TH

Model No.	Case name	Numerical Grid ^a	Infiltration	Thermal Load	Temperature Boundary
1	3-D Case 1	3-D Submodel, no drifts	Mean present day	72.7 kW/acre; no ventilation	1,000 m below the water table
2	3-D Case 2	3-D Submodel, no drifts	Mean present day	72.7 kW/acre; no ventilation	At the water table
3	NS#1 Case 1	2-D Cross Section (NS#1), no drifts	Mean present day	72.7 kW/acre; no ventilation	1,000 m below water table
4	NS#1 Case 2	2-D Cross Section (NS#1) with locally refined drifts	Mean present day	72.7 kW/acre; no ventilation	1,000 m below water table
5	NS#2 Case 1	2-D Cross Section (NS#2) with locally refined drifts	0-600 years, mean present day; 600-2000 years, mean monsoon; 2000+ years, glacial transition	72.7 kW/acre; no ventilation	1,000 m below water table
6	NS#2 Case 2	2-D Cross Section (NS#2) with locally refined drifts	0-600 years, mean present day; 600-2000 years, mean monsoon; 2000+ years, glacial transition	72.7 kW/acre; ventilation, 70% for 50 years	1,000 m below water table

NOTE: ^a DTN: LB991201233129.001

6.8 3-D UNSATURATED-ZONE POTENTIAL REPOSITORY TH SUBMODEL

6.8.1 Modeling Approach

We used the 3-D dual-k submodel to conduct two numerical studies of the effect of thermal load on the mountain-scale UZ system. The rationale for selecting this submodel has been discussed in Section 6.2 (numerical grids) and Section 6.3 (repository thermal load). The modeled cases using the 3-D submodel are 3-D Case 1 and 3-D Case 2. The only difference between these two cases is in the specification of the temperature at the bottom boundary. In the first 3-D simulation, 3-D Case 1 (base-case 3-D TH model), the temperature boundary is located at -270 masl (i.e., 1,000 m below the water table), but the bottom flow boundary is located at the water table. In the second simulation, 3-D Case 2, both the bottom temperature boundary and the bottom flow boundary are located at the water table. Both cases use a thermal load of 72.7 kW/acre, no ventilation, present-day mean infiltration and a smeared heat-source at the repository (i.e., no locally refined elements for the emplacement drifts). The simulations of the nonisothermal fluid and heat flow were conducted for a total thermal-loading period of 100,000 years. The simulation starts at time zero using steady-state initial conditions. The initial conditions were obtained by a nonisothermal EOS3 run (Pruess 1991, pp. 21–23) to steady state, using the boundary conditions defined in Section 6.4 and the present-day mean infiltration rate.

6.8.2 Results of the 3-D TH Simulations

In this section, we present and discuss the evolution of temperature, saturation, and percolation flux for the 3-D TH cases. The results of simulations are discussed using 2-D contour plots of the temperature, saturation and flux. We also present plots of the evolution of temperature, saturation and flux for the entire column at the center of the repository (location #1). For this mountain-scale model, we are interested in the extent of the thermally disturbed zone and the predicted mountain-scale changes in the temperature, saturation, and flux.

6.8.2.1 Model 1; 3-D Case 1

We present the results of this model by using plots along the NS#1 cross section and plots at selected locations. For this base-case model, we use these plots to present and discuss the changes of temperature, saturation, and flux. We also present 2-D plots of the evolution of flux at the repository horizon and at the top of the CHn unit.

Temperature

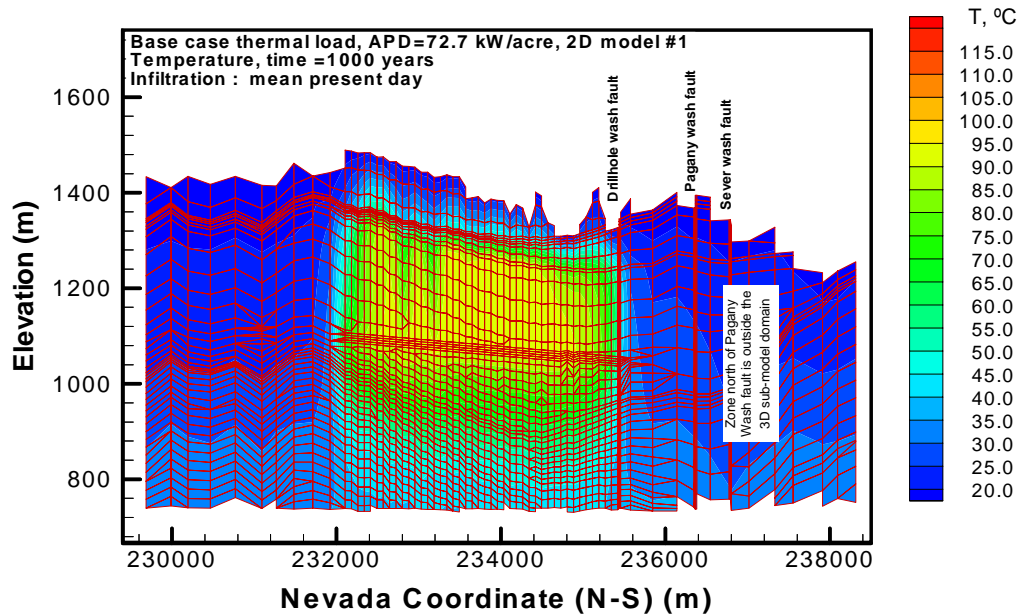
Figures 7–10 show the effects of the emplaced nuclear waste on temperature. The temperatures along cross section NS#1 at 500 and 1,000 years after emplacement are shown in Figures 7 and 8 respectively. Figures 9 show the temperatures in the column at the center of the repository (location #1). Figure 10 shows the temperatures at the repository horizon along the cross section NS#1. These plots show that extensive boiling is predicted only in the area immediately above and at the repository horizon. The 3-D model predicts that temperatures at the repository horizon will rise to boiling conditions (97°C) in about 10 years. The boiling may take place in localized horizons, with heat-pipe conditions developing and being maintained for over 100 years. Beyond 100 years, the temperatures at the repository are predicted to decline. For example, at the center

of location #1, the temperature declines from 97°C to 77°C after 2,000 years (Figure 9). The predicted temperature contours (Figures 7 and 8) show limited lateral extension of the boiling zone. In areas that are 100 m or more outside the repository, no boiling is predicted. For example, the predicted maximum temperature is 37°C 100 m outside the northern boundary and about 40°C about 100 m outside the eastern boundary. This response confirms the convection dominated processes, driven by both boiling and high fracture permeability. The ambient infiltration flux (predominantly vertical) controls the temperature outside the repository boundaries. On top of the CHn, 907 masl, the predicted maximum temperature is 70°C (see Figure 9). The 3-D model predicts little potential for temperature-induced mineralogical changes to occur within the CHn.

Saturation

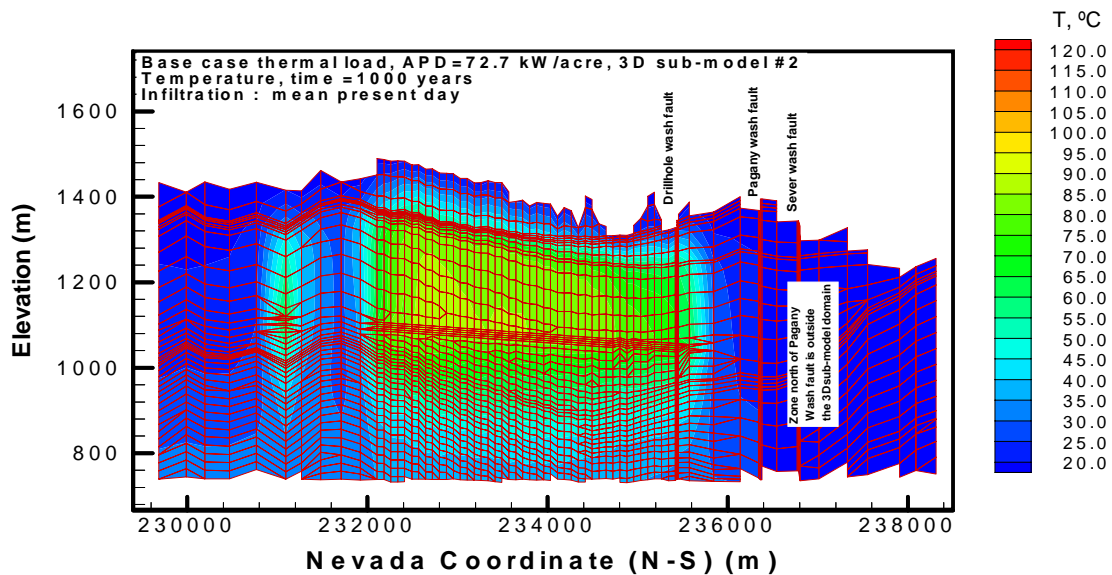
Changes in saturation are important for several reasons. They determine the period during which the repository remains dry. They are also used to assess the potential desaturation-induced changes in porosity and hydraulic conductivity (for example, in the zeolitic units). Finally, they also help identify the onset of rewetting processes and the subsequent potential for possible waste-package corrosion at the repository horizon.

Because of the coarse gridblocks used and because no explicit representation of the drifts is present, the 3-D model predicts very little change in saturation under this thermal-load scenario. Therefore, no large local mobilization of liquid and vapor exists even in those gridblocks with heat generated from the emplaced waste, except in a few columns where local ambient infiltration is low (less than 1.0 mm/year). Figures 11 through 14 show the plots of matrix liquid saturation corresponding to the temperature plots discussed above. The contour plots of the matrix liquid saturation at 500 and 1,000 years of thermal load are shown in Figures 11 and 12. Figures 13 and 14 show the corresponding matrix liquid saturation in Location #1 and at the repository horizon, respectively. The model predicts changes in matrix liquid saturation only in the vicinity of the repository horizon and only in areas of low infiltration rates. Maximum saturation changes occur within the first 100 years after thermal loading in low infiltration washes (for example, near the Drillhole Wash fault). The 3-D numerical model consequently does not predict extensive dry-out zones or zero saturation at any location within the 3-D model domain.



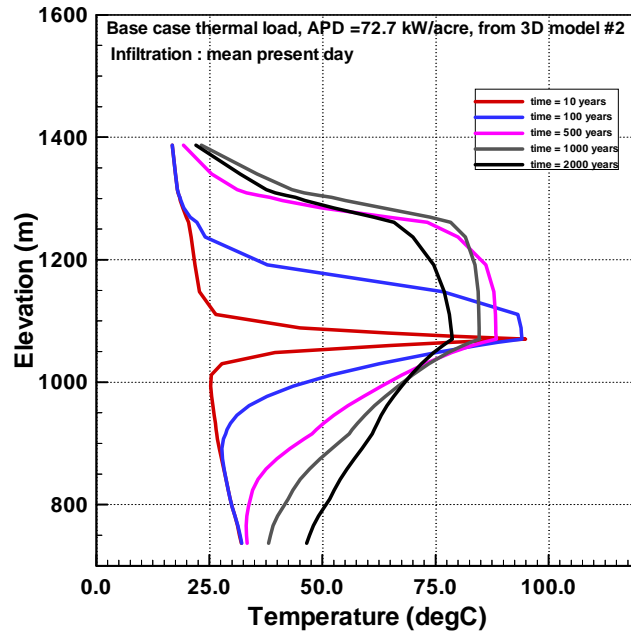
Based on modeling results submitted with this AMR under DTN: LB991201233129.001

Figure 7. Temperature Distribution along NS#1 Cross Section at 500 Years, Model 1.



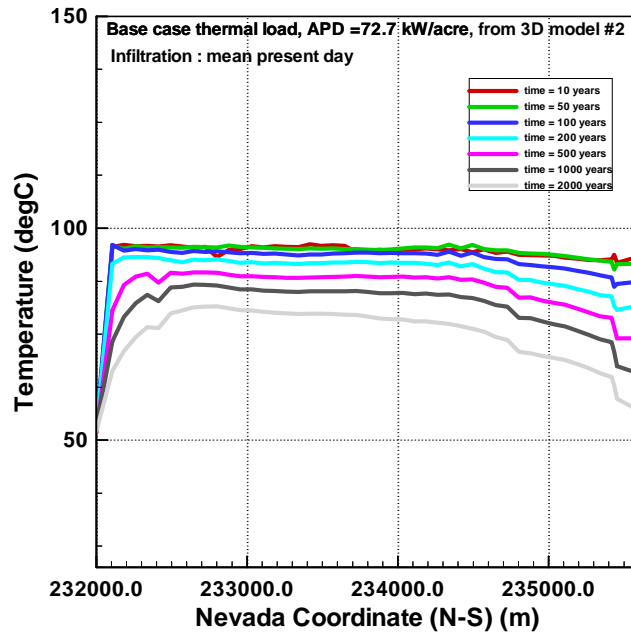
Based on modeling results submitted with this AMR under DTN: LB991201233129.001

Figure 8. Temperature Distribution along NS#1 Cross Section at 1,000 Years, Model 1.



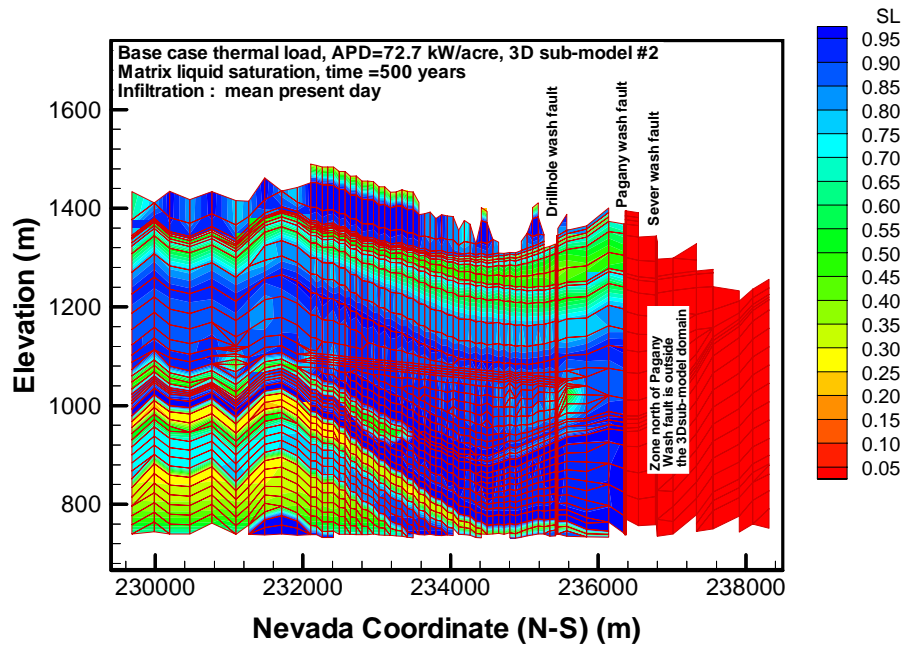
Based on modeling results submitted with this AMR under DTN: LB991201233129.001

Figure 9. Temperature at Location #1, Model 1.



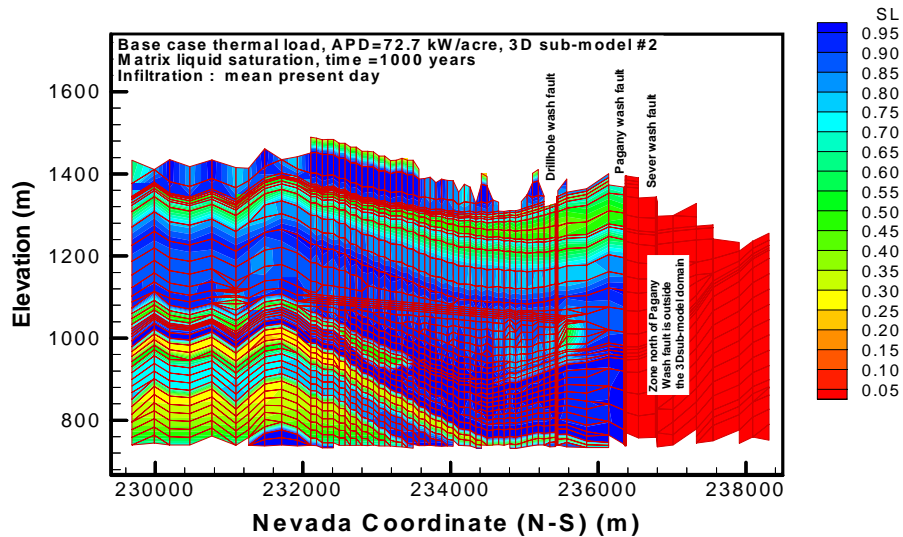
Based on modeling results submitted with this AMR under DTN: LB991201233129.001

Figure 10. Temperature along the Potential Repository at Cross Section NS#1, Model 1.



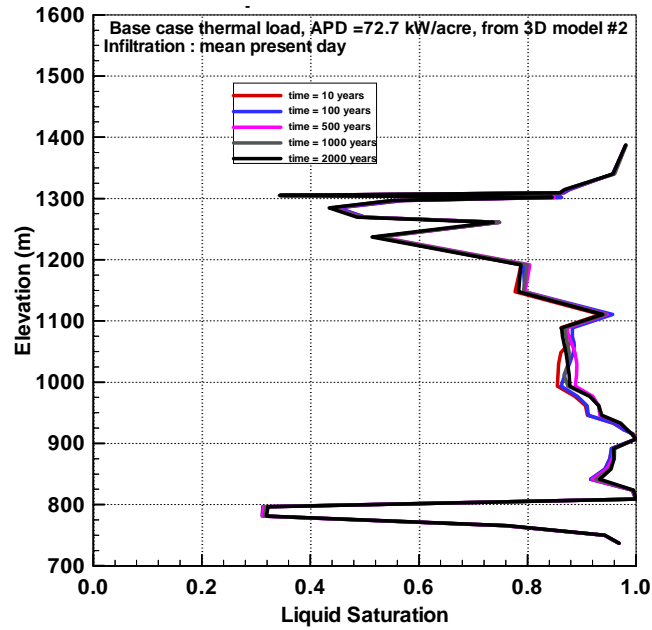
Based on modeling results submitted with this AMR under DTN: LB991201233129.001

Figure 11. Matrix Liquid Saturation (SL), along Cross Section NS#1, 500 Years, Model 1.



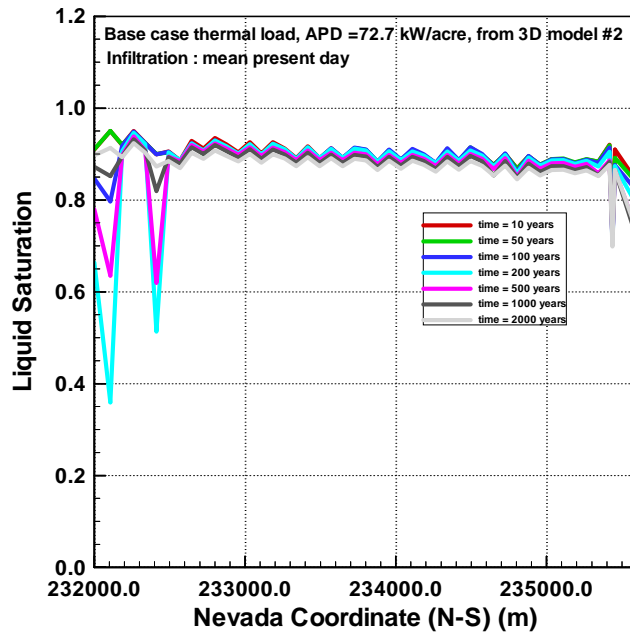
Based on modeling results submitted with this AMR under DTN: LB991201233129.001

Figure 12. Matrix Liquid Saturation (SL), along Cross Section NS#1, 1,000 Years, Model 1.



Based on modeling results submitted with this AMR under DTN: LB991201233129.001

Figure 13. Matrix Liquid Saturation at Location #1, Model 1.



Based on modeling results submitted with this AMR under DTN: LB991201233129.001

Figure 14. Matrix Liquid Saturation along the Potential Repository, at Cross Section NS#1, Model 1.

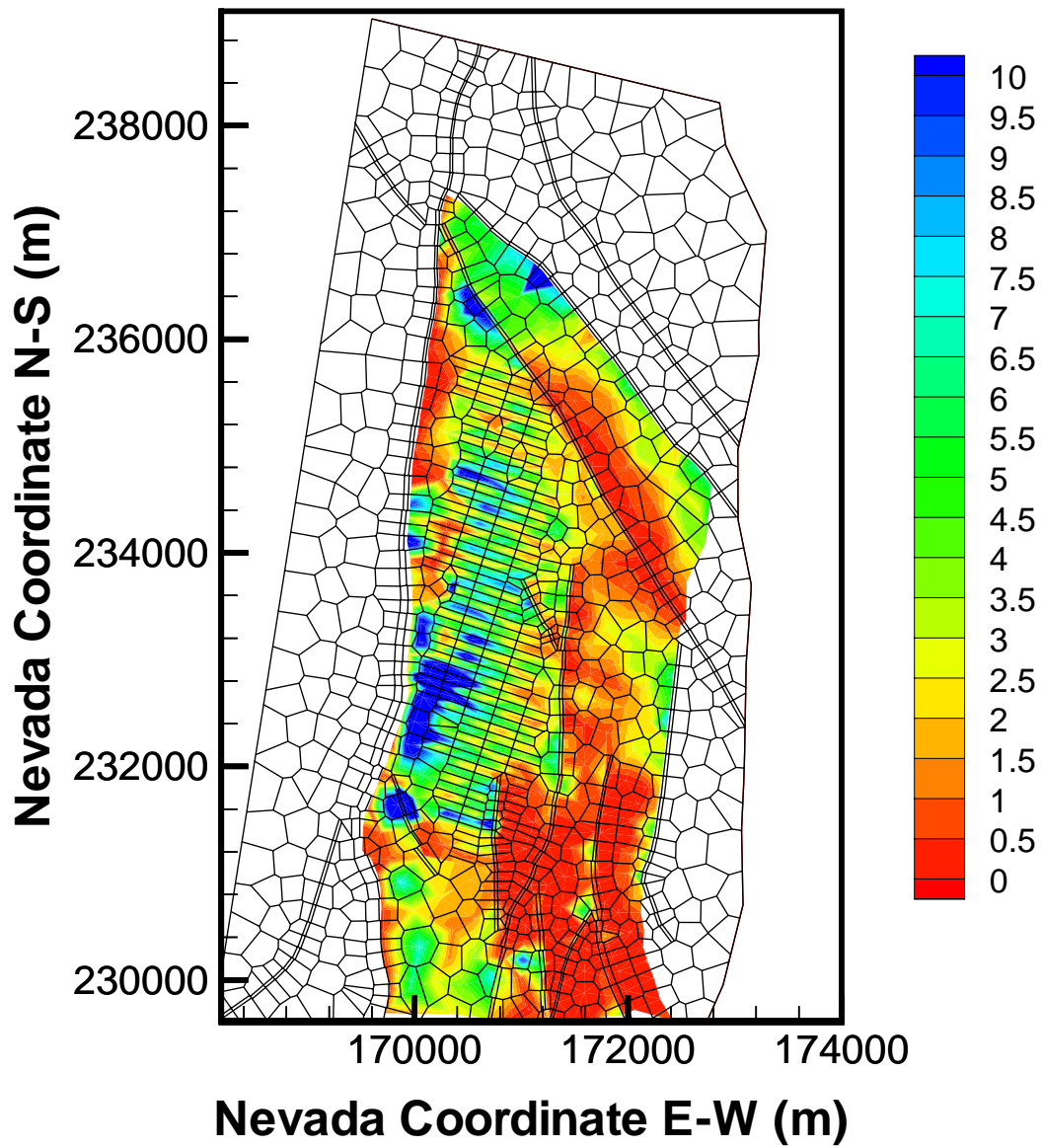
Flux

As noted above, temperature near the repository is increased significantly as a result of heat generated by the emplaced waste. As the repository temperature reaches boiling conditions (about 97°C), rapid vaporization and strong gas flow occur at the repository, which lowers liquid saturation. The lower saturation at the repository creates a sufficient capillary gradient that promotes liquid back flow towards the repository and therefore may enhance percolation fluxes in those areas.

At steady-state ambient conditions, the percolation-flux pattern at the repository is almost the same as the surface-infiltration distribution. This is because lateral flow in the Paintbrush non-welded (PTn) hydrogeologic unit that overlies the potential repository is not significant except at low infiltration areas. Analysis of the thermally induced flux evolution is performed to provide an estimate of the flux that will directly seep towards the waste package (near-field) environment under different thermal-loading and infiltration scenarios.

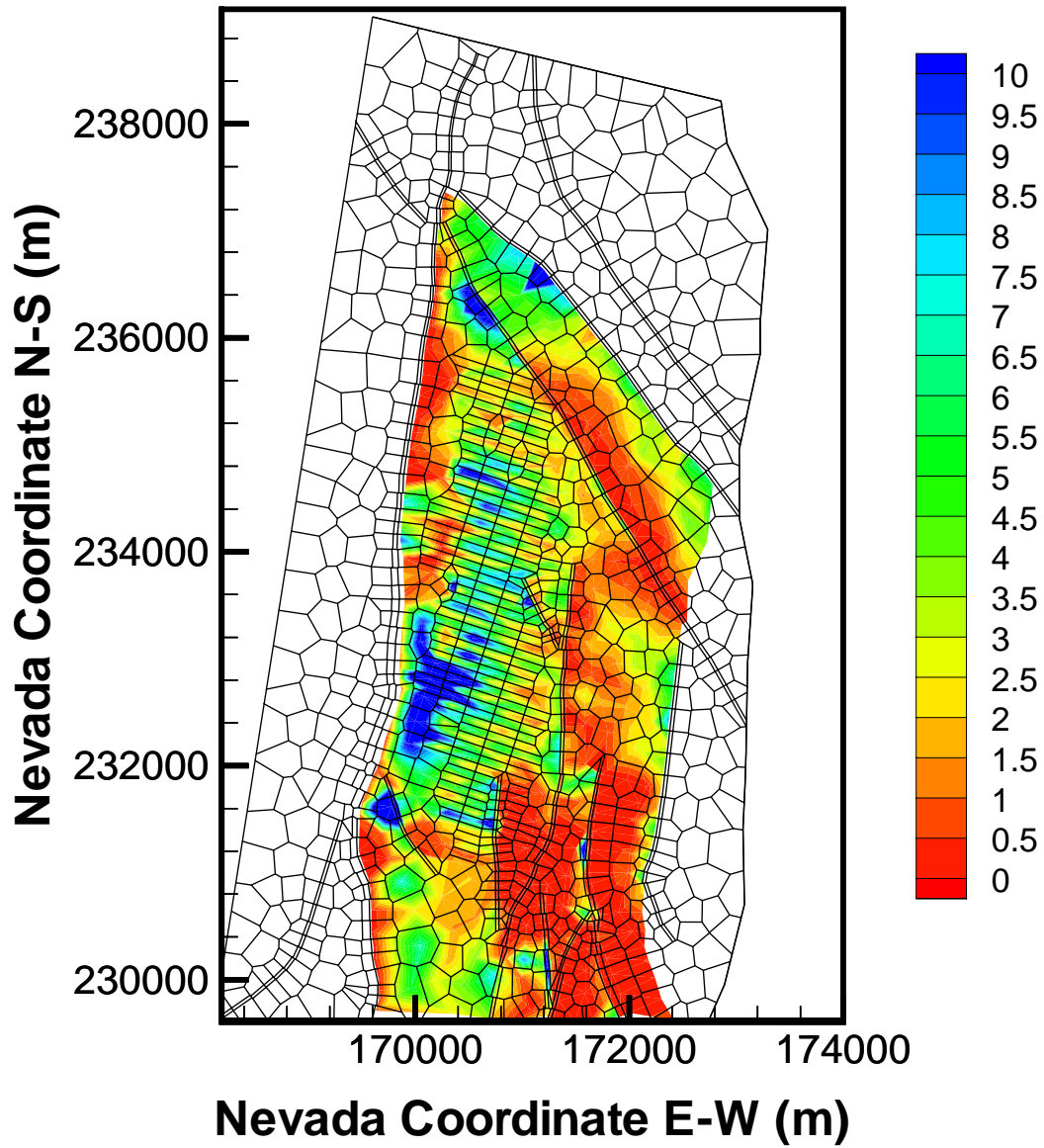
Figures 15 and 16 show the fracture flux after 1,000 years, at the repository horizon and at the top of the CHn, respectively. We present the flux as mass rate, converted to the same unit (mm/year) as the commonly used infiltration map at Yucca Mountain. Because of the continuous heat source used here, the figures show that the repository acts as a barrier to downward liquid flow, except in areas with large infiltration flux, on the Yucca Crest. Figures 17 and 18 show the evolution of flux at the center of the repository and at the repository horizon. In these figures, “positive” flow is downwards and “negative” flow is upwards. In the 2-D cross section, each column has an ambient flux determined by the infiltration map used.

The vertical flux profile through fractures at location #1 is shown in Figure 17. The percolation fluxes above the repository along the NS#1 cross section is shown in Figure 18. These flux plots can be examined in conjunction with the saturation profiles at the same locations (Figures 13 and 14). The figures show that the fracture liquid percolation flux is increased significantly at both the repository horizon and the formations below the PTn, because of changes in fracture saturation from boiling and condensation. At the center of the repository, the model predicts a maximum flux of 75 mm/year (20 times higher than the ambient flux) at 50 years. However, the flux decreases to less than 10 mm/year at 500 years and to near-ambient conditions at 1,000 years. With the coarse grid, the model cannot evaluate detailed flow towards and away from the individual drifts. Outside the repository, no significant changes in the percolation flux are predicted (Figures 15 and 16).



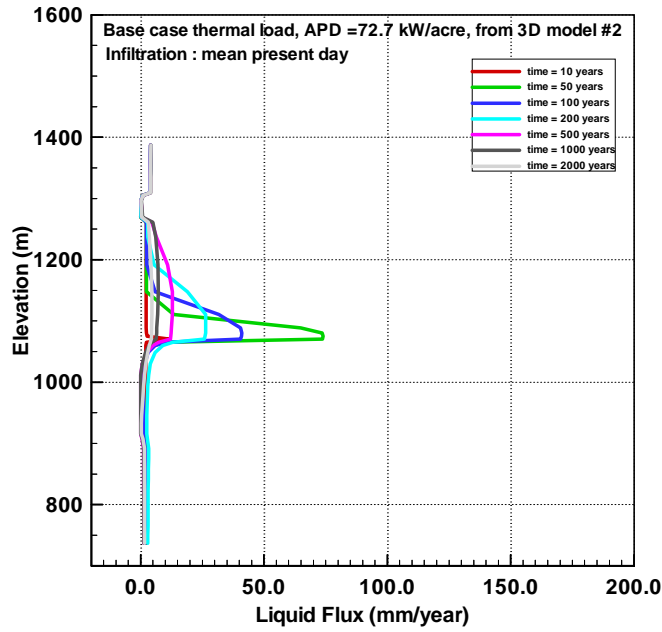
Based on modeling results submitted with this AMR under DTN: LB991201233129.001

Figure 15. Fracture Liquid Flux, at 1,000 Years, at the Potential Repository (mm/year), Model 1.



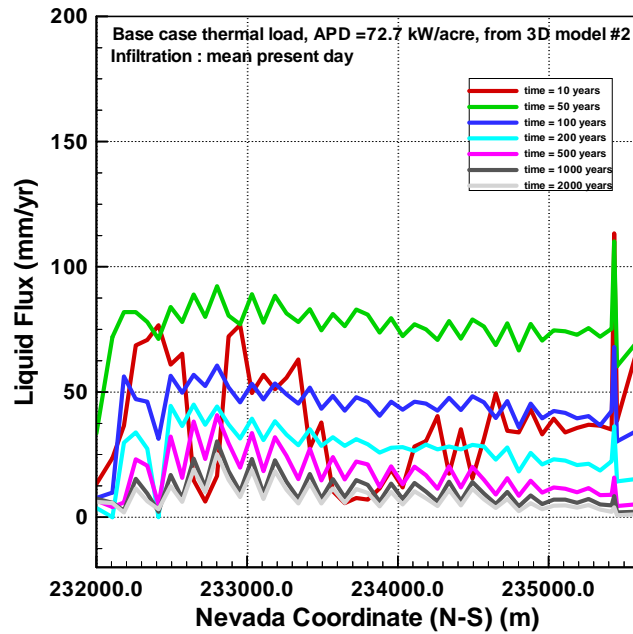
Based on modeling results submitted with this AMR under DTN: LB991201233129.001

Figure 16. Fracture Liquid Flux, at 1,000 Years, at the Top of the CHn (mm/year), Model 1



Based on modeling results submitted with this AMR under DTN: LB991201233129.001

Figure 17. Fracture Liquid Flux, at Location #1, Model 1.



Based on modeling results submitted with this AMR under DTN: LB991201233129.001

Figure 18. Fracture Liquid Flux along the Potential Repository at Cross Section NS#1, Model 1.

6.8.2.2 Model 2, 3-D Case 2

The only difference between this case and the previous case is in the location of the bottom temperature boundary. In this model, the temperature boundary is fixed at the water table. Temperature distribution at this boundary is determined from the calibrated temperature distribution for the UZ 3-D model domain at ambient conditions. The rest of the modeling approach is the same as discussed above. We present the results of the 3-D model using 2-D and 1-D plots of the evolution of temperature and saturation. Because there is little difference in saturation between this case and the previous one, there are no significant differences in predicted percolation flux.

Temperature

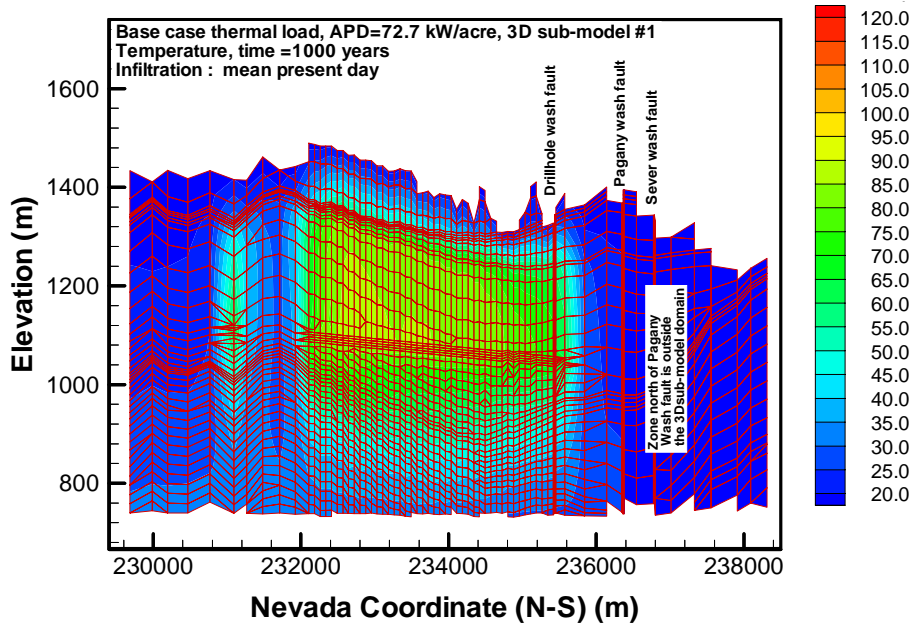
Figure 19 shows the predicted temperature contours along the NS#1 Cross Section after 1,000 years of thermal load. The predicted temperature contours above the repository are nearly the same as in the previous case. Below the repository, the temperature contours are strongly influenced by the fixed temperature boundary at the water table. Figures 20 and 21 show the same vertical profile at the center of the repository and temperature at the repository horizon, respectively. The figures again show that major differences occur only below the repository.

Saturation

Figure 22 shows the corresponding contour plot of liquid saturation along the same cross section. Because most of the changes in liquid saturation are occurring near the repository, the figure is nearly identical to the saturation plots shown in Figure 12.

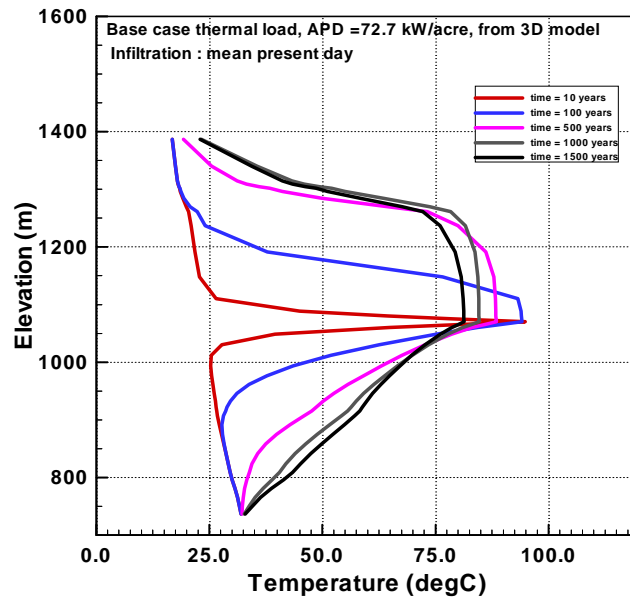
Flux

Changes in saturations lead to changes in capillary pressure gradients, which will change liquid percolation flux. On the other hand, percolation flux is not significantly affected by local variation of temperature if boiling does not take place. Based on the results of this model, the location of the temperature boundary at the water table has little influence on the TH behavior near the repository. This is because boiling zones generated at the repository are small and far away from the bottom temperature boundary.



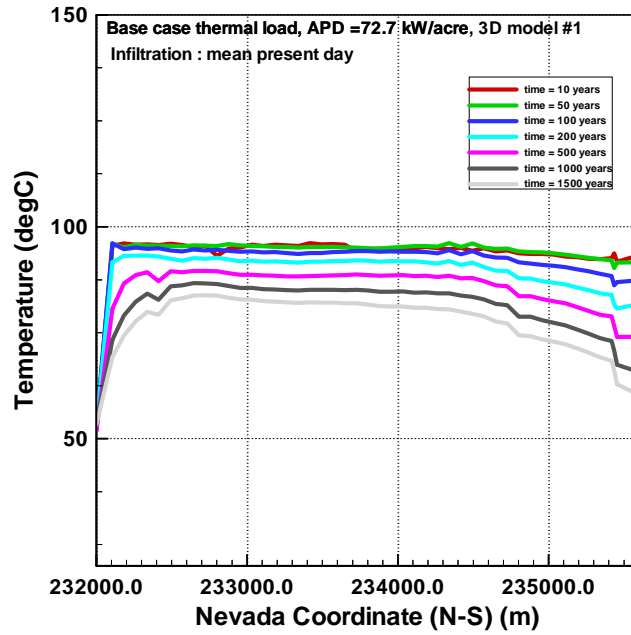
Based on modeling results submitted with this AMR under DTN: LB991201233129.001

Figure 19. Temperature Distribution along NS#1 Cross Section at 1,000 Years, Model 2.



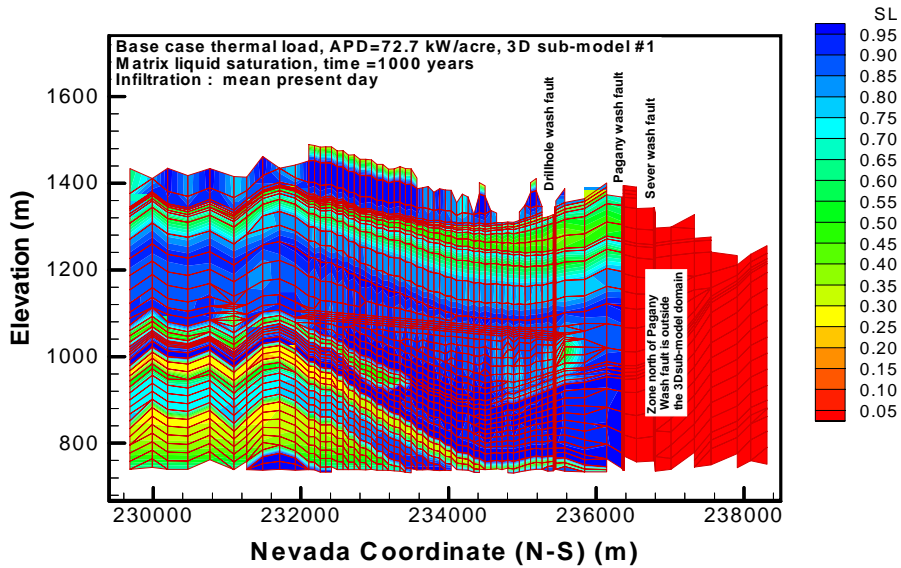
Based on modeling results submitted with this AMR under DTN: LB991201233129.001

Figure 20. Temperature at Location #1, Model 2.



Based on modeling results submitted with this AMR under DTN: LB991201233129.001

Figure 21. Temperature along the Potential Repository Horizon at Cross Section NS#1, Model 2.



Based on modeling results submitted with this AMR under DTN: LB991201233129.001

Figure 22. Matrix Liquid Saturation along Cross Section NS#1, 1,000 Years, Model 2.

6.9 2-D UNSATURATED ZONE TH SIMULATIONS

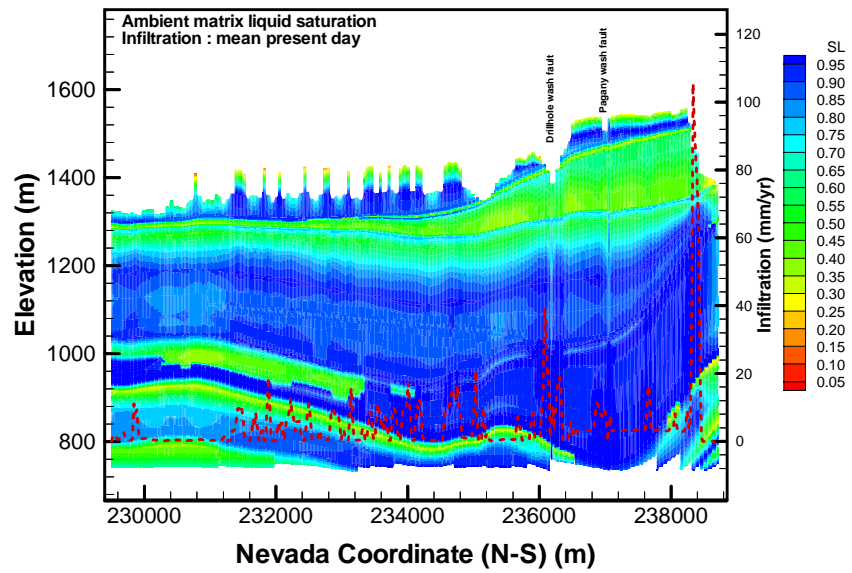
6.9.1 Modeling Approach

We use the 2-D dual-k models to conduct four studies of the effect of repository thermal load on the near- and far-field repository environment. Simulations with these 2-D models are easier to perform computationally compared to full 3-D simulation. We use these models to determine if the mountain-scale 3-D TH processes can be quickly and efficiently predicted by representative 2-D submodel cross sections, which are directly extracted from the 3-D model. We also use the 2-D models to investigate the sensitivity of the TH predictions to the numerical grid resolution using a refined grid model.

Table 5 (in Section 6.7) includes a summary the studies conducted using the 2-D cross section submodels. We use Cross Sections NS#1 and NS#2 (Section 6.3), to conduct these studies.

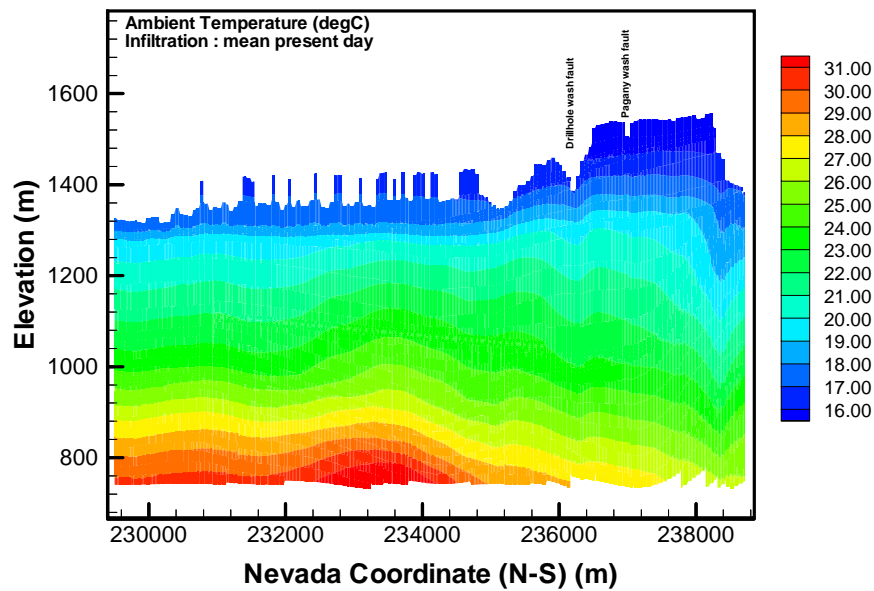
6.9.2 2-D Ambient Conditions

For each of the 2-D models, steady-state model ambient conditions were generated and used as initial conditions for the TH calculations. Since the initial conditions for all the models are identical, we show the results only for the 2-D refined grid model. Figure 23 shows the ambient matrix saturation using the refined NS#2 grid. The mean present-day infiltration (in mm/year) is superimposed on the plot of ambient saturation. The figure shows a large variability in infiltration, from 0 mm/year to over 100 mm/year along this section. The distribution of saturation is controlled by the formation properties as well as by this distribution of infiltration rate. Figure 24 shows the corresponding initial temperature distribution. The temperature distribution is strongly related to the infiltration and the specified boundary temperatures. The definition of the boundary conditions used in these models was discussed in Section 6.4



Based on modeling results submitted with this AMR under DTN: LB991201233129.001

Figure 23. Ambient Matrix Liquid Saturation along Cross Section NS#2. Dotted lines show the distribution of infiltration (mm/year) along the cross section.



Based on modeling results submitted with this AMR under DTN: LB991201233129.001

Figure 24. Ambient Temperature (deg C) along Cross Section NS#2.

6.10 RESULTS OF THE 2-D TH SIMULATIONS AT CROSS SECTION NS#1

We conducted two studies using the NS#1 grid that was directly extracted from the 3-D UZ grid. The results of 2-D models can be compared with the 3-D results discussed in the previous section to examine the significance 3-D effects and the need local refinement at the repository. Both cases use an extended bottom temperature boundary 1,000 m below the water table. For Case 1, we use the mean present-day infiltration rate, 72.7 kW/acre thermal load, no ventilation and a smeared heat source. The simulation was conducted primarily to evaluate 3-D effects by comparing the results of the 2-D TH models with those for the 3-D TH model, as discussed in Section 6.8.1. The second model (NS#1 Case 2) uses the same thermal load, infiltration, and boundary conditions, but also uses a modified locally refined numerical grid described in Section 6.3.3 (Figure 4) to model discrete heat sources at the drifts.

6.10.1 Model 3, NS#1 Case 1

The 2-D grid used for this model is a relatively coarse grid, with the lateral grid spacing equal to the drift spacing (81 m) over the repository horizon. The thermal load is described as a smeared heat source because there is no explicit representation of drifts (i.e., no local refinement).

Temperature

The temperatures along the entire cross section at 1,000 years after waste emplacement are shown in Figure 25. Figure 26 shows the temperatures at location #1 at the center of the repository. Figure 27 shows the temperatures along the repository horizon of the cross section. The plots show that extensive boiling is predicted only in the area at and immediately above the repository horizon, with boiling conditions (97°C) occurring in about 10 years. This 2-D model predicts the same maximum temperature at the repository horizon as the 3-D model. However, because there is no lateral heat conduction across the model into a third dimension, the model predicts less cooling and a larger heat-pipe zone (Figures 25 and 26). The thermally affected zone extends to the base of the PTn (see Figure 2 for the location of the repository and the PTn unit). Beyond 100 years, the modeled temperatures at the repository begin to decline. After 2,000 years, the predicted temperature at the repository is 92°C, compared to 77°C from the 3-D model. The predicted temperature contours (Figure 25) show limited lateral expansion of the boiling zone outside the repository domain. This result confirms the convection-dominated processes, as predicted using the 3-D model. The percolation flux (predominantly vertical) controls the temperature outside the repository boundaries. On top of the CHn, (elevation 900 m, Figure 26) we predict a maximum temperature of about 70°C. These temperature changes in the CHn units make it unlikely that significant thermal-mineralogical alterations of rock properties occur within the CHn unit.

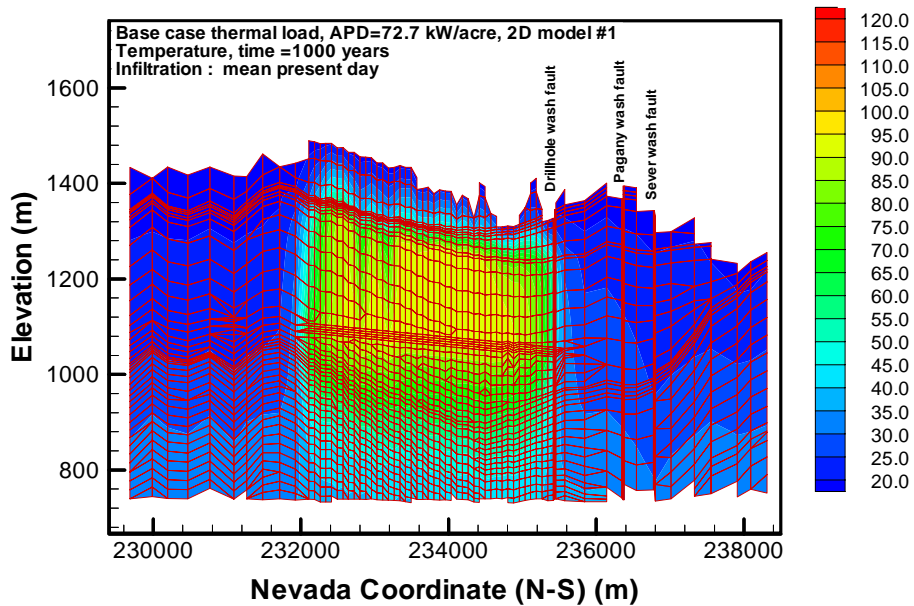
Saturation

Figures 28 to 30 show the plots of matrix liquid saturation corresponding to the temperature plots for the same locations, respectively, as discussed above. The contour plot of the matrix liquid saturation after 1,000 years of thermal loading is shown in Figure 28. The plot shows significant changes in matrix liquid saturation only at or near the repository. Figures 29 and 30 show the corresponding matrix liquid saturation in Column #1 and at the repository horizon, respectively.

The model predicts larger changes in matrix liquid saturation in the vicinity of the repository horizon than those in the 3-D model. Again, however, no complete dry-out regions are predicted (Figure 30). At several locations along the repository, the predicted liquid saturation declines to less than 30%. Under the low-infiltration zones, maximum saturation changes occur during the first 200 years of thermal loading. Beyond 200 years, the saturation recovers. Near-ambient liquid-saturation conditions are re-established after 2,000 years.

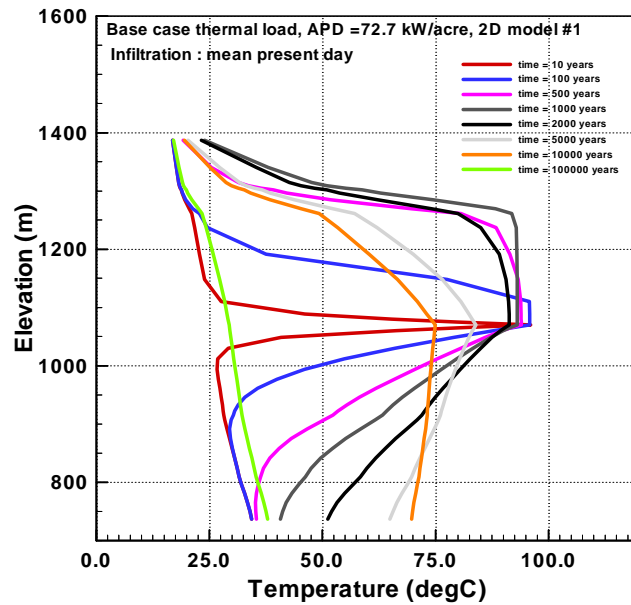
Flux

Figures 31 and 32 show distributions of the simulated flux at the center of the repository and at the repository horizon. Although the figures show a little larger variability in flux than that predicted by the 3-D model, the magnitude and pattern of the fluxes, as indicated by the two models, are similar. The figures show that under thermal load, the repository acts as a barrier to downward liquid flow except in areas under large surface infiltration. The vertical flux profile (Figure 31) shows the maximum flux is still about 75 mm/year after 50 years, which declines to near ambient conditions at 1,000 years. Using the 2-D model, we predict significant increases in percolation flux predominantly in the region between the PTn unit and the repository.



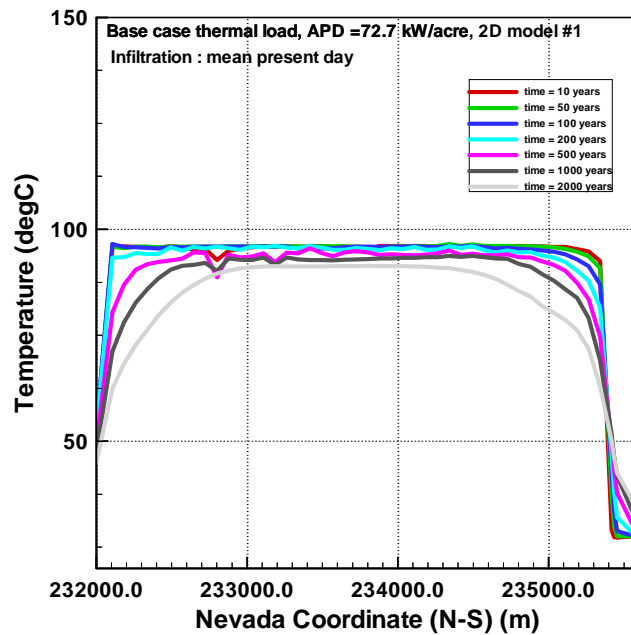
Based on modeling results submitted with this AMR under DTN: LB991201233129.001

Figure 25. Temperature Distribution along NS#1 Cross Section of Grid at 1,000 Years, Model 3.



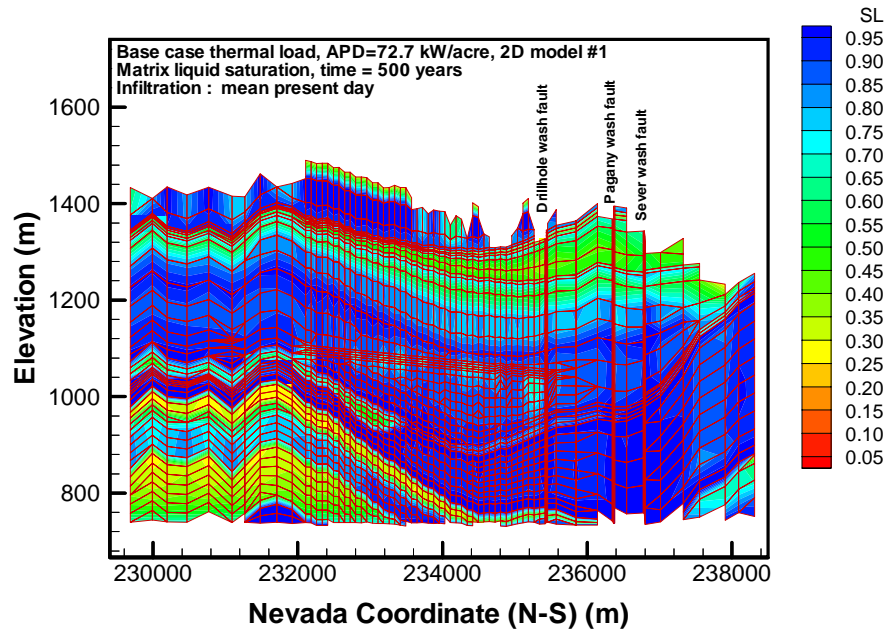
Based on modeling results submitted with this AMR under DTN: LB991201233129.001

Figure 26. Temperature at Location #1, Model 3.



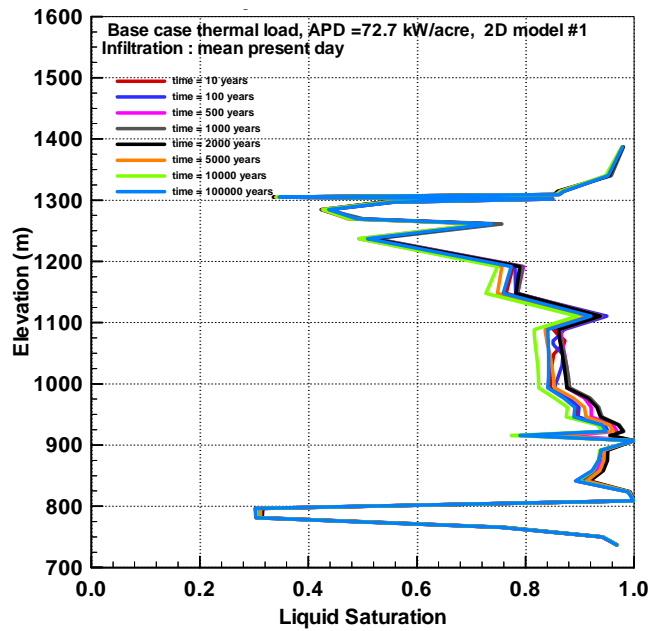
Based on modeling results submitted with this AMR under DTN: LB991201233129.001

Figure 27. Temperature along the Potential Repository Horizon, Model 3.



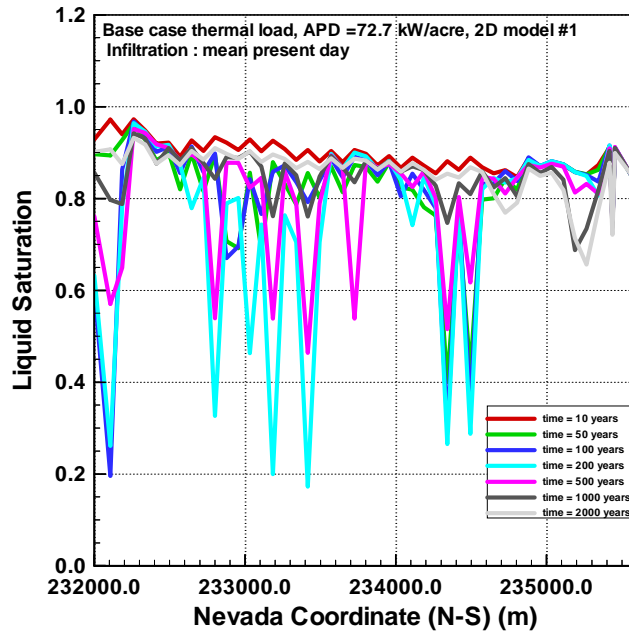
Based on modeling results submitted with this AMR under DTN: LB991201233129.001

Figure 28. Matrix Liquid Saturation along NS#1 Grid at 1,000 Years, Model 3



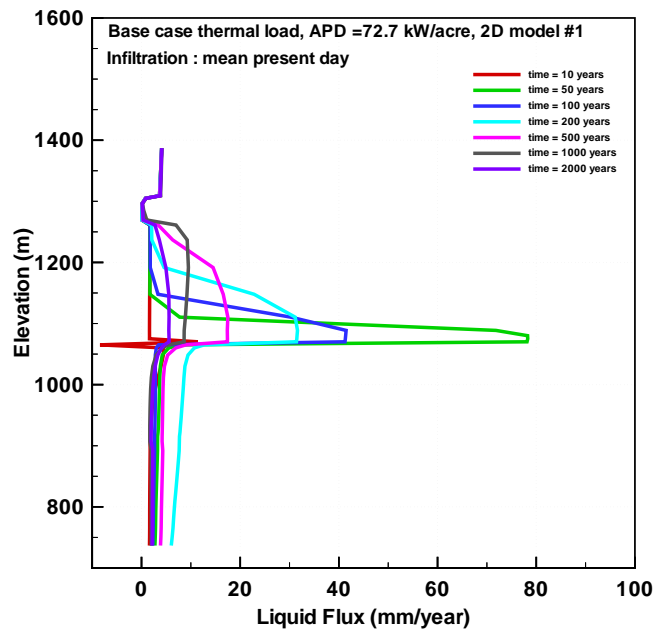
Based on modeling results submitted with this AMR under DTN: LB991201233129.001

Figure 29. Matrix Liquid Saturation at Location #1, Model 3.



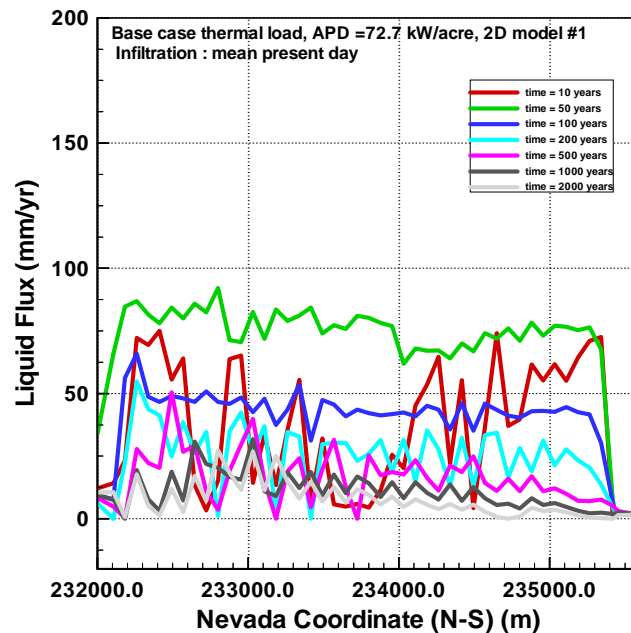
Based on modeling results submitted with this AMR under DTN: LB991201233129.001

Figure 30. Matrix Liquid Saturation along the Potential Repository, Model 3



Based on modeling results submitted with this AMR under DTN: LB991201233129.001

Figure 31. Fracture Liquid Flux at Location #1, Model 3



Based on modeling results submitted with this AMR under DTN: LB991201233129.001

Figure 32. Fracture Liquid Flux along the Potential Repository, Model 3.

6.10.2 Model 4, NS#1 Case 2

This case is almost the same as NS#1 Case 1, except that the grid is modified to model a discrete heat source (drift-by-drift model). This model uses the coarse grid NS#1 with a locally refined 5 m drift element at the repository within each drift column. This provides a model for estimating temperature, saturation, and flux at the repository because it has two elements between the drift elements in the numerical grid. This simple model provides an assessment of the adequacy of such a scheme for resolving the near-drift conditions under thermal loading. We discuss the results of this model using 2-D and 1-D plots of temperature, saturation, and flux.

Temperature

Figures 33 and 34 show the predicted temperature contours along the entire NS#1 cross section after 500 and 1,000 years of thermal load, respectively. The figures show that boiling conditions occur mainly above the repository. The predicted temperature contours above the repository at later times are nearly the same as in the previous case. Figure 35 shows the profiles of location #1 at the center of the repository. Within this column, the predicted temperatures at the repository exceed 103°C after 50 years compared to 97°C for the model without explicit representation of the drifts. At the repository (Figure 36), we predict local peaks where temperatures exceed 150°C in completely dried-out zones. Once boiling is established, the resulting temperature variation is the same as for the nonrefined case except for local peaks at the repository. Beyond 500 years, temperatures begin to decline. Temperatures at the repository decline to 90°C after 2,000 years. Temperatures at a lateral distance of 100 m or more outside the repository remain at near ambient conditions. However, because there is no lateral heat conduction of the model into a third dimension, this 2-D model may also overestimate thermal

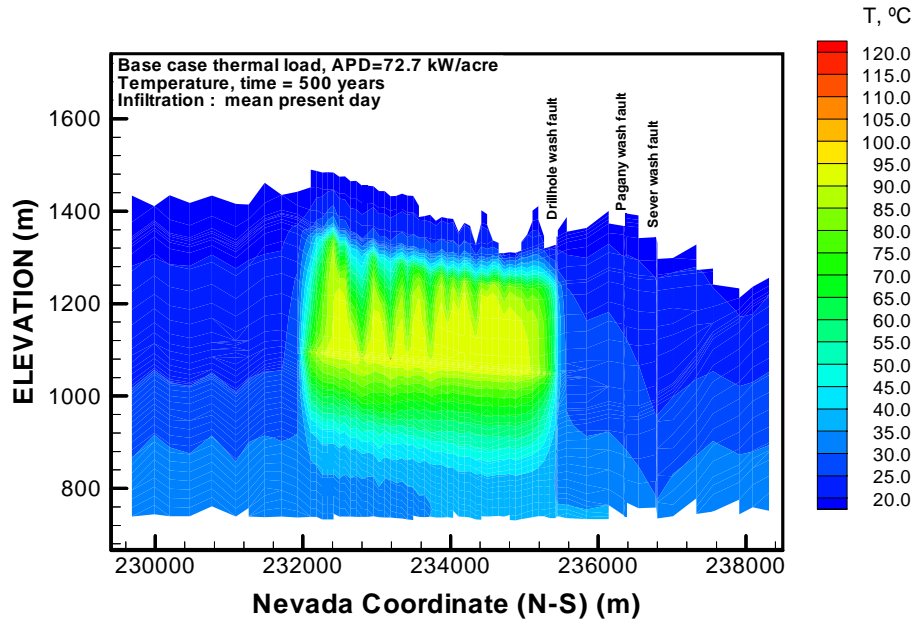
buildup compared to the 3-D case. At the water table, the predicted maximum temperature is about 70°C.

Saturation

Figures 37 to 40 show the plots of matrix liquid saturation corresponding to the temperature plots for the same locations as discussed above. The contour plots of the matrix liquid saturation at 500 and 1,000 years of thermal loading are shown in Figures 37 and 38. The plots show significant changes in matrix liquid saturation only near the repository. Figures 39 and 40 show the corresponding matrix liquid saturation at location #1 and at the repository horizon, respectively. Significant decreases in matrix liquid saturation are simulated in the vicinity of the drifts. However, only a few matrix elements in the drifts become completely dry (Figure 40) between 100 and 500 years. Note that all fractures at the repository are completely dry within the first few years of thermal loading.

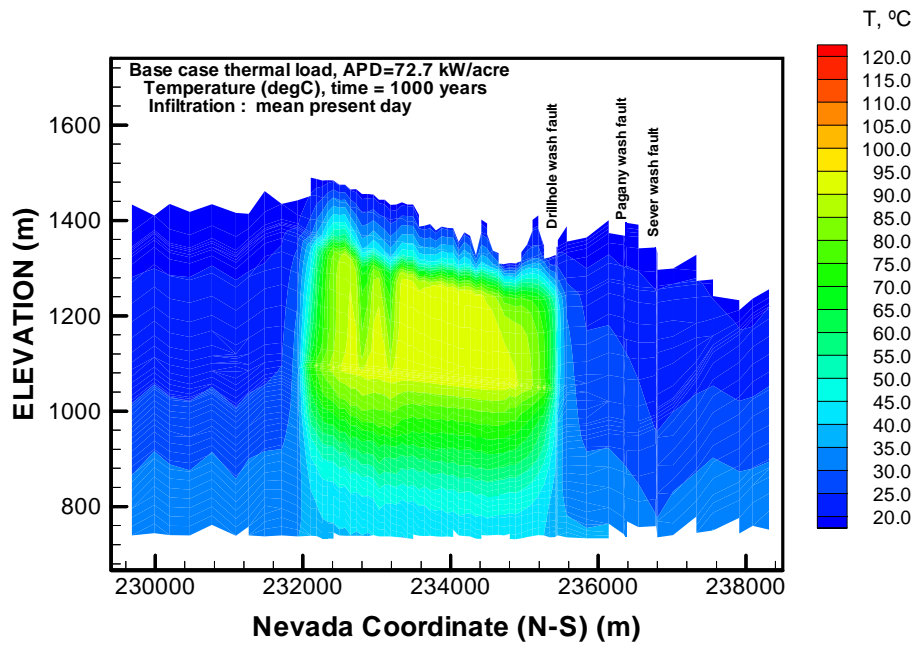
Flux

Figures 41 to 43 show the simulated fluxes through the fracture continua at the center of the repository and along the repository horizon respectively. Because of high capillary suction forces created within the dry zones, the models predict much higher fluxes in the vicinity of the drifts than predicted by the nondiscrete heat-source models discussed above. The vertical-flux profile (Figure 41) shows that the maximum flux exceeds 200 mm/year after five years and declines to less than 30 mm/year after 100 years. The liquid flux at repository horizon (Figure 42) indicates that liquid flux from fractures towards drifts quickly rises to 1,000–1,250 mm/year after 10 years, but drops to zero as the fractures become completely dry. This large flux is confined to the near-field environment and results from the large capillary pressure gradient between the nearly dry drift and the surrounding layers. This liquid flux does not seep into the drifts because the intense heat within the drifts, during this early period of thermal loading, vaporizes all the liquid. Figure 43 shows the matrix liquid flux at the repository for the same period. The matrix liquid flux rises to a maximum of 100–200 mm/year at the drifts, but stays at ambient conditions in the regions between the drifts.



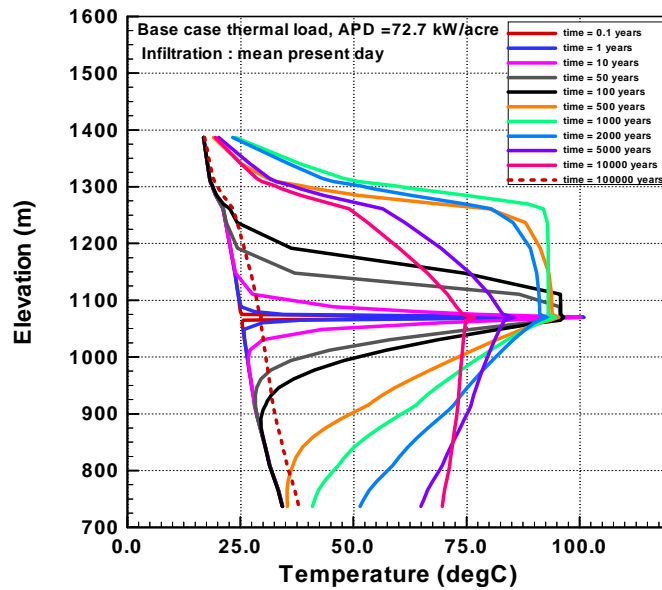
Based on modeling results submitted with this AMR under DTN: LB991201233129.001

Figure 33. Temperature Distribution along NS#1 Grid at 500 Years, Model 4.



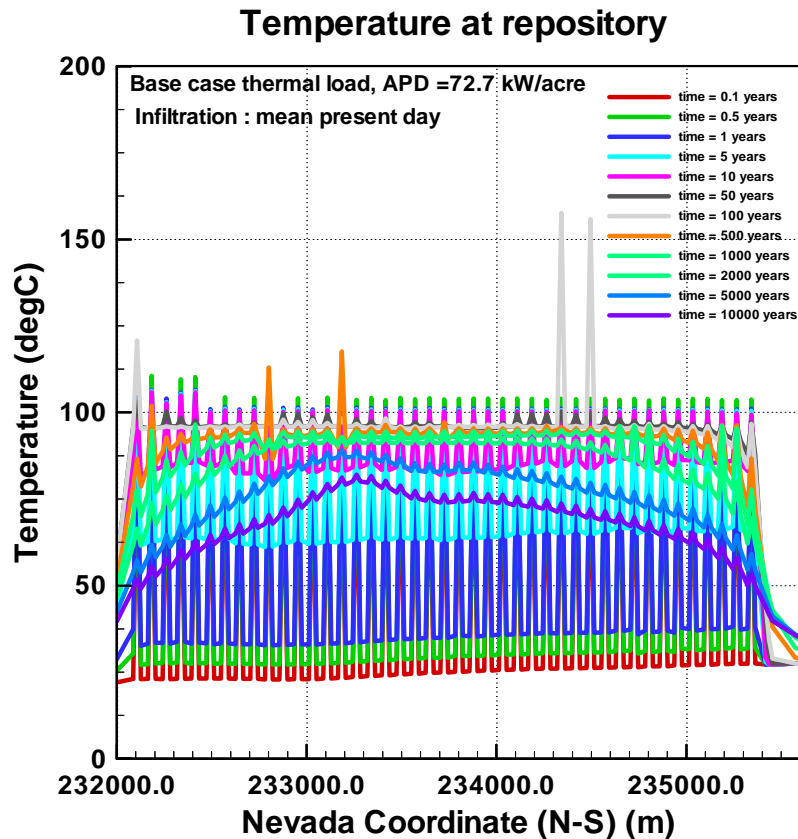
Based on modeling results submitted with this AMR under DTN: LB991201233129.001

Figure 34. Temperature Distribution along NS#1 Grid at 1,000 Years, Model 4.



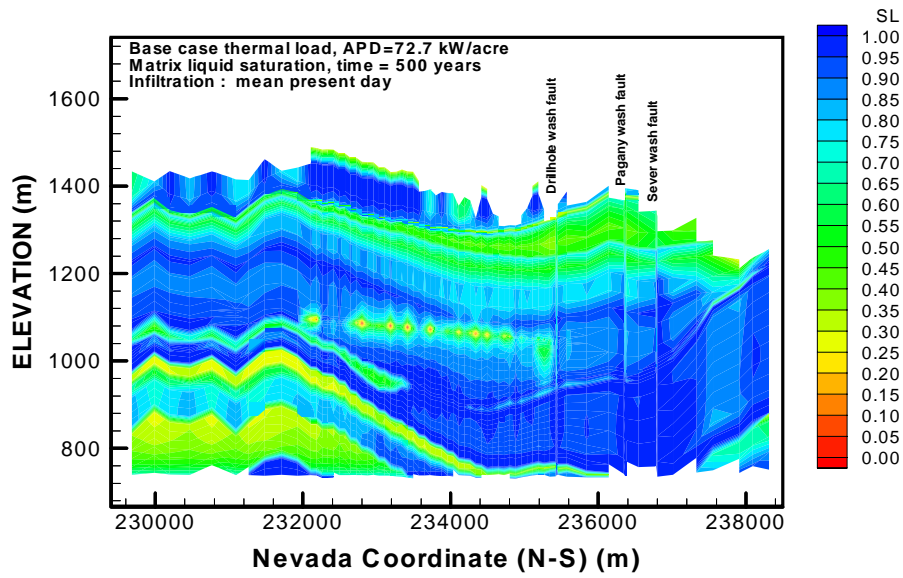
Based on modeling results submitted with this AMR under DTN: LB991201233129.001

Figure 35. Temperature at Location #1, Model 4.



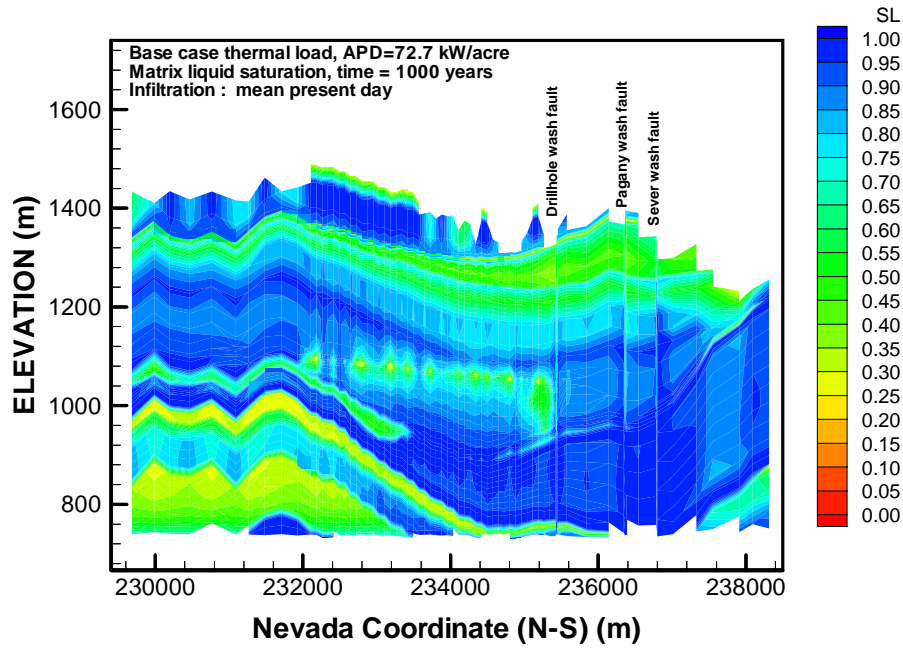
Based on modeling results submitted with this AMR under DTN: LB991201233129.001

Figure 36. Temperature along the Potential Repository Horizon, Model 4.



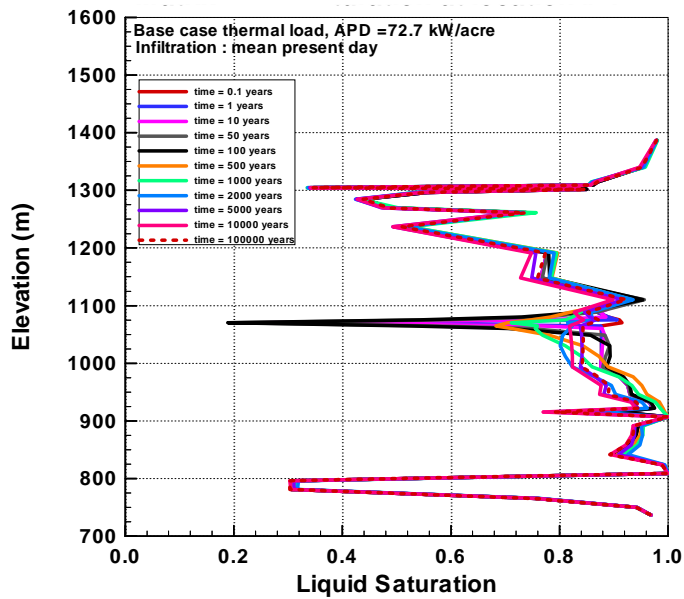
Based on modeling results submitted with this AMR under DTN: LB991201233129.001

Figure 37. Matrix Liquid Saturation (SL) along NS#1 Grid at 500 Years, Model 4.



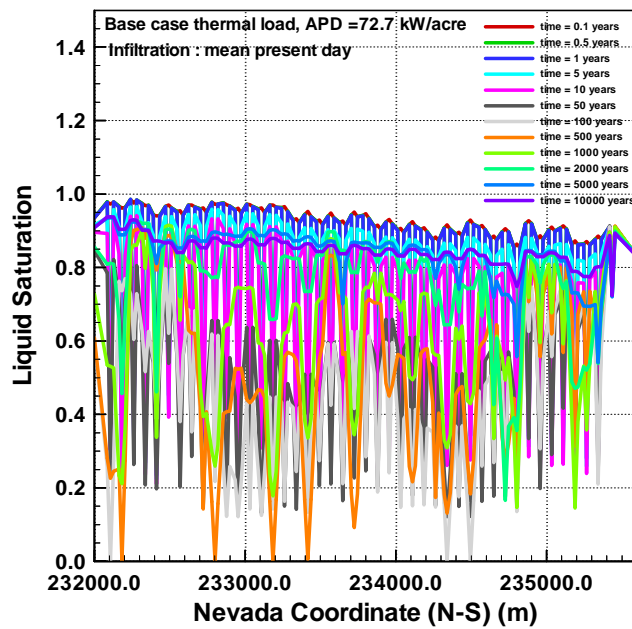
Based on modeling results submitted with this AMR under DTN: LB991201233129.001

Figure 38. Matrix Liquid Saturation (SL) along NS#1 Grid at 1,000 Years, Model 4.



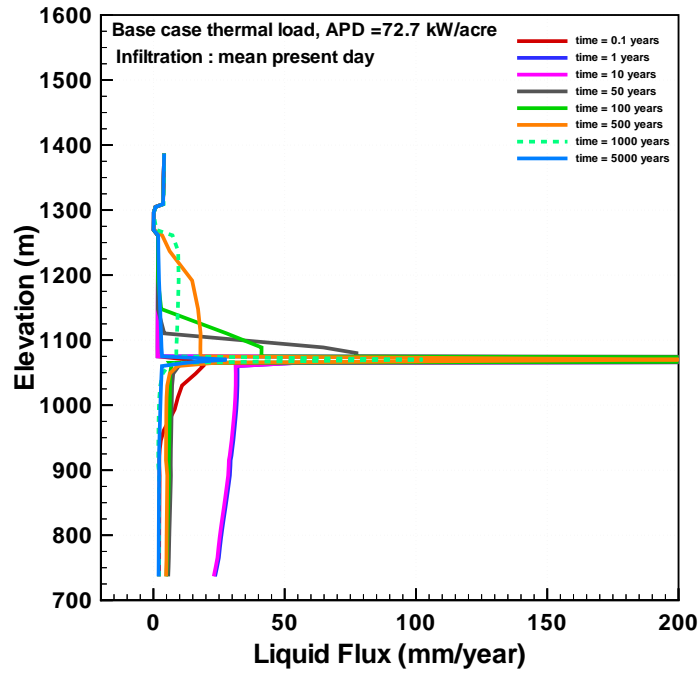
Based on modeling results submitted with this AMR under DTN: LB991201233129.001

Figure 39. Matrix Liquid Saturation at Location #1, Model 4.



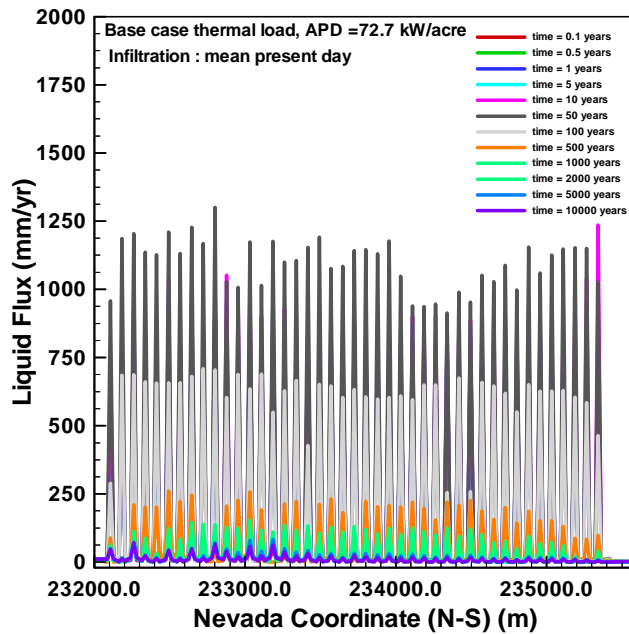
Based on modeling results submitted with this AMR under DTN: LB991201233129.001

Figure 40. Matrix Liquid Saturation along the Potential Repository Horizon, Model 4.



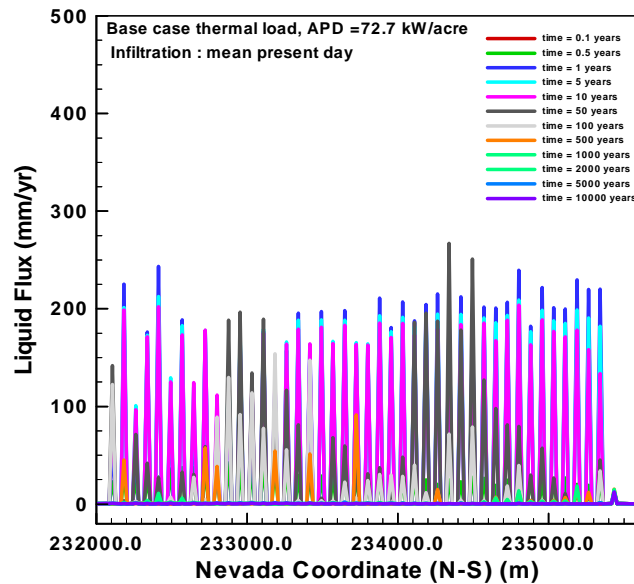
Based on modeling results submitted with this AMR under DTN: LB991201233129.001

Figure 41. Fracture Liquid Flux at Location #1, Model 4.



Based on modeling results submitted with this AMR under DTN: LB991201233129.001

Figure 42. Fracture Liquid Flux along the Potential Repository Horizon, Model 4.



Based on modeling results submitted with this AMR under DTN: LB991201233129.001

Figure 43. Matrix Liquid Flux along the Potential Repository Horizon, Model 4.

6.11 RESULTS OF THE 2-D TH SIMULATIONS AT CROSS SECTION NS#2

In this section, we present and discuss the results of two simulations using the refined north-south numerical grid at Cross Section NS#2. All the simulations with this grid use a locally refined node at the repository to represent the drift (discrete heat source), and the temperature boundary is set at 1,000 m below the water table. In the two models, we also implement changes in infiltration resulting from possible variation in climate over the thermal-loading period. We use mean present-day infiltration for 0–600 years, then mean monsoon climate infiltration for 600–2,000 years, and finally mean glacial transition climate infiltration for the rest of the thermal load period (2,000–100,000 years). The first model, NS#2 Case 1, uses 72.7 kW/acre thermal load, with no ventilation. The second model, NS#2 Case 2, uses the same model parameters as the NS#2 Case 1, but implements a 70% reduction in repository heat. This is the proportion of heat that is removed by ventilation for 50 years.

6.11.1 Model 5, NS#2 Case 1

This model uses a refined 2-D numerical grid, with lateral grid spacing at Cross Section NS#2 equal to one-fourth of the drift spacing. The grid has a locally refined 5 m wide drift element within each drift column (Section 6.3). Thermal loading is 72.7 kW/acre with no ventilation, and we supply the TOUGH2 code with a three-step infiltration rate using the three climates over the thermal-load period as mentioned above.

Temperature

Figures 44 and 45 show temperature contours after 500 and 1,000 years along the entire cross section. The predicted temperature contours show limited lateral extension of the boiling zone outside the repository domain. The results of the two figures again show that the TH processes at and near the repository are convection dominated. Surface infiltration rates have a large impact on temperature outside the repository domain. Figure 46 shows the evolution of temperature within a drift-column (Location #1) at the center of the repository. Temperature in an adjacent column (Location #2) is shown in Figure 47. Location #2 is at a distance of about 21.4 m from Location #1, but separated from it by an 8.2 m locally refined element of the drift column (refer to Section 6.3). The model predicts that local temperature within the drift could rise to over 250°C as both the matrix and the fracture elements of the drift become completely dry. A two-phase boiling zone at 97°C develops and expands to about 50 m above the repository after 500 years. This zone expands to 200 m above the repository between 1,000 to 2,000 years. At the pillars between the drifts, temperatures rise only to boiling conditions.

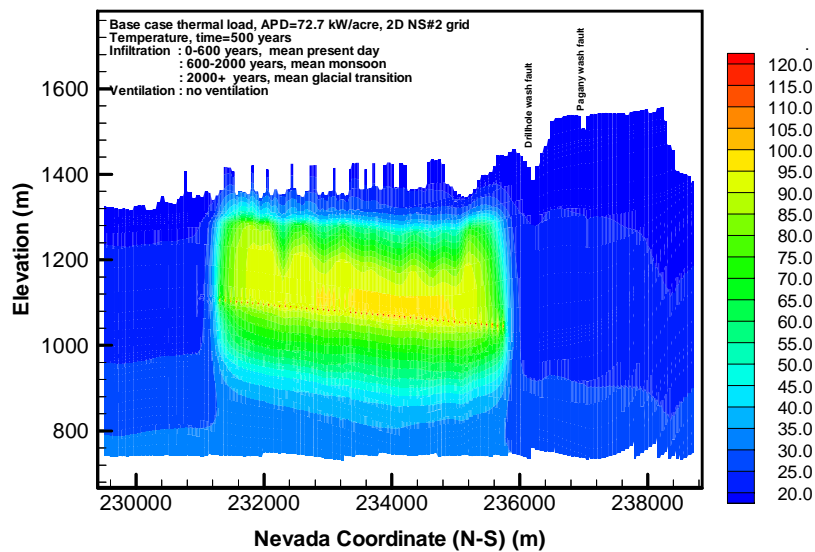
Figure 48 shows the temperature distribution along the repository horizon of this cross section. The temperatures at the repository horizon rise to above boiling conditions (97°C) between 10 and 50 years. Although most of the drifts are at 100°C at ten years, the temperatures rise to over 260°C in the completely dry drifts at the north end of the repository, where the surface infiltration rate is nearly zero. At 50 years, the temperatures in all the drifts reach 210–235°C. At this period, the minimum temperature between the drifts is only 80–85°C. Beyond 50 years, the temperatures at the repository decline rapidly as a result of strong rewetting by strong capillary suction in the near-field environment. After 100 years, temperatures within the drifts are still 160–180°C, and temperatures at the entire repository horizon (except at the ends) remain at or above boiling conditions. After 400 years, the temperature range of the drifts is 120–135°C over the entire repository horizon. However, as discussed in the previous models, use of a 2-D model may overestimate elevated temperature compared with a 3-D model, which may partly account for the higher predicted temperatures.

Saturation

Figures 49 to 52 show the plots of matrix liquid saturation corresponding to the temperature plots discussed above. Contour plots of the matrix liquid saturation at 500 and 1,000 years of thermal loading are shown in Figures 49 and 50 respectively. The plots show large changes in matrix liquid saturation only near the repository. Note that all fractures at the repository are completely dry within the first few years of thermal loading. Figures 51 and 52 show the matrix liquid saturation in Column #1 and at the repository horizon, respectively, for the same periods. Similarly, significant changes in matrix liquid saturation occur only near the drifts. The model predicts completely dry conditions (Figures 51 and 52) for all the drifts between 10 and 50 years. Both the matrix and the fracture continuum at the drifts remain dry as the repository heat immediately vaporizes any liquid flowing towards the drifts. The matrix liquid saturation between the drifts drops to a minimum of 40% after 400 years. Liquid saturation outside the repository remains at near-ambient conditions.

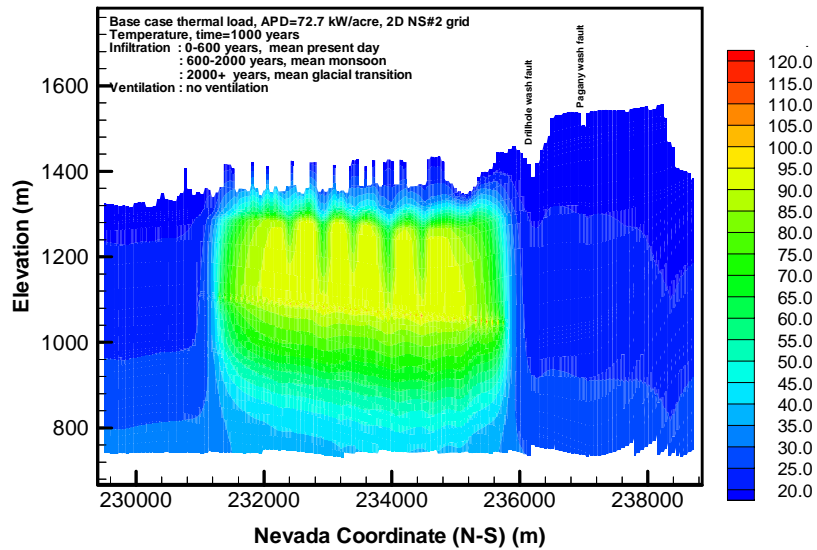
Flux

Figures 53 to 57 show the fluxes simulated at the center of the repository and along the repository horizon. Because of an extensive drying zone developed at the repository, the model predicts much higher percolation fluxes in the vicinity of the drifts than predicted by the 3-D coarse grid and the 2-D NS#1 grid models. The vertical flux profile at Location #1 (Figure 53) shows that the maximum flux towards the drifts exceeds 400 mm/year at 5 years, but declines to less than 30 mm/year at 400 years. Note that flux at Location #1 is calculated based on the entire column area. At the repository, a drift (see Section 6.3) represents each column. To get the apparent flux towards the drift, we need to multiply the drift flux by the ratio of column area to drift area ($21.39/5.0 = 4.3$). This is the liquid flux pattern at the top of the repository horizon plotted in Figures 54 through 57. The figures show that liquid flux through the fractures towards the drifts rises to between 1250–1600 mm/year after 10 years, but drops to zero as the fracture continua at and above the drifts become completely dry. The fracture liquid flux in the pillars between the drifts also increases during this period because of the decrease in liquid saturation within the fracture continua at the repository horizon. After 500 years, the average fracture liquid flux between drifts is about 20 mm/year, about 5 times higher than the ambient flux. Figures 56 and 57 show the corresponding matrix liquid flux at the top of the repository horizon at the same times. The matrix liquid flux rises to a maximum of 400–450 mm/year at the drifts, but stays at ambient conditions between the drifts. As the matrix continuum of the drifts becomes completely dry, this liquid flux also drops to zero (Figure 57).



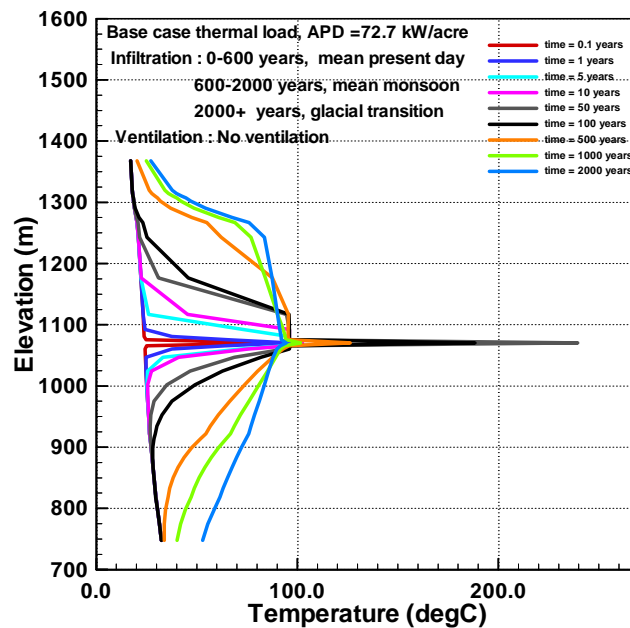
Based on modeling results submitted with this AMR under DTN: LB991201233129.001

Figure 44. Temperature Distribution along NS#2 Grid at 500 Years, Model 5.



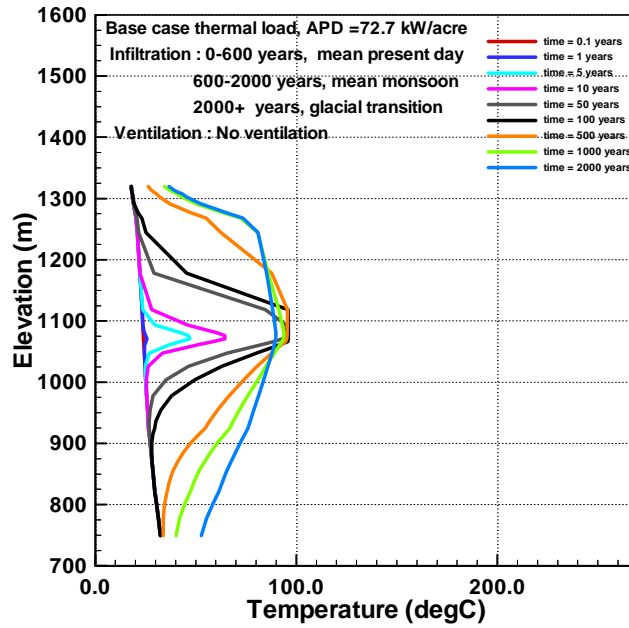
Based on modeling results submitted with this AMR under DTN: LB991201233129.001

Figure 45. Temperature Distribution along NS#2 Grid at 1,000 Years, Model 5.



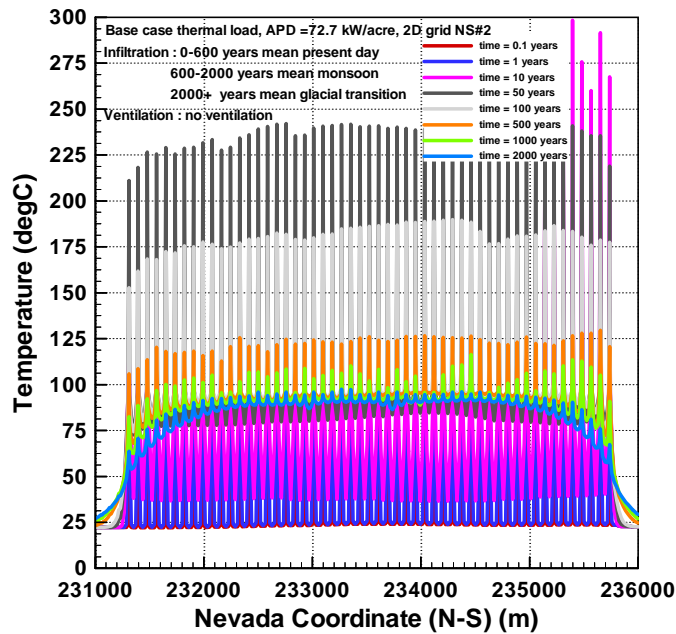
Based on modeling results submitted with this AMR under DTN: LB991201233129.001

Figure 46. Temperature at Location #1, NS#2 Grid, Model 5.



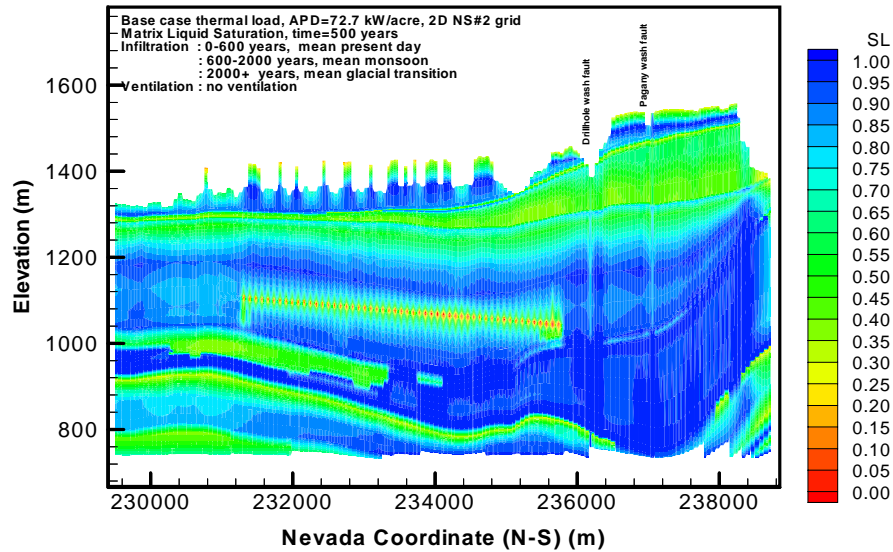
Based on modeling results submitted with this AMR under DTN: LB991201233129.001

Figure 47. Temperature at Location #2, NS#2 Grid, Model 5.



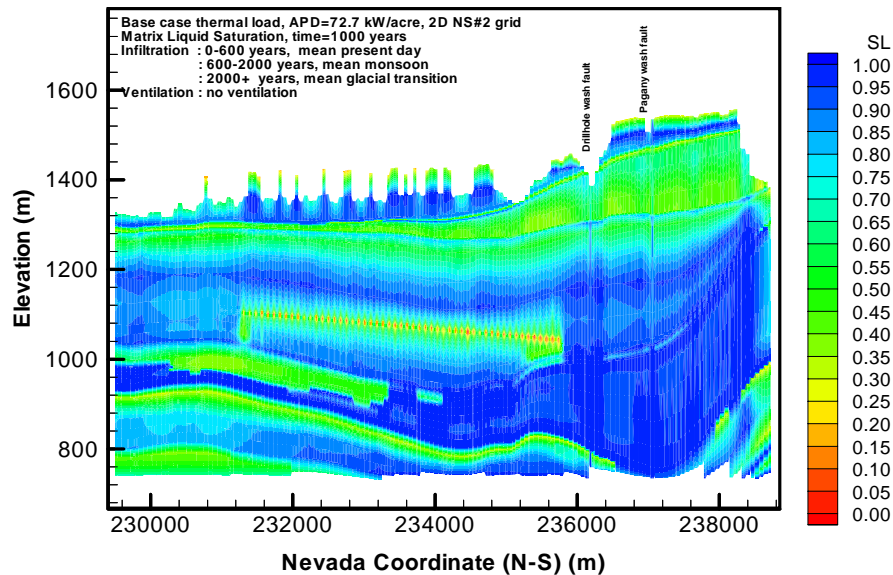
Based on modeling results submitted with this AMR under DTN: LB991201233129.001

Figure 48. Temperature along the Potential Repository Horizon NS#2 Grid, Model 5.



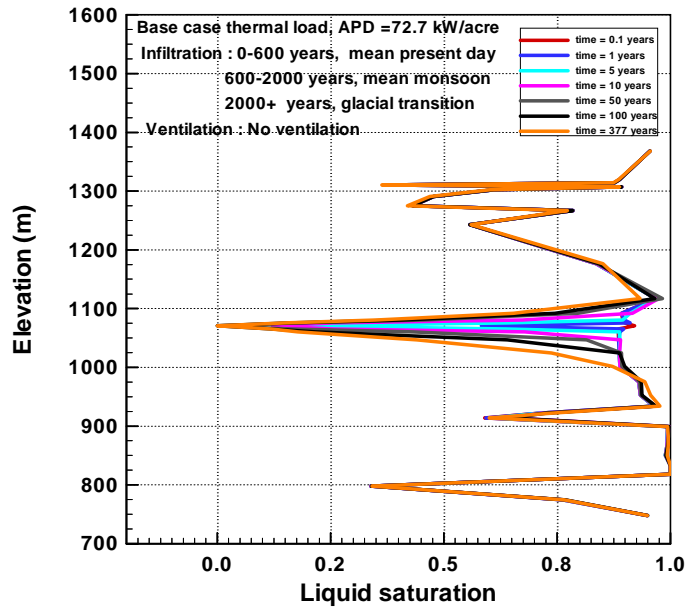
Based on modeling results submitted with this AMR under DTN: LB991201233129.001

Figure 49. Matrix Liquid Saturation (SL) along NS#2 Grid at 500 Years, Model 5.



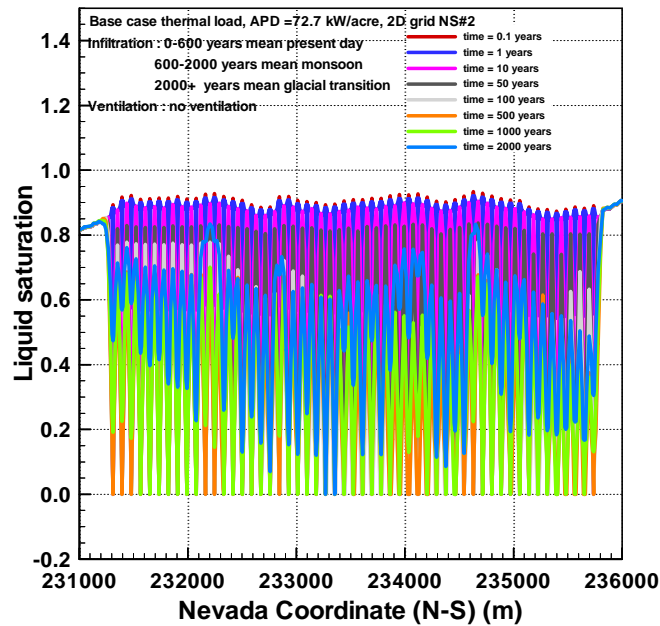
Based on modeling results submitted with this AMR under DTN: LB991201233129.001

Figure 50. Matrix Liquid Saturation (SL) along NS#2 Grid at 1,000 Years, Model 5.



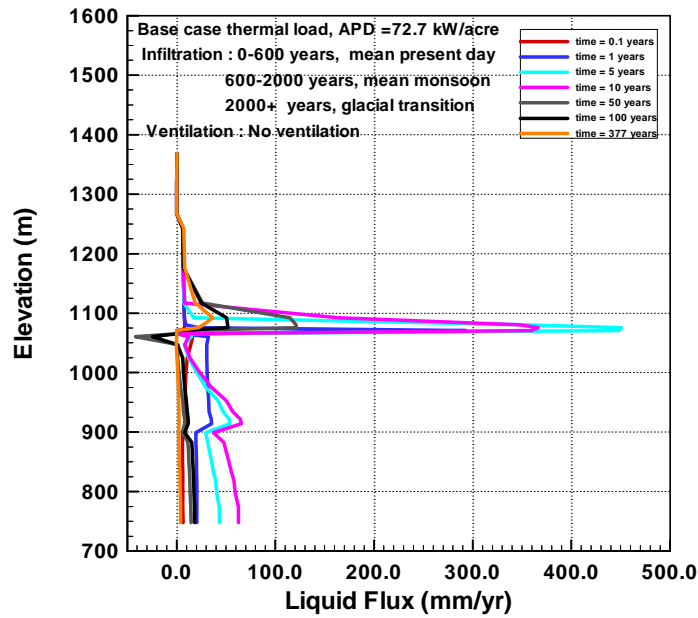
Based on modeling results submitted with this AMR under DTN: LB991201233129.001

Figure 51. Matrix Liquid Saturation Location #1, Model 5.



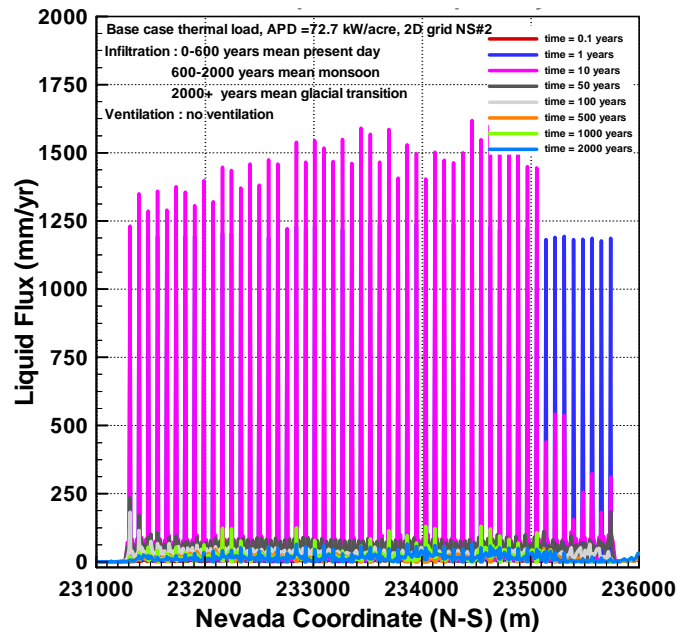
Based on modeling results submitted with this AMR under DTN: LB991201233129.001

Figure 52. Matrix Liquid Saturation along the Potential Repository Horizon, NS#2 Grid, Model 5.



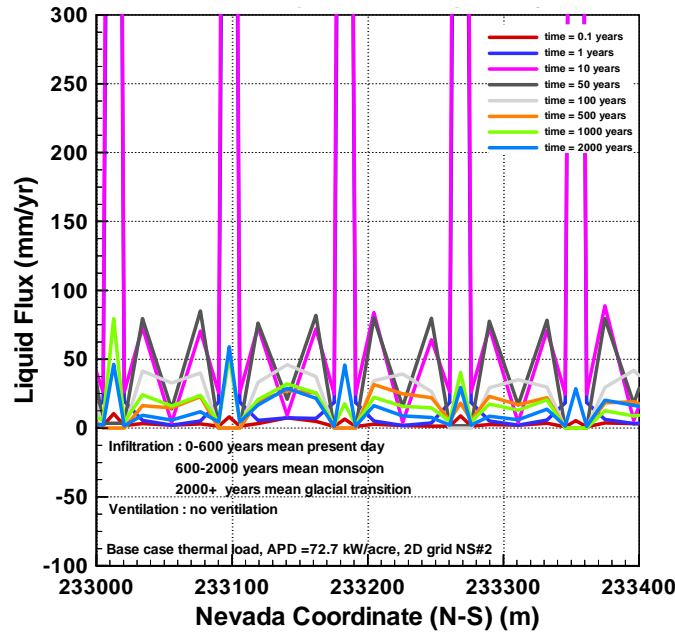
Based on modeling results submitted with this AMR under DTN: LB991201233129.001

Figure 53. Fracture Liquid Flux at Location #1, NS#2 Grid, Model 5.



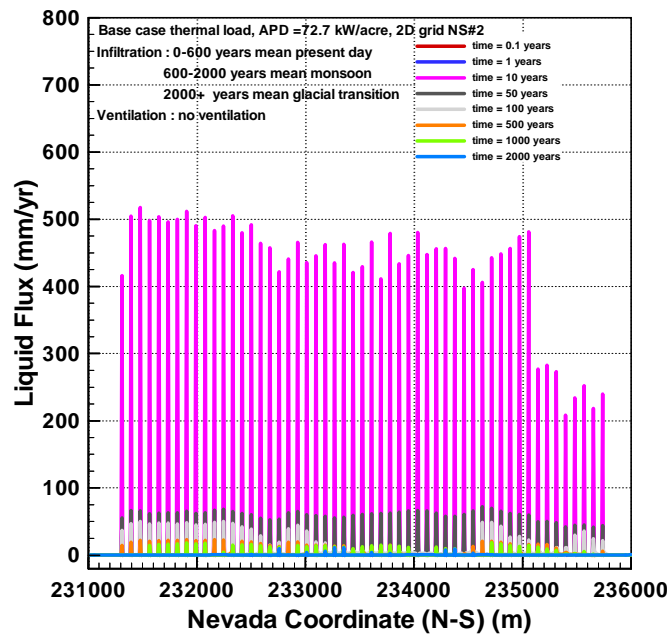
Based on modeling results submitted with this AMR under DTN: LB991201233129.001

Figure 54. Fracture Liquid Flux along the Potential Repository Horizon NS#2 Grid, Model 5.



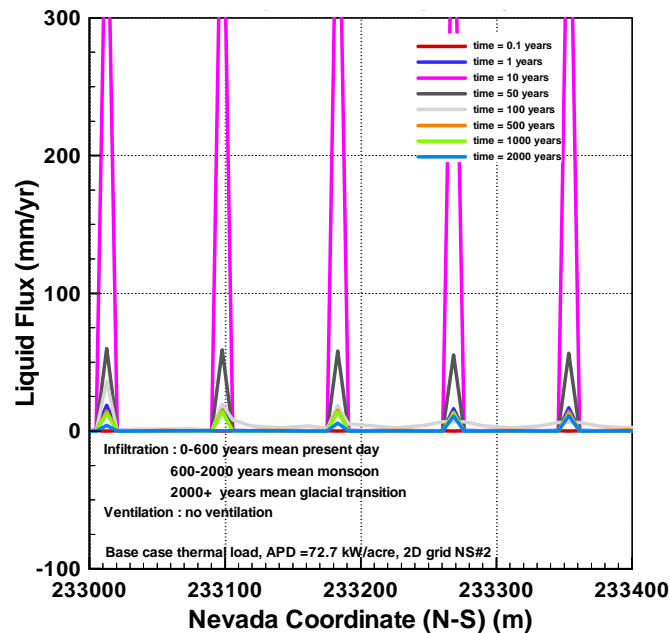
Based on modeling results submitted with this AMR under DTN: LB991201233129.001

Figure 55. Repository Fracture Liquid Flux along the Potential Repository Horizon NS#2 Grid, Model 5 (detail plot).



Based on modeling results submitted with this AMR under DTN: LB991201233129.001

Figure 56. Matrix Liquid Flux along the Potential Repository Horizon NS#2 Grid, Model 5.



Based on modeling results submitted with this AMR under DTN: LB991201233129.001

Figure 57. Fracture Liquid Flux along the Potential Repository Horizon NS#2 Grid, Model 5 (detail plot).

6.11.2 Model 6, NS#2 Case 2

This case is the same as Case 1 above, except that 70% of the heat is removed by ventilation for 50 years. This is the design base-case thermal load scenario. In this section, we discuss the effects of ventilation and variation in climate on the predicted TH conditions. In this discussion we highlight the differences between the model predictions for this case, and all the previous, cases over the thermal-loading period.

Temperature

Figures 58 and 59 show the temperature after 500 and 1,000 years of thermal loading, respectively. Even with ventilation, a two-phase heat-pipe region is developed at the repository horizon. However, it is limited to within a few meters above the repository. The model predicts much lower elevated temperatures resulting from ventilation cooling. Zones at about 100 m from the northern and southern ends of the repository have a maximum temperature rise of only 10-15°C during the thermal-loading period. Areas more than 200 m from the edges of the repository remain at near-ambient thermal conditions throughout the thermal-loading period. After the 50 years of ventilation ends, the temperatures within the central part of the repository are predicted to rise. The average temperature within the drifts rises to boiling conditions (97°C), although in a few locations temperatures rise to above 110°C (Figure 62). Figures 60 and 61 show the temperature profiles within a drift-column (Location #1) at the center of the repository and in an adjacent column (Location #2) as discussed in the previous section. The model predicts that although local temperature within the drift will rise to a boiling point, temperatures in the adjacent column rise to only 90°C, and the temperature in the pillars will only rise to 80-85 °C.

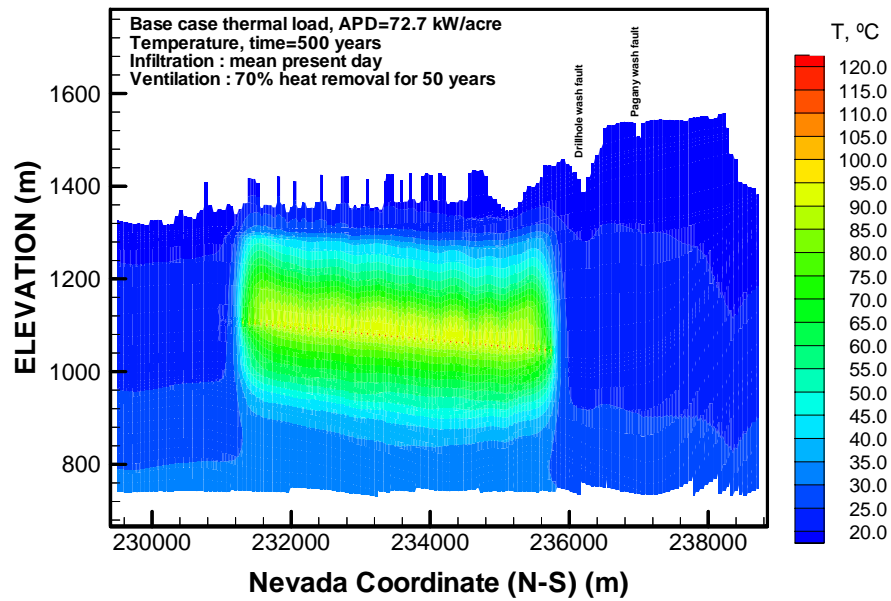
Saturation

Figures 63 to 66 present the plots and contours of matrix liquid saturation. The contour plots of the matrix liquid saturation after 500 and 1,000 years of thermal load are shown in Figures 63 and 64, respectively. The plots again show that significant drying or a decrease in matrix liquid saturation occurs only at or near the repository. Figures 65 and 66 show the matrix liquid saturation profiles in Column #1 and at the repository horizon, respectively. We predict completely dry conditions to occur only in a few matrix elements of the drifts where local surface infiltration rate is low. The matrix liquid saturation in several drifts with high ambient infiltration is above 90% after 1,000 years (note that this is within the monsoon climate). After 5,000 years, matrix liquid saturation recovers to ambient conditions (of the glacial infiltration climate).

Flux

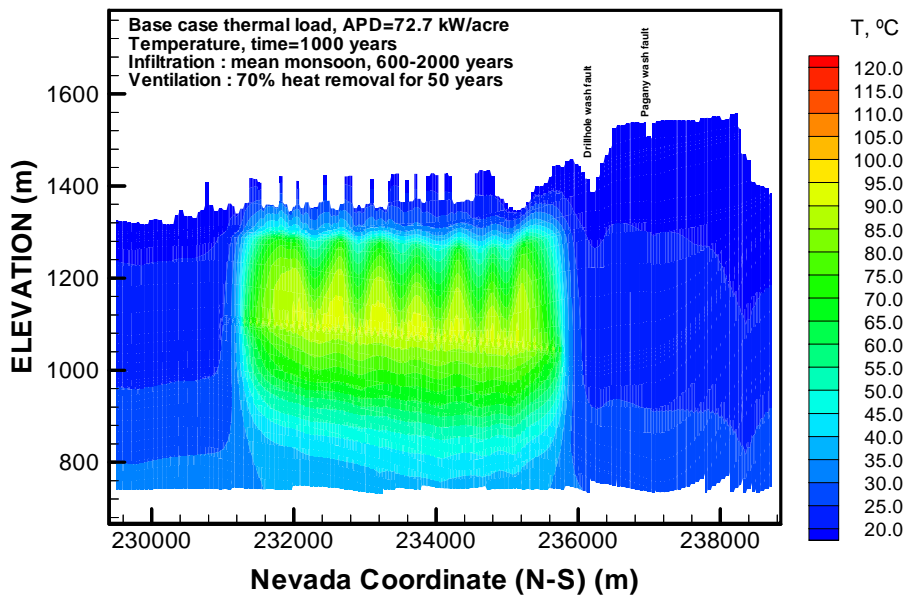
Figures 67 to 71 show that the modeled percolation fluxes are much lower than those for the no-ventilation scenario. The vertical flux profile (Figure 67) shows the average liquid flux towards the drifts rises to a maximum of only 50 mm/year at 5 years. At the repository (Figures 68-69) this fracture liquid flux rises to a maximum of 270-300 mm/year at 10 years, but drops to less than 10 mm/year after 100 years. The flux recovers to over 150 mm/year at 500 years as a result of increased heating at the end of ventilation. After 1,000 years, the fracture flux declines to rates primarily controlled by the prevailing ambient climate. The fracture liquid flux in the pillars remains above ambient conditions throughout the thermal-loading period. This flux may rise to 15-20 mm (about 2 to 3 times the ambient flux) at 500 years because of condensate drainage. Beyond 500 years, the flux rises because of the high ambient infiltration during the monsoon and glacial transition climates. Figures 70 and 71 show the matrix liquid flux during thermal load. The matrix liquid flux rises to a maximum of 20-30 mm/year at the drifts after 500 years, but remains at ambient conditions between the drifts throughout the thermal-loading period (Figure 71).

Figures 72 to 73 show the evolution of mountain-scale gas flux through the fracture continuum after 500 and 1,000 years of thermal load. The increase in gas flux is confined to the repository horizon for the duration of boiling (up to 2000 years). Much smaller gas flux is expected in the matrix continuum because of the lower permeability. The simulations of mountain-scale TH with ventilation, therefore, predict no large-scale thermally driven gas movement in the mountain.



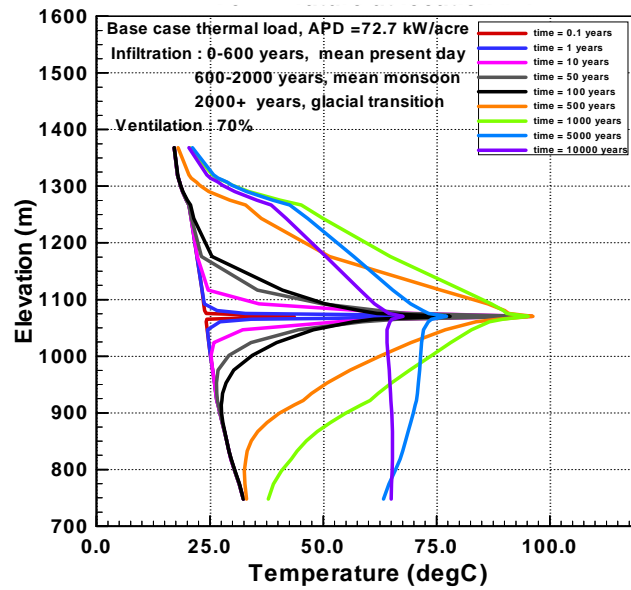
Based on modeling results submitted with this AMR under DTN: LB991201233129.001

Figure 58. Temperature Distribution along NS#2 Grid at 500 Years, Model 6.



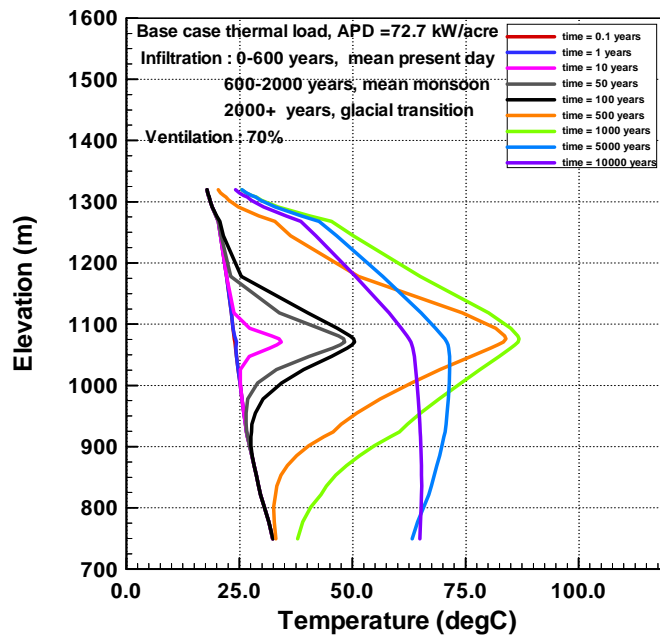
Based on modeling results submitted with this AMR under DTN: LB991201233129.001

Figure 59. Temperature Distribution along NS#2 Grid at 1,000 Years, Model 6.



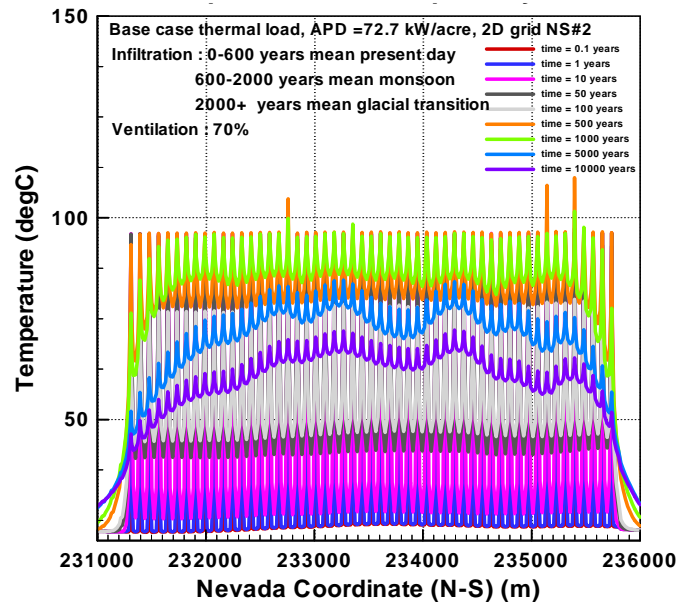
Based on modeling results submitted with this AMR under DTN: LB991201233129.001

Figure 60. Temperature at Location #1 (see Figures 1 and 3), NS#2 Grid, Model 6.



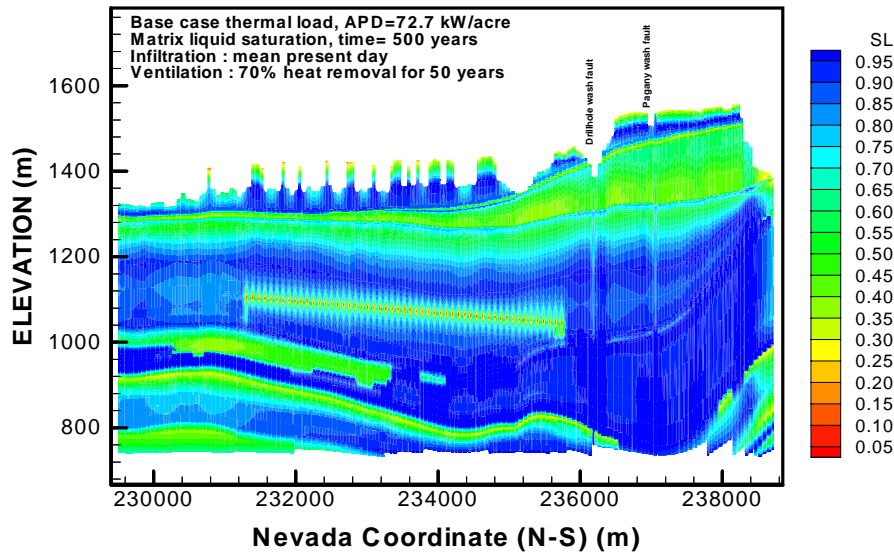
Based on modeling results submitted with this AMR under DTN: LB991201233129.001

Figure 61. Temperature at Location #2 (see Figures 1 and 3), NS#2 Grid, Model 6.



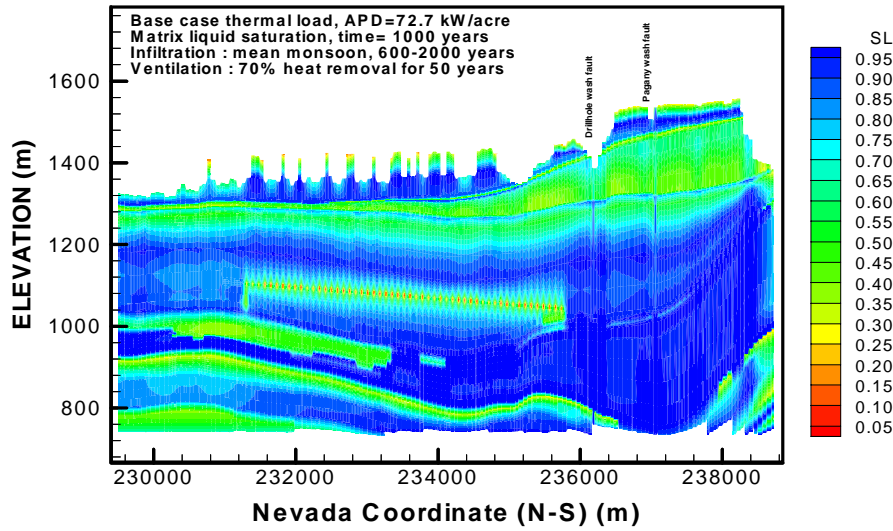
Based on modeling results submitted with this AMR under DTN: LB991201233129.001

Figure 62. Temperature along the Potential Repository Horizon NS#2 Grid, Model 6.



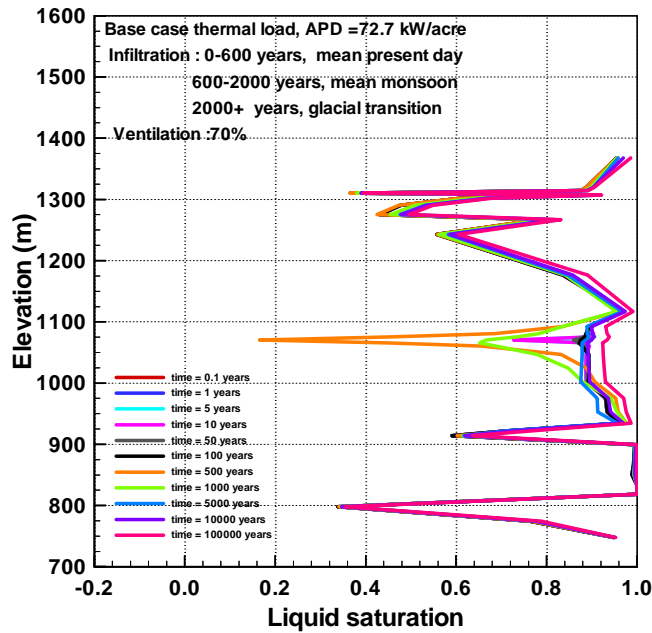
Based on modeling results submitted with this AMR under DTN: LB991201233129.001

Figure 63. Matrix Liquid Saturation (SL) along NS#2 Grid at 500 Years, Model 6.



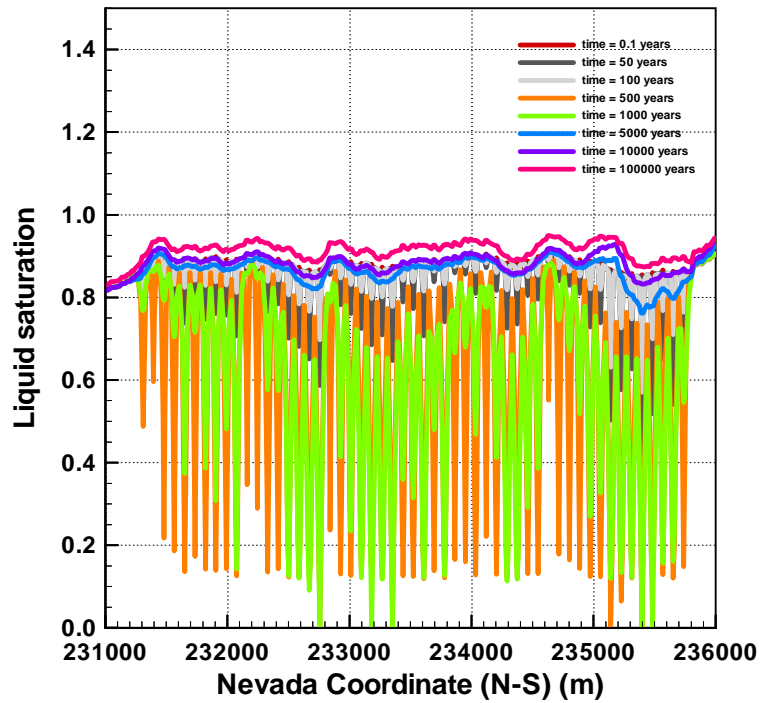
Based on modeling results submitted with this AMR under DTN: LB991201233129.001

Figure 64. Matrix Liquid Saturation (SL) along NS#2 Grid at 1,000 Years, Model 6.



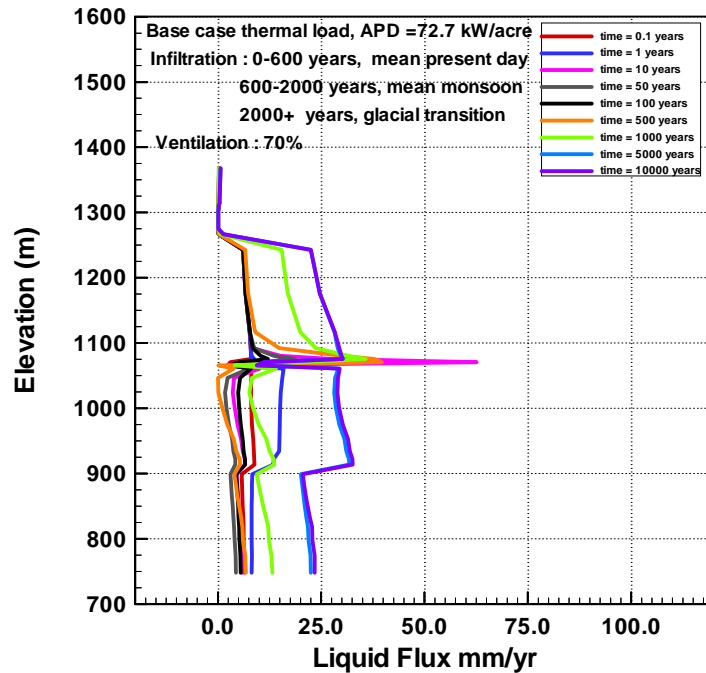
Based on modeling results submitted with this AMR under DTN: LB991201233129.001

Figure 65. Matrix Liquid Saturation at Location #1, Model 6.



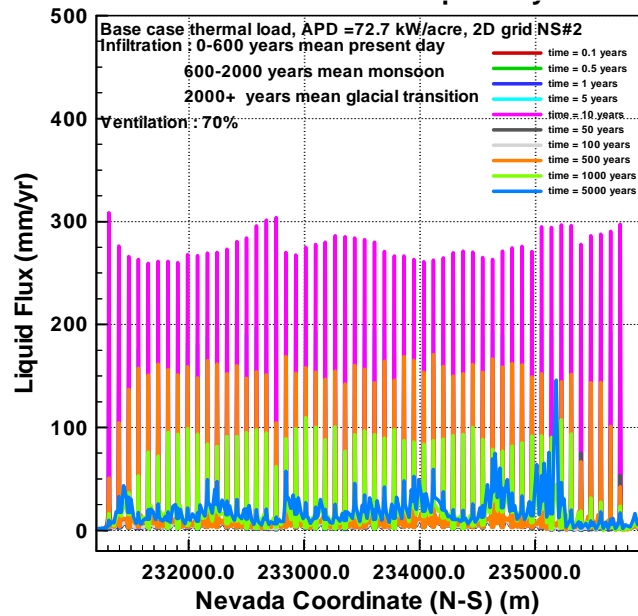
Based on modeling results submitted with this AMR under DTN: LB991201233129.001

Figure 66. Matrix Liquid Saturation along the Potential Repository NS#2 Grid, Model 6.



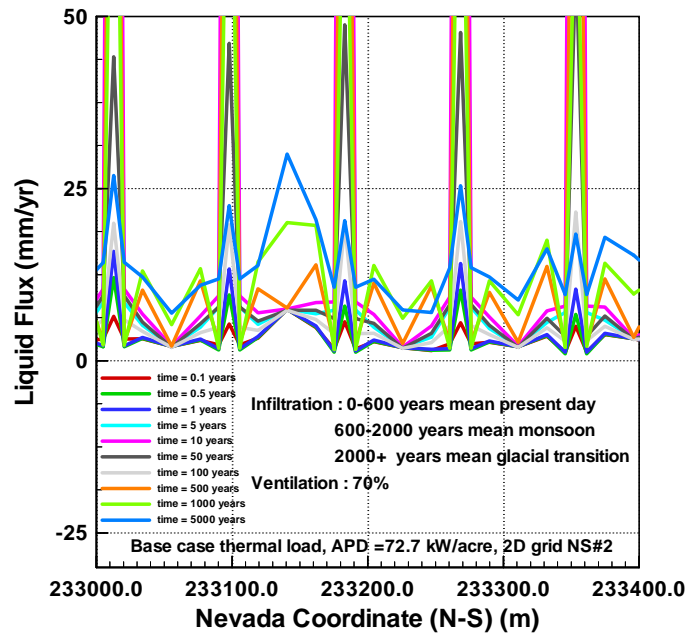
Based on modeling results submitted with this AMR under DTN: LB991201233129.001

Figure 67. Fracture Liquid Flux at Location #1, Model 6.



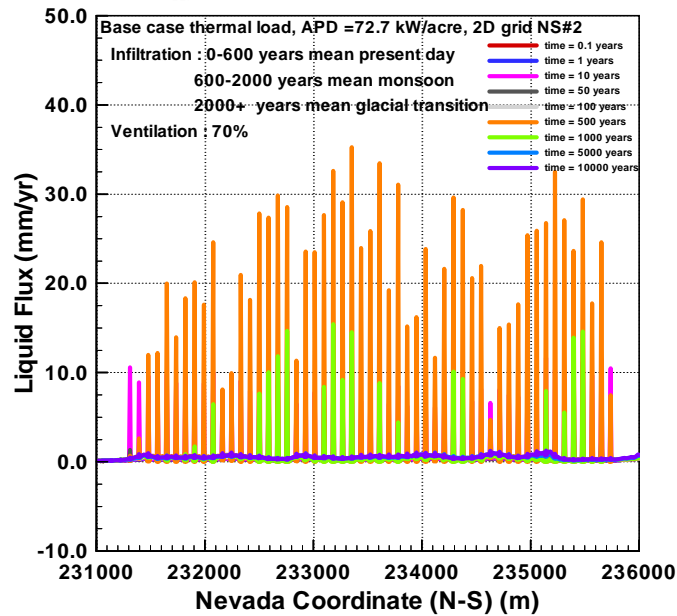
Based on modeling results submitted with this AMR under DTN: LB991201233129.001

Figure 68. Fracture Liquid Flux along the Potential Repository Horizon NS#2 Grid, Model 6.



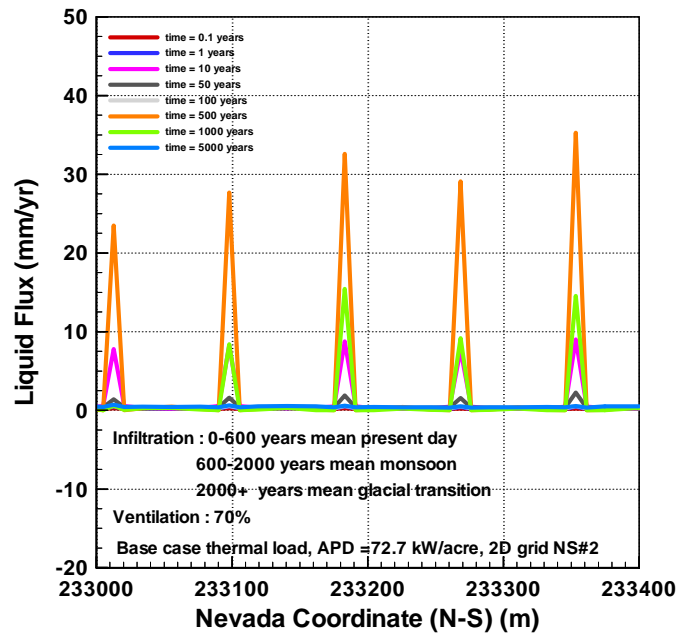
Based on modeling results submitted with this AMR under DTN: LB991201233129.001

Figure 69. Fracture Liquid Flux along the Potential Repository NS#2 Grid, Model 6 (detail plot).



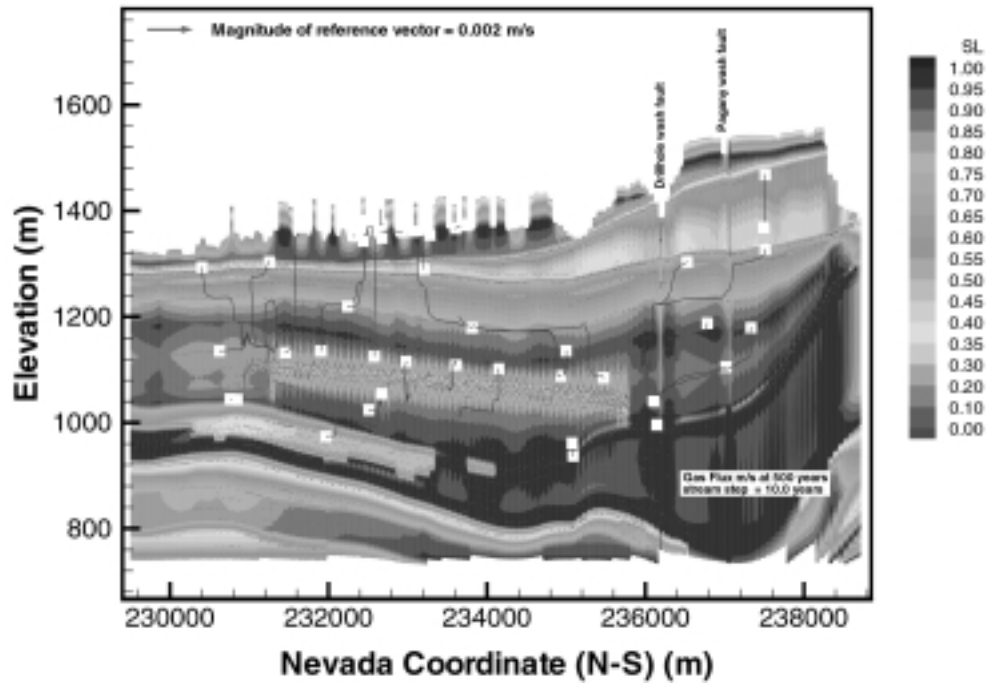
Based on modeling results submitted with this AMR under DTN: LB991201233129.001

Figure 70. Matrix Liquid Flux along the Potential Repository Horizon NS#2 Grid, Model 6.



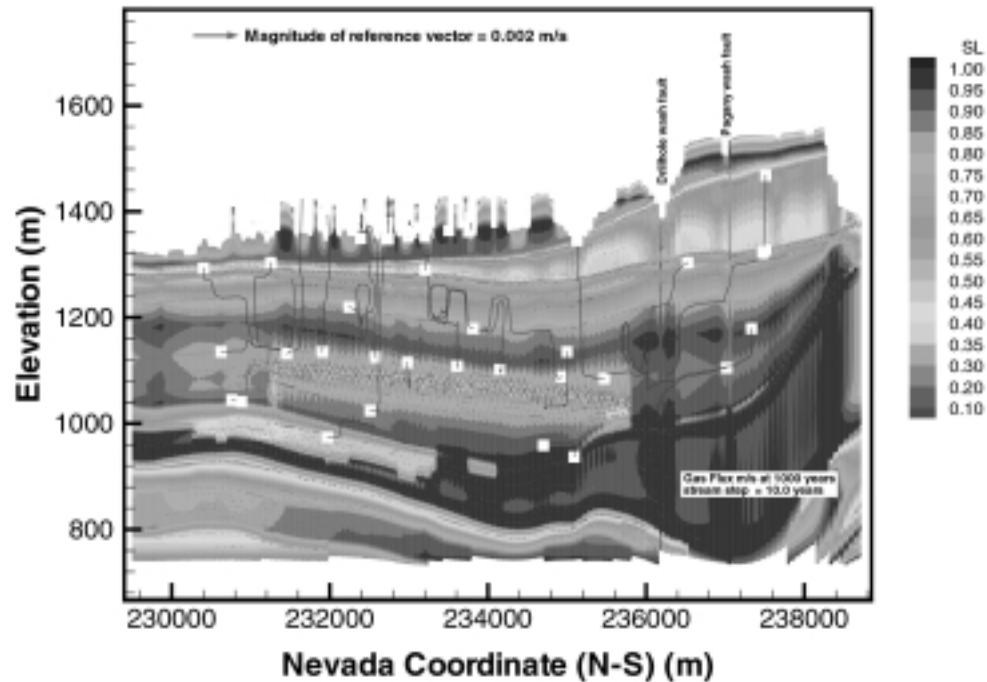
Based on modeling results submitted with this AMR under DTN: LB991201233129.001

Figure 71. Matrix Liquid Flux along the Potential Repository Horizon NS#2 Grid, Model 6 (detail plot).



Based on modeling results submitted with this AMR under DTN: LB991201233129.001

Figure 72. Fracture Gas Flux along the NS#2 Cross Section at 500 Years, Model 6. Purple lines show gas flux vectors at the interfaces of connected elements, red lines show streamline traces and direction of gas flow. The contour floods show liquid saturation in the matrix.



Based on modeling results submitted with this AMR under DTN: LB991201233129.001

Figure 73. Fracture Gas Flux along the NS#2 Cross Section at 1,000 Years, Model 6. Purple lines show gas flux vectors at the interfaces of connected elements, red lines show streamline traces and direction of gas flow. The contour floods show liquid saturation in the matrix.

6.12 MODEL VALIDATION

Numerical modeling of mountain-scale thermal hydrology (TH) can provide insight into the performance of the repository under thermal loading. The intended use for the TH model has been discussed in Section 6.1. This discussion includes an estimation of the qualitative and quantitative impact of heat generated by the high-level nuclear waste emplaced within the drifts on ambient conditions. Criteria include:

- The extent of the thermally affected zone and the two-phase zone within the UZ
- The temperature of the drifts, pillars, CHn zeolites, and water table
- The moisture redistribution in the UZ and formation of dry-out and condensation zones
- The liquid and gas flux in the UZ, drainage towards the drifts and between the pillars
- The potential for temperature and precipitation induced changes in flow and transport properties of the PTn and the CHn zeolites
- The impact of climate and ventilation on the predicted TH response.

Prediction of the range of the TH conditions during thermal loading allows for an evaluation of the adequacy of the design repository environment to safely store heat-generating nuclear waste over a period of up to 100,000 years.

The problem to be modeled here is essentially that of coupled two-phase fluid and heat flow in a fractured geological medium. Approaches to developing the numerical models to simulate two-phase processes, are (in such systems) generally based on geothermal and petroleum reservoir simulation methods. Numerical models of geothermal and petroleum systems can be validated from a wealth of field-scale tests and production data. Validation of a TH model requires field data on a mountain scale, which can only be available when the repository is fully operational. Because no such data is available, we demonstrate the validity of model predictions and modeling approach using corroborative work in this field and the previously published UZ numerical modeling studies and small-scale tests.

Experiments to determine the near-field (repository) scale process under thermal loading have been designed and are being conducted (Tsang and Birkholzer 1999, pp. 385–425). For example, the Single Heater Test (SHT), after a nine-month heating period, is now in a cooling phase. The larger Drift Scale Test (DST) will last up to 10 years (with a heating period of 4 years). However, because both the repository drift and the waste packages are on a much smaller scale compared to the UZ Mountain-Scale Model, the thermal tests will provide only limited data for calibration and validation of the numerical models. The small spatial and temporal scales limit validation of the mountain-scale submodels, based on SHT and DST tests. The validation is also limited by the uncertainties arising from parameter estimates in a geologically complex system and the upscaling of drift-scale results to the UZ Mountain-Scale Model.

Therefore, numerical modeling of mountain-scale TH will play a crucial role in understanding the impact of thermal loading on the performance of the UZ. Validations of such models, although incorporating results of SHT and DST tests, will rely mainly on the conceptual and mathematical validity of the models and the associated numerical grids as documented in this AMR. Performance-assessment models based on numerical simulation of fluid and heat flow can include all important physical and chemical processes affecting repository and host rock

behavior. In these models, we can explicitly represent relevant thermal-hydrologic conditions at the potential repository over the applicable time and space scale. The analyses conducted in this AMR are intended to provide the mountain-scale response to thermal loading under the proposed design conditions. The numerical models are used to determine the effect of thermal loading on mountain-scale liquid and gas flux, temperature, and moisture distribution in the UZ. The formulation of simulation code TOUGH2 V 1.4 allows numerical modeling of such processes.

Versions of TOUGH2 have been used in a number of numerical models for evaluating the thermal-hydrologic effects of thermal loading at Yucca Mountain (Pruess and Tsang 1994; Buscheck et al. 1994; Haukwa et al. 1999, pp. 217–255). Model conceptualizations have focused mainly on large-scale average behavior or on local simplified domains of two-dimensional representations. Both the ECM and dual-k methods have been used.

These previous versions have also been used in sensitivity studies on thermal-hydrological conditions near an infinite linear string of waste packages, as reported by Pruess and Wang (1984). They modeled fluid and heat flow (including phase change effects) in a one-dimensional cylindrical geometry. They found that strong two-phase vapor-liquid counter flow (heat pipe) occurred in some cases. Tsang and Pruess (1987, pp. 1958-1966) conducted repository-scale simulations with an emphasis on thermally driven natural convection. Nitao (1988) considered details of temperature, saturation, and gas-phase composition in the hydrothermally disturbed zone. This was modeled using a 3 km diameter, disk-shaped repository to examine the thermal-hydrological responses. Pruess et al. (1990a, 1990b) used a previous version of TOUGH2 to perform a comprehensive modeling study of simultaneous transport of heat, liquid water, vapor, and air in a partially saturated fractured porous rock. They used a two-dimensional idealized model and included an explicit consideration of fracture effects. Their model included most of the physical effects that are important in multiphase fluid and heat flow. They demonstrated the capability of modeling multiphase, nonisothermal flow of water and air with phase changes in a fractured medium.

Many simulations have been conducted at Lawrence Livermore National Laboratory (LLNL) to predict the thermal-hydrologic conditions at the repository (Nitao 1988; Ramspott 1991; Buscheck and Nitao 1991, 1992, 1993a, 1993b, 1993c; Buscheck et al. 1993, 1994; and Buscheck and Nitao 1994). Pruess and Tsang (1994) provide detailed investigations into strongly heat-driven flow processes at small scales to look at heterogeneity effects. They concluded through these studies that for a highly heterogeneous fractured-porous hydrogeologic system at Yucca Mountain, water infiltration across the unsaturated zone might be dominated by highly localized phenomena. The phenomena include "fast" channeled flow along preferential paths in fractures and frequent local ponding. The active fracture concept used in this AMR is intended to capture such effects.

The TOUGH2 family of codes has also been used in several numerical models of the natural state of geothermal systems (Bodvarsson et al. 1984a, 1986, 1988; Hanano 1992; Ingebritsen et al. 1988; O'Sullivan et al. 1990) and in the predictions of their performance under exploitation (Bodvarsson et al. 1984b, 1987a, 1987b, 1990, 1993; Garg et al. 1990; Hunt et al. 1990; Lam et al. 1988; Menzies et al. 1991). Mathematical models of the two-phase flow in such systems are identical to numerical modeling of TH response to thermal loading described in this AMR. Major differences exist, mainly in equations correlating flow and saturation and the existence of

preferential flow paths in UZ flow even for fairly heterogeneous media (e.g., fingering and flow channeling). The other major difference is in the time scale of modeled behavior. For example evolution of the natural state of geothermal systems is typically modeled over a period of a few hundred to several hundred thousand years. The exploitation prediction is over a period of 30-50 years, the economic life of such systems, based measured field response. On the other hand, modeling of the mountain-scale TH response requires numerical prediction for tens of thousands of years in a system where little field data exist. In many ways, however, the process for setting up the conceptual model, building the numerical grid, specifying boundary conditions, developing the natural state, and conducting numerical model predictions is the same and is documented in the cited references as well as in this AMR.

The modeling efforts described above demonstrate the capability of TOUGH2 to model TH processes on a mountain scale, in addition to the validity of process models and the assumptions used. The numerical grids employed are sufficiently simplified to allow for models consistent with the distribution of measured field data. On the other hand, the grids are detailed enough to adequately resolve key ambient hydrology parameters, e.g., fluid saturation and percolation flux at the repository. Numerical models in this AMR therefore use several grids to provide a range of sensitivity in the predicted mountain-scale TH response

The TOUGH2 TH models that are developed in this AMR match closely the observed conditions from the SHT and DST heater tests. Both the results of the heater tests and the TH models suggest no major adverse conditions in terms of temperature changes, moisture redistribution near the drifts, or liquid drainage towards the drifts and within the pillars. The TH models in addition show no major moisture redistribution in the UZ except near the heated drifts. The models also show only a moderate temperature increase within the zeolites and at the water table. We consider the TH models developed here validated because of this good agreement with the heater test models, the validity of the geothermal analog models, and the documented theoretical and physical validity of similar unsaturated flow studies with and without heat.

7. DISCUSSION AND CONCLUSIONS

In this AMR, we conduct a systematic modeling study to investigate the effects of thermal loading on the TH processes in the UZ of Yucca Mountain. This study uses several 3-D and 2-D dual-permeability submodels of the 3-D UZ Model and incorporates material properties developed using the Calibrated Properties Model (documented in separate AMRs). The 2-D models employ different refined lateral grids as well as explicit drift representation at the repository.

These models provide the mountain-scale TH response and the sensitivity to thermal loading distribution, based on surface infiltration rate, numerical grid discretization, and the effects of ventilation. The models allow for the temperature to vary at the water table. This is achieved by shifting the UZ-model bottom boundary with a fixed temperature condition to 1,000 m below the water table. The numerical model grids used in this study are still relatively coarse for resolving the drift-scale phenomena expected near the waste packages. However, the models provide sufficient resolution for determining mountain-scale, long-term TH behavior resulting from thermal load within the drifts. This is because the detailed TH processes and descriptions at the drifts affect only a small distance (tens of meters and at early times less than 100 years) relative to the mountain-scale model domain. The far-field, mountain-scale TH behavior of the UZ system is determined mainly by a long-term average heat source at the repository.

Three-dimensional effects of TH processes are investigated by comparing the simulation results of the 3-D models with the 2-D model (NS#1 Case 1 Sections 6.8 and 6.9). In both models, the thermal load is applied to the entire drift column (continuous/smeared heat source over the repository block). Except for a few locations, the 2-D and 3-D models predict very similar temperature contours for the simulated domain. Significant differences in the modeled temperature profiles between the two models occur only at the center of the repository along the repository horizon. With the 3-D model, we predict more rapid cooling at the end of the boiling period than the 2-D models, because of lateral heat conduction into a third dimension. After 2,000 years, the predicted temperature at the repository is 77°C from the 3-D model compared to 92°C from the 2-D model. The predicted maximum temperature at the water table is 70°C in both cases for the current thermal-loading, scenario using the mean present-day infiltration and no ventilation.

In addition to the surface infiltration rates and the actual thermal load to be emplaced into the drifts, the model-predicted TH processes also depend on other factors. These factors include how the waste distribution is represented in the model, whether ventilation is used, and the resolution of numerical grids. This study indicates that the available heat and ambient infiltration flux are the determining factors for boiling and rewetting processes at the repository. The average infiltration rate for the modeled cases is 4.8 mm/year for the mean present-day infiltration rate, 11.3 mm/year for the mean monsoon-climate average infiltration, and 16.9 mm/year for the mean glacial-transition climate. With both the 2-D coarse and refined grid models without ventilation, heat-pipe conditions are developed in a region above the repository during 10-100 years. Complete dry-out conditions are predicted near the drifts, mainly within fracture elements, with drift temperatures exceeding 100°C for hundreds of years.

In the rock mass between the drifts, temperatures may rise to boiling conditions and saturation may be slightly reduced. No complete dry-out conditions are predicted except in zones under low surface infiltration rates. The liquid flux towards the drifts may exceed 1,200 mm/year, particularly in the low infiltration areas. This is because of drier conditions and consequentially high capillary pressure gradients. However, the high percolation fluxes occur only at early times (less than 100 years) and do not represent liquid seepage into the drifts because it is vaporized by the heat within the drifts. The refined 2-D model predicts that although vertical flow crossing the interval between the drifts continues at a rate close to the ambient percolation fluxes for most of the thermal-loading period, this flux may be enhanced by condensate drainage for the first 1,000 years of thermal load. The results also show that major changes to flow occur mainly above the potential repository horizon. The increase in flow here is associated with boiling, lowering of liquid saturation (high capillary suction), or increase in saturation through condensation (increased relative permeability). Only small increases in liquid flux are predicted below the repository horizon.

Thermal loading at the repository results in significant changes in the temperature conditions and moisture distribution, both at the repository and at the zone directly above and below the repository. Without ventilation, strong liquid and gas flow fields are developed. These flow fields are several orders of magnitude higher than the ambient conditions at the repository drifts and at earlier times. Two-phase heat-pipe conditions occur only in a region above the repository, a region extending up to 200 m above the repository to the base of the PTn hydrogeologic unit. These conditions occur between 500–1,000 years. Complete dry-out of both the fracture and matrix continua at the repository develops over the first 100 years. Return to the ambient saturation occurs during 500–5,000 years. Localized dry-out of the matrix at the repository and in areas with low infiltration rates is predicted even with ventilation. Temperatures may be elevated to approximately 250°C within the completely dry drifts, when no ventilation is implemented. However, most of the repository remains at boiling temperature (about 97°C) for nearly 1,000 years. When ventilation is employed, only localized boiling at the drifts is predicted. The maximum temperature at the repository in this case is 97°C, which is the boiling temperature at repository.

Without ventilation and with the present-day mean infiltration for the entire thermal load period, the models predict a nearly 30 to 35°C temperature increase at the water table to an average of 70°C. With ventilation and change in infiltration owing to changes in the climate, the predicted maximum temperature at the water table drops to about 65°C. This indicates that the models with a fixed temperature boundary applied at the water table may overestimate the cooling rate of the repository, because it imposes a higher temperature gradient between the repository and the water table.

At the top of the CHn hydrogeologic unit, the predicted maximum temperature rises to 75–80°C for a period between 2,000 and 7,000 years. The predicted near surface temperatures (top of the TCw hydrogeologic unit) are dominated by the top temperature condition, as specified in the models, and may not correctly represent the evolution of near-surface temperature conditions under thermal loading.

Even with ventilation, the models predict a zone with substantial changes in matrix liquid saturation that extends about 50 m below and above the potential repository horizon. From the

2-D models, we predict surface infiltration rates resulting from simulated monsoon and glacial climates have little impact on the duration and extent of boiling zones at the repository. However, higher liquid recharge rates from these two climates during the cooling phase speed up the processes of cooling and re-saturation beyond 2,000 years, and elevate the ambient percolation flux.

The 2-D models used here show good agreement with the results of 3-D models showing that 3-D effects do not adversely impact the conclusions derived using the detailed NS#2 grid. Because there is no heat-transfer in the 3rd dimension, the 2-D models provide an upper bound estimate of TH impact heat on the UZ environment compared to the 3-D models. Furthermore, because the predicted thermally affected zone does not laterally extend more than 100 m outside the repository, the predicted TH response can apply to an E-W or any cross section through the repository over which similar flow properties, thermal load distribution, and infiltration pattern apply.

8. INPUTS AND REFERENCES

8.1 CITED DOCUMENTS

Bodvarsson, G.S.; Bjornsson, S.; Gunnarsson, A.; Gunnlaugsson, E.; Sigurdsson, O.; Stefansson, V.; and Steingrimsson, B. 1988. "A Summary of Modeling Studies of the Nesjavellir Geothermal Field, Iceland." *Thirteenth Workshop on Geothermal Reservoir Engineering, Stanford University*, 83–91. Stanford, California: Stanford University. TIC: 246824.

Bodvarsson, G.S.; Gislason, G.; Gunnlaugsson, E.; Sigurdsson, O.; Stefansson, V.; and Steingrimsson, B. 1993. "Accuracy of Reservoir Predictions for the Nesjavellir Geothermal Field, Iceland." *Eighteenth Workshop on Geothermal Reservoir Engineering, Stanford University*, 273–278. Stanford, California: Stanford University. TIC: 246821.

Bodvarsson, G.S.; Pruess, K.; Haukwa, C.; and Ojiambo, S. B. 1990. "Evaluation of Reservoir Model Predictions for Olkaria East Geothermal Field, Kenya." *Geothermics*, 19 (5), 399–414. Oxford, UK: Pergamon Press. TIC: 246739.

Bodvarsson, G.S.; Pruess, K.; and Lippmann, M. J. 1986. "Modeling of Geothermal Systems." *Journal of Petroleum Technology September*, 1007–1021. Richardson, Texas: Society of Petroleum Engineers. TIC: 246733.

Bodvarsson, G.S.; Pruess, K.; Stefansson, V.; Bjornsson, S.; and Ojiambo, S. B. 1987a. "East Olkaria Geothermal Field, Kenya, 1. History Match With Production and Pressure Decline Data." *Journal of Geophysical Research*, 92 (B1), 521–539. Washington, D.C.: American Geophysical Union. TIC: 236629.

Bodvarsson, G.S.; Pruess, K.; Stefansson, V.; Bjornsson, S.; and Ojiambo, S. B. 1987b. "East Olkaria Geothermal Field, Kenya, 2. Predictions of Well Performance and Reservoir Depletion." *Journal of Geophysical Research*, 92 (B1), 541–554. Washington, D.C.: American Geophysical Union. TIC: 246738.

Bodvarsson, G.S.; Pruess, K.; Stefansson, V.; and Eliasson, E.T. 1984a. "The Krafla Geothermal Field, Iceland, 2. The Natural State of the System." *Water Resources Research*, 20 (11), 1531–1544. Washington, D.C.: American Geophysical Union. TIC: 246734.

Bodvarsson, G.S.; Pruess, K.; Stefansson, V.; and Eliasson, E.T. 1984b. "The Krafla Geothermal Field, Iceland, 3, The Generating Capacity of the Field." *Water Resources Research*, 20 (11), 1545–1559. Washington, D.C.: American Geophysical Union. TIC: 246737.

Brooks, R.H. and Corey, A.T. 1966. "Properties of Porous Media Affecting Fluid Flow." *Journal of Irrigation and Drainage Division: Proceedings of the American Society of Civil Engineers*, 92 (IR2), 61–88. Washington, D.C.: American Society of Civil Engineers. TIC: 216867.

Buscheck, T.A. and Nitao, J.J. 1992. "Impact of Thermal Loading on Repository Performance at Yucca Mountain." *Proceedings of the Third Annual International Conference High Level Radioactive Waste Management, Las Vegas, Nevada, April 12-16, 1992*, 11003–1017. La Grange Park, Illinois: American Nuclear Society. TIC: 204231.

Buscheck, T.A. and Nitao, J.J. 1993a. "Repository-Heat-Driven Hydrothermal Flow at Yucca Mountain, Part I: Modeling and Analysis." *Nuclear Technology*, 104 (3), 418–448. La Grange Park, Illinois: American Nuclear Society. TIC: 224039.

Buscheck, T.A. and Nitao, J.J. 1993b. "The Analysis of Repository-Heat-Driven Hydrothermal Flow at Yucca Mountain." *High Level Radioactive Waste Management, Proceedings of the Fourth Annual International Conference 1, Las Vegas, Nevada, April 26-30, 1993*, 847–867. La Grange Park, Illinois: American Nuclear Society. TIC: 208542.

Buscheck, T.A. and Nitao, J.J. 1993c. *The Impact of Repository-Heat-Driven Hydrothermal Flow on Hydrological Performance at Yucca Mountain*. Report UCRL-JC-114791. Livermore, California: Lawrence Livermore National Laboratory. ACC: NNA.19940121.0144.

Buscheck, T.A. and Nitao, J.J. 1993d. "Modeling Hydrothermal Flow in Variably Saturated, Fractured, Welded Tuff During the Prototype Engineered Barrier System Field Test of the Yucca Mountain Project." *Proceedings of the Fifth Workshop on Flow and Transport through Unsaturated Fractured Rock, Tucson, Arizona*. Livermore, California: Lawrence Livermore National Laboratory. TIC: 207128.

Buscheck, T.A. and Nitao, J.J. 1995. "The Importance of Thermal Loading Conditions to Waste Package Performance at Yucca Mountain." *Proceedings of the XVIII International Symposium on the Scientific Basis for Nuclear Waste Management, Kyoto, Japan, October 23-27, 1994*. TIC: 216341.

Buscheck, T.A.; Nitao, J.J.; and Saterlie, S.F. 1994. "Evaluation of Thermo-Hydrological Performance in Support of the Thermal Loading Systems Study." *High Level Radioactive Waste Management, Proceedings of the Fifth Annual International Conference 2, Las Vegas, Nevada, May 22-26, 1994*, 592–610. La Grange Park, Illinois: American Nuclear Society. TIC: 210984.

Buscheck, T.A.; Nitao, J.J.; and Wilder, D.G. 1993. "Repository Heat-Driven Hydrothermal Flow at Yucca Mountain, Part II: Large-Scale in Situ Heater Tests." *Nuclear Technology*, 104 (3), 449–471. La Grange Park, Illinois: American Nuclear Society. TIC: 235095.

CRWMS M&O (Civilian Radioactive Waste Management System, Management & Operating Contractor) 1999a. *Analysis & Modeling Development Plan (DP) for U0105, Mountain-Scale Coupled Processes (TH) Models Rev. 00*. TDP-NBS-HS-000012. Las Vegas, Nevada: CRWMS M&O. ACC: MOL.19990830.0382.

CRWMS M&O 1999b. *M&O Site Investigations*. Activity Evaluation. Las Vegas, Nevada: CRWMS M&O. ACC: MOL.19990317.0330.

CRWMS M&O 1999c. *M&O Site Investigations. Activity Evaluation.* Las Vegas, Nevada: CRWMS M&O. ACC: MOL.19990928.0224.

CRWMS M&O 1999d. *Rainfall/Runoff/Runon 1999 Simulations.* Input Transmittal LBL-USG-99248.T. Las Vegas, Nevada: CRWMS M&O. ACC: MOL.19991014.0102.

Doughty, C. 1999. "Investigation of Conceptual and Numerical Approaches for Evaluating Moisture, Gas, Chemical, and Heat Transport in Fractured Unsaturated Rock." *Journal Of Contaminant Hydrology* 38 (1-3), 69–106. Amsterdam, The Netherlands: Elsevier Science. TIC: 244160.

Driscoll, F.G. 1986. *Groundwater and Wells.* 2nd Edition. St. Paul, Minnesota: Johnson Filtration Systems. TIC: 217555.

Dyer, J.R. 1999. "Revised Interim Guidance Pending Issuance of New U.S. Nuclear Regulatory Commission (NRC) Regulations (Revision 01, July 22, 1999), for Yucca Mountain, Nevada." Letter from J.R. Dyer (DOE) to D.R. Wilkins (CRWMS M&O), September 9, 1999, OL&RC:SB-1714, with enclosure, "Interim Guidance Pending Issuance of New U.S. Nuclear Regulatory Commission (NRC) Regulations (Revision 01)." ACC: MOL.19990910.0079.

Francis, N.D. 1997. "The Base-Case Thermal Properties for TSPA-VA Modeling." Memorandum from N.D. Francis (SNL) to Distribution, April 16, 1997. Albuquerque, New Mexico: Sandia National Laboratories. ACC: MOL.19980518.0229.

Garg, S.K. and Pritchett, J.W. 1990. "Cold Water Injection Into Single- and Two-Phase Geothermal Reservoir." *Water Resources Research*, 26 (2), 331–338. Washington, D.C.: American Geophysical Union. TIC: applied for.

Hanano, M. 1992. "Reservoir Engineering Studies of the Matsukawa Geothermal Field, Japan." *Geothermal Resources Council Transactions, 16 October*, 643–650. Davis, California: Geothermal Resources Council. TIC: 247116.

Haukwa, C.B.; Wu, Y.S.; and Bodvarsson, G.S. 1999. "Thermal Loading Studies Using the Yucca Mountain Unsaturated Zone Model." *Journal of Contaminant Hydrology* 38 (1–3), 217–255. Amsterdam, The Netherlands: Elsevier Science Publishers. TIC: 244160.

Ho, C.K. and Francis, N.D. 1997. "Correction to Base-Case Thermal Properties for TSPA-VA Modeling." Memo from Ho, C.K. and Francis, N.D. to Distribution, August 7, 1997. Albuquerque, New Mexico: Sandia National Laboratories. ACC: MOL.19980518.0230.

Hunt, T.M.; Allis, R.G.; Blakeley, M.R.; and O'Sullivan, M. J. 1990. "Testing Reservoir Simulation Models for the Broadlands Geothermal Field using Precision Gravity Data." *Geothermal Resources Council Transactions, 14, Part II August*, 1287–1294. Davis, California: Geothermal Resources Council. TIC: 246942.

Ingebritsen, S.E. and Sorey, M.L. 1988. "Vapor-Dominated Zones within Hydrothermal Systems: Evolution and Natural State." *Journal of Geophysical Research*, 93 (B11), 13635–13655. Washington, D.C.: American Geophysical Union. TIC: applied for.

Klavetter, E.A. and Peters, R.R. 1986. *Estimation of Hydrologic Properties of an Unsaturated Fractured Rock Mass*. Report SAND84-2642. Albuquerque, New Mexico: Sandia National Laboratories. TIC: 202727.

Lam, S.T.; Hunsbedt, A.; Kruger, P.; and Pruess, K. 1988. "Analysis of the Stanford Geothermal Reservoir Model Experiments Using the LBL Reservoir Simulator." *Geothermics*, 17 (4), 595–605. Amsterdam, The Netherlands: Elsevier Science Publishers. TIC: 247098.

Liu, H.H.; Doughty, C.; and Bodvarsson, G.S. 1998. "An Active Fracture Model for Unsaturated Flow and Transport in Fractured Rocks." *Water Resources Research*, 34 (10), 2633–2646. Washington, D.C.: American Geophysical Union. TIC: 243012.

Menzies, A.J.; Granados, E.E.; Sanyal, S.K.; Merida-I, L. and Caicedo-A, A. 1991. "Numerical Modeling of the Initial State and Matching of Well Test Data from the Zunil Geothermal Field, Guatemala." *Sixteenth Workshop on Geothermal Reservoir Engineering, Stanford University*, 193–210. Stanford, California: Stanford University. TIC: applied for.

Montazer, P. and Wilson, W.E. 1984. *Conceptual Hydrologic Model of Flow in the Unsaturated Zone, Yucca Mountain, Nevada*. Water-Resources Investigations Report 84-4345. Lakewood, Colorado: U.S. Geological Survey. ACC: NNA.19890327.0051.

Nitao, J.J. 1988. *Numerical Modeling of the Thermal and Hydrological Environment around a Nuclear Waste Package Using the Equivalent Continuum Approximation: Horizontal Emplacement*. UCID-21444. Livermore, California: Lawrence Livermore National Laboratory. ACC: NNA-19890317.0021.

O'Sullivan, M. J.; Barnett, B. G.; and Razali, M. Y. 1990. "Numerical Simulation of the Kamojang Geothermal Field, Indonesia." *Geothermal Resources Council Transactions*, 14, Part II (August), 1317–1324. Davis, California: Geothermal Resources Council. TIC: applied for.

Pruess, K. 1987. *TOUGH User's Guide*. Nuclear Regulatory Commission, Report NUREG/CR-4645, Report LBL-20700. Berkeley, California: Lawrence Berkeley National Laboratory. ACC: MOL.19960314.0434.

Pruess, K. 1991. *TOUGH2-A General Purpose Numerical Simulator for Multiphase Fluid and Heat Flow*. Report LBL-29400, UC-251. Berkeley, California: Lawrence Berkeley National Laboratory. ACC: NNA.19940202.0088.

Pruess, K. and Narasimhan, T.N. 1985. "A Practical Method for Modeling Fluid and Heat Flow in Fractured Porous Media." *Society of Petroleum Engineers Journal*, 25 (1), 14–26. Richardson, Texas: Society of Petroleum Engineers. TIC: 221917.

Pruess, K. and Tsang, Y.W. 1994. *Thermal Modeling for a Potential High-Level Nuclear Waste Repository at Yucca Mountain, Nevada*. Report LBL-35381, UC-600. Berkeley, California: Lawrence Berkeley National Laboratory. ACC: NNA.19940427.0248.

Pruess, K. and Wang, J.S.Y. 1984. *TOUGH—A Numerical Model for Non-isothermal Unsaturated Flow to Study Waste Canister Heating Effects*. New York, New York: Elsevier Science Publishers. TIC: 221408.

Pruess, K.; Wang, J.S.Y.; and Tsang, Y.W. 1990a. “On Thermohydrologic Conditions near High-Level Nuclear Wastes Emplaced in Partially Saturated Fractured Tuff, Part I. Simulation Studies with Explicit Consideration of Fracture Effects.” *Water Resources Research*, 26 (6), 1235–1248. Washington, D.C.: American Geophysical Union. TIC: 221923.

Pruess, K.; Wang, J.S.Y.; and Tsang, Y.W. 1990b. “On the Thermohydrologic Conditions near High-Level Nuclear Wastes Emplaced in Partially Saturated Fractured Tuff, Part 2. Effective Continuum Approximation.” *Water Resources Research*, 26 (6), 1249–1261. Washington, D.C.: American Geophysical Union. TIC: 224854.

Ramspott, L.D. 1991. “The Constructive Use of Heat in an Unsaturated Tuff Repository.” *Proceedings of the Second International Conference on High Level Radioactive Waste Management*, 2, 1602–1607. La Grange Park, Illinois: American Nuclear Society. TIC:209272.

Tsang, Y.W. and Birkholzer, J.T. 1999. “Predictions and Observations of the Thermal-Hydrological Conditions in the Single Heater Test.” *Journal of Contaminant Hydrology*, 38 (1–3), 385–425. Amsterdam, The Netherlands: Elsevier Science Publishers. TIC: 244160.

Tsang, Y.W. and Pruess, K. 1987. “A Study of Thermally Induced Convection near a High-level Nuclear Waste Repository in Partially Saturated Fractured Tuff.” *Water Resources Research*, 23 (10), 1958–1966. Washington, DC: American Geophysical Union. TIC: 240715.

van Genuchten, M. 1980. “A Closed-Form Equation for Predicting the Hydraulic Conductivity of Unsaturated Soils.” *Soil Science Society of America Journal*, 44 (5), 892–898. Madison, Wisconsin: Soil Science Society of America. TIC: 217327.

Wemheuer, R.F. 1999. “First Issue of FY00 NEPO QAP-2-0 Activity Evaluations.” Interoffice correspondence from R.F. Wemheuer (CRWMS M&O) to R.A. Morgan (CRWMS M&O), October 1, 1999, LV.NEPO.RTPS.TAG.10/99-155, with attachments, Activity Evaluation for Work Package #1401213UM1. ACC: MOL.19991028.0162.

Wu, Y.S. 1996. *On the Effective Continuum Method for Modeling Multiphase Flow, Multicomponent Transport and Heat Transfer in Fractured Rock*. LBNL-42720. Berkeley, California: Lawrence Berkeley National Laboratory. TIC: 245761.

Wu, Y.S.; Haukwa, C. and Bodvarsson, G.S. 1999a. “A Site-Scale Model for Fluid and Heat Flow in the Unsaturated Zone of Yucca Mountain, Nevada.” *Journal of Contaminant Hydrology* 38, (1–3), 185–215. Amsterdam, The Netherlands: Elsevier Science Publishers. TIC: 244160.

Wu, Y.S.; Ritcey, A.C.; and Bodvarsson, G.S. 1999b. "A Modeling Study of Perched Water Phenomena in the Unsaturated Zone at Yucca Mountain." *Journal of Contaminant Hydrology* 38, (1-3), 157-184. Amsterdam, The Netherlands: Elsevier Science Publishers. TIC: 244160.

Software cited:

Software Code: TOUGH2 V 1.4. STN: 10007-1.4-01.

Software Code: EXT V1.0. STN: 10047-1.0-00.

Software Code: WinGridder V 1.0. STN: 10024-1.0-00.

Software Code: Inf2grd V 1.6. STN: 10077-1.6-00.

Software Routine: thbcgen-v0.f, Version 1.0, STN: 10219-1.0-00

Software Routine: gen-incon-v0.f, Version 1.0, STN: 10220-1.0-00

Software Routine: get_a_layer_v0.f, Version 1.0, STN: 10221-1.0-00

Software Routine: get_temp_v0.f, Version 1.0, STN: 10222-1.0-00

Software Routine: add_rep_v0.f, Version 1.0, STN: 10223-1.0-00

Software Routine: toptemp_v0.f, Version 1.0, STN: 10224-1.0-00

Software Routine: hsource_v0.f, Version 1.0, STN: 10225-1.0-00

Software Routine: dk2ecm_mat_v0.f, Version 1.0, STN: 10226-1.0-00

8.2 CODES, STANDARDS, REGULATIONS, AND PROCEDURES

AP-3.10Q, Rev. 1, ICN 1. *Analyses and Models*. Washington, D.C.: U.S. Department of Energy, Office of Civilian Radioactive Waste Management. ACC: MOL.19991019.0467.

AP-3.14Q, Rev. 0, ICN 0. *Transmittal of Input*. Washington, D.C.: U.S. Department of Energy, Office of Civilian Radioactive Waste Management. ACC: MOL.19990701.0621.

AP-3.17Q, Rev. 0. *Impact Reviews*. Washington, D.C.: U.S. Department of Energy, Office of Civilian Radioactive Waste Management. ACC: MOL.19990702.0306.

AP-SI.1Q, Rev. 2, ICN 2. *Software Management*. Washington, D.C.: U.S. Department of Energy, Office of Civilian Radioactive Waste Management. ACC: MOL.19991214.0627.

AP-SI.1Q, Rev. 2, ICN 4. *Software Management*. Washington, D.C.: U.S. Department of Energy, Office of Civilian Radioactive Waste Management. ACC: MOL.20000223.0508.

AP-SIII.3Q, Rev. 0, ICN 2. *Submittal and Incorporation of Data to the Technical Data Management System*. Las Vegas, Nevada: CRWMS M&O. ACC: MOL.19991214.0632.

DOE (U.S. Department of Energy) 1998. *Quality Assurance Requirements and Description*. DOE/RW-0333P, REV 8. Washington D.C.: DOE OCRWM. ACC: MOL.19980601.0022.

QAP-2-0, Rev. 5. *Conduct of Activities*. Las Vegas, Nevada: CRWMS M&O. ACC: MOL.19980826.0209.

YAP-SV.1Q, Rev. 0, ICN 1. *Control of the Electronic Management of Data*. Las Vegas, Nevada: CRWMS M&O. ACC: MOL.19991008.0209.

YMP-LBNL-QIP-6.1, Rev. 5, Mod. 0. *Document Review*. Berkeley, California: Lawrence Berkeley National Laboratory. ACC: MOL.19991210.0091.

YMP-LBNL-QIP-SV.0, Rev. 0, Mod. 0. *Control of the Electronic Management of Data*. Berkeley, California: Lawrence Berkeley National Laboratory. ACC: MOL.19990726.0092.

8.3 SOURCE DATA, LISTED BY DATA TRACKING NUMBER

GS950208312232.003. Data, Including Water Potential, Pressure and Temperature, Collected from Boreholes USW NRG-6 and USW NRG-7a from Instrumentation through March 31, 1995. Submittal date: 02/13/1995.

GS951108312232.008. Data, Including Water Potential, Pressure and Temperature, Collected from Boreholes UE-25 UZ#4 & UZ#5 from Instrumentation through September 30, 1995, and from USW NRG-6 & NRG-7A from April 1 through September 30, 1995. Submittal date: 11/21/1995.

GS960308312232.001. Deep Unsaturated Zone Surface-Based Borehole Instrumentation Program Data from Boreholes USW NRG-7A, USW NRG-6, UE-25 UZ#4, UE-25 UZ#5, USW UZ-7A, and USW SD-12 for the Time Period 10/01/95 through 3/31/96. Submittal date: 04/04/1996.

GS970108312232.002. Deep Unsaturated Zone, Surface-Based Borehole Instrumentation Program - Raw Data Submittal for Boreholes USW NRG-7A, USW NRG-6, UE-25 UZ#4, UE-25 UZ#5, USW UZ-7A, and USW SD-12, for the Period 8/16/96 through 12/31/96. Submittal date: 01/22/1997.

GS970808312232.005. Deep Unsaturated Zone Surface-Based Borehole Instrumentation

Program Data from Boreholes USW NRG-7A, UE-2 5 UZ#4, UE-25 UZ#5, USW UZ-7A and USW SD-12 for the Time Period 1/1/97 – 6/30/97. Submittal date: 08/28/1997.

GS971108312232.007. Deep Unsaturated Zone Surface-Based Borehole Instrumentation Program Data from Boreholes USW NRG-7A, UE-2 5 UZ #4, UE-25 UZ #5, USW UZ-7A and USW SD-12 for the Time Period 7/1/97 - 9/30/97. Submittal date: 11/18/1997.

GS980408312232.001. Deep Unsaturated Zone Surface-Based Borehole Instrumentation Program Data from Boreholes USW NRG-7A, UE-2 5 UZ #4, USW NRG-6, UE-25 UZ #5, USW UZ-7A and USW SD-12 for the Time Period 10/01/97 - 03/31/98. Submittal date: 04/16/1998.

LB990501233129.004. 3-D UZ Model Calibration Grids for AMR U0000, "Development of Numerical Grids of UZ Flow and Transport Modeling." Submittal date: 09/24/1999.

LB990701233129.001. 3-D UZ Model Grids for Calculation of Flow Fields for PA for AMR U0000, "Development of Numerical Grids For UZ Flow and Transport Modeling." Submittal date: 09/24/1999

LB991091233129.006. Thermal Properties and Tortuosity Factor for the UZ Model Layers. Submittal date: 10/15/1999. Initial use.

LB997141233129.001. Calibrated Base case Infiltration 1-D Parameter Set for the UZ Flow and Transport Model, FY99. Submittal date: 07/21/1999.

MO9901MWDGFM31.000. Geologic Framework Model. Submittal date: 01/06/1999.

SN9907T0872799.001. Heat Decay Data and Repository Footprint for Thermal-Hydrologic and Conduction-Only Models for TSPA-SR (Total System Performance Assessment-Site Recommendation). Submittal date: 07/27/1999.

8.4 OUTPUT DATA, LISTED BY DATA TRACKING NUMBER

LB991201233129.001. The Mountain-Scale Thermal-Hydrologic Model Simulations for AMR U0105, "Mountain-Scale Coupled Processes (TH) Models

9. ATTACHMENTS

Attachment I – Document Input Reference System

Attachment II – List of Model Input and Output Files

INTENTIONALLY LEFT BLANK

**OFFICE OF CIVILIAN RADIOACTIVE WASTE MANAGEMENT
DOCUMENT INPUT REFERENCE SHEET**

1. Document Identifier No./Rev.: MDL-NBS-HS-000007/Rev. 00		Change:	Title: Mountain-Scale Coupled Processes (TH) Models						
Input Document			4. Input Status	5. Section Used in	6. Input Description	7. TBV/TBD Priority	8. TBV Due To		
2. Technical Product Input Source Title and Identifier(s) with Version		3. Section					Unqual.	From Uncontrolled Source	Un-confirmed
2a									
1.	DTN: GS950208312232.003. Data, Including Water Potential, Pressure and Temperature, Collected from Boreholes USW NRG-6 and USW NRG-7a from Instrumentation through March 31, 1995. Submittal date: 02/13/1995.	S98010.003	N/A- Qualified-Verification Level 2	6.4 6.8- 6.11	Temperature, collected from boreholes USW NRG-6 and NRG-7a from instrumentation through March 31, 1995.	N/A	N/A	N/A	N/A
2.	DTN: GS951108312232.008. Data, Including Water Potential, Pressure and Temperature, Collected from Boreholes UE-25 UZ#4 & UZ#5 from Instrumentation through September 30, 1995, and from USW NRG-6 & NRG-7A from April 1 through September 30, 1995. Submittal date: 11/21/1995.	S98009.003	N/A- Qualified-Verification Level 2	6.4 6.8- 6.11	Temperature, collected from boreholes UE-25 UZ#4 and UZ#5 from instrumentation through September 30, 1995, and from USW NRG-6 and NRG-7a from April 1 through September 30, 1995.	N/A	N/A	N/A	N/A

**OFFICE OF CIVILIAN RADIOACTIVE WASTE MANAGEMENT
DOCUMENT INPUT REFERENCE SHEET**

1. Document Identifier No./Rev.: MDL-NBS-HS-000007/Rev. 00		Change:	Title: Mountain-Scale Coupled Processes (TH) Models						
Input Document		4. Input Status	5. Section Used in	6. Input Description	7. TBV/TBD Priority	8. TBV Due To			
2. Technical Product Input Source Title and Identifier(s) with Version						3. Section	Unqual.	From Uncontrolled Source	Un-confirmed
2a									
3.	DTN: GS960308312232.001. Deep Unsaturated Zone Surface-Based Borehole Instrumentation Program Data from Boreholes USW NRG-7A, USW NRG-6, UE-25 UZ#4, UE-25 UZ#5, USW UZ-7A, and USW SD-12 for the Time Period 10/01/95 through 3/31/96. Submittal date: 04/04/1996.	S98008.003	N/A- Qualified-Verification Level 2	6.4 6.8-6.11	Temperature for boreholes USW NRG-7a, USW NRG-6, UE-25 UZ#4, UE-25 UZ#5, USW UZ-7a, and USW SD-12 for the time period 10/01/95 through 3/31/96. Data include temperature, pressure, and water potential. VA Supporting Data.	N/A	N/A	N/A	N/A
4.	DTN: GS970108312232.002. Deep Unsaturated Zone, Surface-Based Borehole Instrumentation Program - Raw Data Submittal for Boreholes USW NRG-7A, USW NRG-6, UE-25 UZ#4, UE-25 UZ#5, USW UZ-7A, and USW SD-12, for the Period 8/16/96 through 12/31/96. Submittal date: 01/22/1997.	S98006.003	N/A- Qualified-Verification Level 2	6.4 6.8-6.11	Temperature for boreholes USW NRG-7a, USW NRG-6, UE-25 UZ#4, UE-25 UZ#5, USW UZ-7a and USW SD-12 for the period 8/16/96 through 12/31/96.	N/A	N/A	N/A	N/A

**OFFICE OF CIVILIAN RADIOACTIVE WASTE MANAGEMENT
DOCUMENT INPUT REFERENCE SHEET**

1. Document Identifier No./Rev.: MDL-NBS-HS-000007/Rev. 00		Change:	Title: Mountain-Scale Coupled Processes (TH) Models						
Input Document			4. Input Status	5. Section Used in	6. Input Description	7. TBV/TBD Priority	8. TBV Due To		
2. Technical Product Input Source Title and Identifier(s) with Version		3. Section					Unqual.	From Uncontrolled Source	Un-confirmed
2a									
5.	DTN: GS970808312232.005. Deep Unsaturated Zone Surface-Based Borehole Instrumentation Program Data from Boreholes USW NRG-7A, UE-2 5 UZ#4, UE-25 UZ#5, USW UZ-7A and USW SD-12 for the Time Period 1/1/97 – 6/30/97. Submittal date: 08/28/1997.	S98005.003	N/A- Qualified-Verification Level 2	6.4 6.8- 6.11	Temperature for boreholes USW NRG-7a, UE-25 UZ#4, UE-25 UZ#5, USW UZ-7a and USW SD-12 for the time period 1/1/97 - 6/30/97.	N/A	N/A	N/A	N/A
6.	DTN: GS971108312232.007. Deep Unsaturated Zone Surface-Based Borehole Instrumentation Program Data from Boreholes USW NRG-7A, UE-2 5 UZ #4, UE-25 UZ #5, USW UZ-7A and USW SD-12 for the Time Period 7/1/97 - 9/30/97. Submittal date: 11/18/1997.	S98004.003	N/A- Qualified-Verification Level 2	6.4 6.8 6.9 6.10 6.11	Temperature for boreholes USW NRG-7a, UE-25 UZ#4, UE-25 UZ#5, USW UZ-7a and USW SD-12 for the time period 7/1/97 - 9/30/97.	N/A	N/A	N/A	N/A

**OFFICE OF CIVILIAN RADIOACTIVE WASTE MANAGEMENT
DOCUMENT INPUT REFERENCE SHEET**

1. Document Identifier No./Rev.: MDL-NBS-HS-000007/Rev. 00		Change:	Title: Mountain-Scale Coupled Processes (TH) Models						
Input Document		4. Input Status	5. Section Used in	6. Input Description	7. TBV/TBD Priority	8. TBV Due To			
2. Technical Product Input Source Title and Identifier(s) with Version						3. Section	Unqual.	From Uncontrolled Source	Un-confirmed
2a									
7.	DTN: GS980408312232.001. Deep Unsaturated Zone Surface-Based Borehole Instrumentation Program Data from Boreholes USW NRG-7A, UE-2 5 UZ #4, USW NRG-6, UE-25 UZ #5, USW UZ-7A and USW SD-12 for the Time Period 10/01/97 - 03/31/98. Submittal date: 04/16/1998.	S98155.003	N/A- Qualified- Verificatio n Level 2	6.4 6.8 6.9 6.10 6.11	Temperature for boreholes USW NRG-7a, UE-25 UZ#4, UE-25 UZ#5, USW UZ-7a and USW SD-12 for the time period 10/1/97 - 03/31/98.	N/A	N/A	N/A	N/A
8.	DTN: LB990501233129.004. 3-D UZ Model Calibration Grids for AMR U0000, "Development of Numerical Grids of UZ Flow and Transport Modeling." Submittal date: 09/24/1999.	./3-D_Grid_Ca lib/	N/A- Technical Product Output	6.4	3-D UZ Model Grid used properties calibration	N/A	N/A	N/A	N/A
9.	DTN: LB990701233129.001. 3-D UZ Model Grids for Calculation of Flow Fields for PA for AMR U0000, "Development of Numerical Grids For UZ Flow and Transport Modeling." Submittal date: 09/24/1999.	./3-D_Grid_TS PA	N/A- Technical Product Output	6.2 6.8 6.9	3D UZ model grid used for TSPA flow fields	N/A	N/A	N/A	N/A

**OFFICE OF CIVILIAN RADIOACTIVE WASTE MANAGEMENT
DOCUMENT INPUT REFERENCE SHEET**

1. Document Identifier No./Rev.: MDL-NBS-HS-000007/Rev. 00		Change:	Title: Mountain-Scale Coupled Processes (TH) Models						
Input Document		4. Input Status	5. Section Used in	6. Input Description	7. TBV/TBD Priority	8. TBV Due To			
2. Technical Product Input Source Title and Identifier(s) with Version						3. Section	Unqual.	From Uncontrolled Source	Un-confirmed
2a									
10.	DTN: LB991091233129.006. Thermal Properties and Tortuosity Factor for the UZ Model Layers. Submittal date: not yet submitted. Initial use.	Entire	N/A- Technical Product Output	6.5 6.8 6.9 6.10 6.11	Thermal properties for model layers	N/A	N/A	N/A	N/A
11.	DTN: LB997141233129.001. Calibrated Basecase Infiltration 1-D Parameter Set for the UZ Flow and Transport Model, FY99. Submittal date: 07/21/1999.	Entire	N/A- Technical Product Output	6.2 6.8 6.9 6.10 6.11	Calibrated fracture and matrix properties sets (basecase)	N/A	N/A	N/A	N/A
12.	DTN: MO9901MWDGFM31.000. Geologic Framework Model. Submittal date: 01/06/1999.	Entire	N/A- Technical Product Output	6.2	Borehole locations, lithological contacts	N/A	N/A	N/A	N/A
13.	DTN: SN9907T0872799.001. Heat Decay Data and Repository Footprint for Thermal-Hydrologic and Conduction-Only Models for TSPA-SR (Total System Performance Assessment-Site Recommendation). Submittal date: 07/27/1999.	heatTSPA-SR-9918 4-Ta.xls	N/A- Qualified-Verification Level 2	6.3 6.8 6.9 6.10 6.11	Heat Loading Thermal decay curve ventilation	N/A	N/A	N/A	N/A

**OFFICE OF CIVILIAN RADIOACTIVE WASTE MANAGEMENT
DOCUMENT INPUT REFERENCE SHEET**

1. Document Identifier No./Rev.: MDL-NBS-HS-000007/Rev. 00		Change:	Title: Mountain-Scale Coupled Processes (TH) Models						
Input Document			4. Input Status	5. Section Used in	6. Input Description	7. TBV/TBD Priority	8. TBV Due To		
2. Technical Product Input Source Title and Identifier(s) with Version		3. Section					Unqual.	From Uncontrolled Source	Un-confirmed
2a									
14.	Bodvarsson, G.S.; Bjornsson, S.; Gunnarsson, A.; Gunnlaugsson, E.; Sigurdsson, O.; Stefansson, V.; and Steingrimsson, B. 1988. "A Summary of Modeling Studies of the Nesjavellir Geothermal Field, Iceland." <i>Thirteenth Workshop on Geothermal Reservoir Engineering, Stanford University</i> , 83 – 91. Stanford, California: Stanford University. TIC: 246824.	Entire	N/A-Reference only	6.12	N/A	N/A	N/A	N/A	N/A
15.	Bodvarsson, G.S.; Gislason, G.; Gunnlaugsson, E.; Sigurdsson, O.; Stefansson, V.; and Steingrimsson, B. 1993. "Accuracy of Reservoir Predictions for the Nesjavellir Geothermal Field, Iceland." <i>Eighteenth Workshop on Geothermal Reservoir Engineering, Stanford University</i> , 273–278. Stanford, California: Stanford University. TIC: 246821.	Entire	N/A-Reference only	6.12	N/A	N/A	N/A	N/A	N/A

**OFFICE OF CIVILIAN RADIOACTIVE WASTE MANAGEMENT
DOCUMENT INPUT REFERENCE SHEET**

1. Document Identifier No./Rev.: MDL-NBS-HS-000007/Rev. 00		Change:	Title: Mountain-Scale Coupled Processes (TH) Models						
Input Document		4. Input Status	5. Section Used in	6. Input Description	7. TBV/TBD Priority	8. TBV Due To			
2. Technical Product Input Source Title and Identifier(s) with Version	3. Section					Unqual.	From Uncontrolled Source	Un-confirmed	
2a									
16.	Bodvarsson, G.S.; Pruess, K.; Haukwa, C.; and Ojiambo, S. B. 1990. "Evaluation of Reservoir Model Predictions for Olkaria East Geothermal Field, Kenya." <i>Geothermics</i> , 19 (5), 399-414. Oxford, United Kingdom: Pergamon Press. TIC: 246739.	Entire	N/A-Reference only	6.12	N/A	N/A	N/A	N/A	N/A
17.	Bodvarsson, G.S.; Pruess, K.; and Lippmann, M. J. 1986. "Modeling of Geothermal Systems." <i>Journal of Petroleum Technology September</i> , 1007-1021. Richardson, Texas: Society of Petroleum Engineers. TIC: 246733.	Entire	N/A-Reference only	6.12	N/A	N/A	N/A	N/A	N/A

**OFFICE OF CIVILIAN RADIOACTIVE WASTE MANAGEMENT
DOCUMENT INPUT REFERENCE SHEET**

1. Document Identifier No./Rev.: MDL-NBS-HS-000007/Rev. 00		Change:	Title: Mountain-Scale Coupled Processes (TH) Models						
Input Document			4. Input Status	5. Section Used in	6. Input Description	7. TBV/TBD Priority	8. TBV Due To		
2. Technical Product Input Source Title and Identifier(s) with Version		3. Section					Unqual.	From Uncontrolled Source	Un-confirmed
2a									
18.	Bodvarsson, G.S.; Pruess, K.; Stefansson, V.; Bjornsson, S.; and Ojiambo, S. B. 1987a. "East Olkaria Geothermal Field, Kenya, 1. History Match With Production and Pressure Decline Data." <i>Journal of Geophysical Research</i> , 92 (B1), 521–539. Washington, D.C.: American Geophysical Union. TIC: 236629.	Entire	N/A-Reference only	6.12	N/A	N/A	N/A	N/A	N/A
19.	Bodvarsson, G.S.; Pruess, K.; Stefansson, V.; Bjornsson, S.; and Ojiambo, S. B. 1987b. "East Olkaria Geothermal Field, Kenya, 2. Predictions of Well Performance and Reservoir Depletion." <i>Journal of Geophysical Research</i> , 92 (B1), 541–554. Washington, D.C.: American Geophysical Union. TIC: 246738.	Entire	N/A-Reference only	6.12	N/A	N/A	N/A	N/A	N/A

**OFFICE OF CIVILIAN RADIOACTIVE WASTE MANAGEMENT
DOCUMENT INPUT REFERENCE SHEET**

1. Document Identifier No./Rev.: MDL-NBS-HS-000007/Rev. 00		Change:	Title: Mountain-Scale Coupled Processes (TH) Models						
Input Document			4. Input Status	5. Section Used in	6. Input Description	7. TBV/TBD Priority	8. TBV Due To		
2. Technical Product Input Source Title and Identifier(s) with Version		3. Section					Unqual.	From Uncontrolled Source	Un-confirmed
2a									
20.	Bodvarsson, G.S.; Pruess, K.; Stefansson, V.; and Eliasson, E.T. 1984a. "The Krafla Geothermal Field, Iceland, 2. The Natural State of the System." <i>Water Resources Research</i> , 20 (11), 1531–1544. Washington, D.C.: American Geophysical Union. TIC: 246734.	Entire	N/A-Reference only	6.12	N/A	N/A	N/A	N/A	N/A
21.	Bodvarsson, G.S.; Pruess, K.; Stefansson, V.; and Eliasson, E.T. 1984b. "The Krafla Geothermal Field, Iceland, 3, The Generating Capacity of the Field." <i>Water Resources Research</i> , 20 (11), 1545–1559. Washington, D.C.: American Geophysical Union. TIC: 246737.	Entire	N/A-Reference only	6.12	N/A	N/A	N/A	N/A	N/A

**OFFICE OF CIVILIAN RADIOACTIVE WASTE MANAGEMENT
DOCUMENT INPUT REFERENCE SHEET**

1. Document Identifier No./Rev.: MDL-NBS-HS-000007/Rev. 00		Change:	Title: Mountain-Scale Coupled Processes (TH) Models						
Input Document		4. Input Status	5. Section Used in	6. Input Description	7. TBV/TBD Priority	8. TBV Due To			
2. Technical Product Input Source Title and Identifier(s) with Version	3. Section					Unqual.	From Uncontrolled Source	Un-confirmed	
2a									
22.	Brooks, R.H. and Corey, A.T. 1966. "Properties of Porous Media Affecting Fluid Flow." <i>Journal of Irrigation and Drainage Division: Proceedings of the American Society of Civil Engineers, 92</i> (IR2), 61-88. Washington, D.C.: American Society of Civil Engineers. TIC: 216867.	Entire	N/A-Reference only	Entire	N/A	N/A	N/A	N/A	N/A
23.	Buscheck, T.A. and Nitao, J.J. 1992. "Impact of Thermal Loading on Repository Performance at Yucca Mountain." <i>High Level Radioactive Waste Management, Proceedings of the Third International Conference, Las Vegas, Nevada, April 12-16, 1992, 1</i> , 1003-1017. La Grange Park, Illinois: American Nuclear Society. TIC: 204231	Entire	N/A-Reference only	6.12	N/A	N/A	N/A	N/A	N/A

**OFFICE OF CIVILIAN RADIOACTIVE WASTE MANAGEMENT
DOCUMENT INPUT REFERENCE SHEET**

1. Document Identifier No./Rev.: MDL-NBS-HS-000007/Rev. 00		Change:	Title: Mountain-Scale Coupled Processes (TH) Models						
Input Document		4. Input Status	5. Section Used in	6. Input Description	7. TBV/TBD Priority	8. TBV Due To			
2. Technical Product Input Source Title and Identifier(s) with Version						3. Section	Unqual.	From Uncontrolled Source	Un-confirmed
2a									
24.	Buscheck, T.A. and Nitao, J.J. 1993a. "Repository-Heat-Driven Hydrothermal Flow at Yucca Mountain, Part I: Modeling and Analysis." <i>Nuclear Technology</i> , 104 (3), 418-448. La Grange Park, Illinois: American Nuclear Society. TIC: 224039.	Entire	N/A-Reference only	6.12	N/A	N/A	N/A	N/A	N/A
25.	Buscheck, T.A. and Nitao, J.J. 1993b. "The Analysis of Repository-Heat-Driven Hydrothermal Flow at Yucca Mountain." <i>Proceedings of the Fourth Annual International Conference on High Level Radioactive Waste Management, 1, Las Vegas, Nevada, April 26-30, 1993</i> , 847-867. La Grange Park, Illinois: American Nuclear Society. TIC: 208542.	Entire	N/A-Reference only	6.12	N/A	N/A	N/A	N/A	N/A

**OFFICE OF CIVILIAN RADIOACTIVE WASTE MANAGEMENT
DOCUMENT INPUT REFERENCE SHEET**

1. Document Identifier No./Rev.: MDL-NBS-HS-000007/Rev. 00		Change:	Title: Mountain-Scale Coupled Processes (TH) Models						
Input Document			4. Input Status	5. Section Used in	6. Input Description	7. TBV/TBD Priority	8. TBV Due To		
2. Technical Product Input Source Title and Identifier(s) with Version		3. Section					Unqual.	From Uncontrolled Source	Un-confirmed
2a									
26.	Buscheck, T.A. and Nitao, J.J. 1993c. <i>The Impact of Repository Heat on Thermo-Hydrological Performance at Yucca Mountain</i> . UCRL-JC-114791. Livermore, California: Lawrence Livermore National Laboratory. ACC: NNA.19940121.0144.	Entire	N/A-Reference only	6.12	N/A	N/A	N/A	N/A	N/A

**OFFICE OF CIVILIAN RADIOACTIVE WASTE MANAGEMENT
DOCUMENT INPUT REFERENCE SHEET**

1. Document Identifier No./Rev.: MDL-NBS-HS-000007/Rev. 00		Change:	Title: Mountain-Scale Coupled Processes (TH) Models						
Input Document		4. Input Status	5. Section Used in	6. Input Description	7. TBV/TBD Priority	8. TBV Due To			
2. Technical Product Input Source Title and Identifier(s) with Version	3. Section					Unqual.	From Uncontrolled Source	Un-confirmed	
2a									
27.	Buscheck, T.A. and Nitao, J.J. 1993d. "Modeling Hydrothermal Flow in Variably Saturated, Fractured, Welded Tuff During the Prototype Engineered Barrier System Field Test of the Yucca Mountain Project." <i>Proceedings of the Fifth Workshop on Flow and Transport Through Unsaturated Fractured Rock-Related to High-Level Radioactive Waste Disposal, Tucson, Arizona, January 7-10, 1991.</i> Evans, D.D. and Nicholson, T.J., eds. NUREG/CP-0040, 147-152. Washington, D.C.: U.S. Nuclear Regulatory Commission. TIC: 207128.	Entire	N/A-Reference only	6.12	N/A	N/A	N/A	N/A	N/A

**OFFICE OF CIVILIAN RADIOACTIVE WASTE MANAGEMENT
DOCUMENT INPUT REFERENCE SHEET**

1. Document Identifier No./Rev.: MDL-NBS-HS-000007/Rev. 00		Change:	Title: Mountain-Scale Coupled Processes (TH) Models						
Input Document			4. Input Status	5. Section Used in	6. Input Description	7. TBV/TBD Priority	8. TBV Due To		
2. Technical Product Input Source Title and Identifier(s) with Version		3. Section					Unqual.	From Uncontrolled Source	Un-confirmed
2a									
28.	Buscheck, T.A. and Nitao, J.J. 1995. "The Importance of Thermal Loading Conditions to Waste Package Performance at Yucca Mountain." Scientific Basis for Nuclear Waste Management XVIII, Symposium held October 23-27, 1994, Kyoto, Japan. Murakami, T. and Ewing, R.C., eds. 353, 403-410. Pittsburgh, Pennsylvania: Materials Research Society. TIC: 216341.	Entire	N/A-Reference only	6.12	N/A	N/A	N/A	N/A	N/A

**OFFICE OF CIVILIAN RADIOACTIVE WASTE MANAGEMENT
DOCUMENT INPUT REFERENCE SHEET**

1. Document Identifier No./Rev.: MDL-NBS-HS-000007/Rev. 00		Change:	Title: Mountain-Scale Coupled Processes (TH) Models						
Input Document		4. Input Status	5. Section Used in	6. Input Description	7. TBV/TBD Priority	8. TBV Due To			
2. Technical Product Input Source Title and Identifier(s) with Version	3. Section					Unqual.	From Uncontrolled Source	Un-confirmed	
2a									
29.	Buscheck, T.A.; Nitao, J.J.; and Saterlie, S.F. 1994. "Evaluation of Thermo-Hydrological Performance in Support of the Thermal Loading Systems Study." <i>High Level Radioactive Waste Management, Proceedings of the Fifth Annual International Conference, Las Vegas, Nevada, May 22-26, 1994. 2, 592-610.</i> La Grange Park, Illinois: American Nuclear Society. TIC: 210984.	Entire	N/A-Reference only	6.12	N/A	N/A	N/A	N/A	N/A
30.	Buscheck, T.A.; Nitao, J.J.; and Wilder, D.G. 1993. "Repository-Heat-Driven Hydrothermal Flow at Yucca Mountain, Part II: Large-Scale In Situ Heater Tests." <i>Nuclear Technology, 104 (3), 449-471.</i> La Grange Park, Illinois: American Nuclear Society. TIC: 235095.	Entire	N/A-Reference only	6.12	N/A	N/A	N/A	N/A	N/A

**OFFICE OF CIVILIAN RADIOACTIVE WASTE MANAGEMENT
DOCUMENT INPUT REFERENCE SHEET**

1. Document Identifier No./Rev.: MDL-NBS-HS-000007/Rev. 00		Change:	Title: Mountain-Scale Coupled Processes (TH) Models						
Input Document			4. Input Status	5. Section Used in	6. Input Description	7. TBV/TBD Priority	8. TBV Due To		
2. Technical Product Input Source Title and Identifier(s) with Version		3. Section					Unqual.	From Uncontrolled Source	Un-confirmed
2a									
31.	CRWMS M&O (Civilian Radioactive Waste Management System, Management & Operating Contractor) 1999a. <i>Analysis & Modeling Development Plan (DP) for U0105, Mountain-Scale Coupled Processes (TH) Models Rev. 00.</i> TDP-NBS-HS-000012. Las Vegas, Nevada: CRWMS M&O. ACC: MOL.19990830.0382.	Entire	N/A - Reference only	2	Standards, Codes & Regulations	N/A	N/A	N/A	N/A
32.	CRWMS M&O 1999b. <i>M&O Site Investigations.</i> Activity Evaluation. Las Vegas, Nevada: CRWMS M&O. ACC: MOL.19990317.0330.	Entire	N/A - Reference only	2	Standards, Codes & Regulations	N/A	N/A	N/A	N/A
33.	CRWMS M&O 1999c. <i>M&O Site Investigations.</i> Activity Evaluation. Las Vegas, Nevada: CRWMS M&O. ACC: MOL.19990928.0224.	Entire	N/A - Reference only	2	Standards, Codes & Regulations	N/A	N/A	N/A	N/A

**OFFICE OF CIVILIAN RADIOACTIVE WASTE MANAGEMENT
DOCUMENT INPUT REFERENCE SHEET**

1. Document Identifier No./Rev.: MDL-NBS-HS-000007/Rev. 00		Change:	Title: Mountain-Scale Coupled Processes (TH) Models						
Input Document		4. Input Status	5. Section Used in	6. Input Description	7. TBV/TBD Priority	8. TBV Due To			
2. Technical Product Input Source Title and Identifier(s) with Version	3. Section					Unqual.	From Uncontrolled Source	Un-confirmed	
2a									
34.	CRWMS M&O 1999d. <i>Rainfall/Runoff/Runon 1999 Simulations</i> . Input Request LBL-USG-99248.T. Las Vegas, Nevada: CRWMS M&O. ACC: MOL.19991014.0102.	base-case, present day simulation	TBV-3164	6.4 6.8 6.9 6.10 6.11	Net Infiltration data	1	N/A	✓	N/A
35.	CRWMS M&O 1999d. <i>Rainfall/Runoff/Runon 1999 Simulations</i> . Input Transmittal LBL-USG-99248.T. Las Vegas, Nevada: CRWMS M&O. ACC: MOL.19991014.0102.	base-case, future monsoon simulation	TBV-3164	6.4 6.8 6.9 6.10 6.11	Net Infiltration data	1	N/A	✓	N/A
36.	CRWMS M&O 1999d. <i>Rainfall/Runoff/Runon 1999 Simulations</i> . Input Transmittal LBL-USG-99248.T. Las Vegas, Nevada: CRWMS M&O. ACC: MOL.19991014.0102.	Base-case, future glacial transition simulation	TBV-3164	6.4 6.8 6.9 6.10 6.11	Net Infiltration data	1	N/A	✓	N/A

**OFFICE OF CIVILIAN RADIOACTIVE WASTE MANAGEMENT
DOCUMENT INPUT REFERENCE SHEET**

1. Document Identifier No./Rev.: MDL-NBS-HS-000007/Rev. 00		Change:	Title: Mountain-Scale Coupled Processes (TH) Models						
Input Document			4. Input Status	5. Section Used in	6. Input Description	7. TBV/TBD Priority	8. TBV Due To		
2. Technical Product Input Source Title and Identifier(s) with Version		3. Section					Unqual.	From Uncontrolled Source	Un-confirmed
2a									
37.	Doughty, C. 1999. "Investigation of Conceptual and Numerical Approaches for Evaluating Moisture, Gas, Chemical, and Heat Transport in Fractured Unsaturated Rock." <i>Journal Of Contaminant Hydrology</i> 38 (1-3), 69-106. Amsterdam, The Netherlands: Elsevier Science. TIC: 244160.	69-106	N/A-Reference only	6.1 6.12	N/A	N/A	N/A	N/A	N/A
38.	Driscoll, F.G. 1986. Groundwater and Wells. 2nd Edition. St. Paul, Minnesota: Johnson Filtration Systems. TIC: 217555.	pp. 49-51	N/A-Reference only	6.4 6.8 6.9 6.10 6.11	N/A	N/A	N/A	N/A	N/A

**OFFICE OF CIVILIAN RADIOACTIVE WASTE MANAGEMENT
DOCUMENT INPUT REFERENCE SHEET**

1. Document Identifier No./Rev.: MDL-NBS-HS-000007/Rev. 00		Change:	Title: Mountain-Scale Coupled Processes (TH) Models						
Input Document		4. Input Status	5. Section Used in	6. Input Description	7. TBV/TBD Priority	8. TBV Due To			
2. Technical Product Input Source Title and Identifier(s) with Version						3. Section	Unqual.	From Uncontrolled Source	Un-confirmed
2a									
39.	Dyer, J.R. 1999. "Revised Interim Guidance Pending Issuance of New U.S. Nuclear Regulatory Commission (NRC) Regulations (Revision 01, July 22, 1999), for Yucca Mountain, Nevada." Letter from J.R. Dyer (DOE) to D.R. Wilkins (CRWMS M&O), September 9, 1999, OL&RC:SB-1714, with enclosure, "Interim Guidance Pending Issuance of New U.S. Nuclear Regulatory Commission (NRC) Regulations (Revision 01)." ACC: MOL.19990910.0079.	Entire	N/A Reference only	4.2	Interim Guidance	N/A	N/A	N/A	N/A
40.	Francis, N.D. 1997. "The Base-Case Thermal Properties for TSPA-VA Modeling." Memorandum from N.D. Francis (SNL) to Distribution, April 16, 1997. Albuquerque, New Mexico: Sandia National Laboratories. ACC: MOL.19980518.0229.	Entire	N/A-Reference only	6.5 6.8 6.9 6.10 6.11	N/A	N/A	N/A	N/A	N/A

**OFFICE OF CIVILIAN RADIOACTIVE WASTE MANAGEMENT
DOCUMENT INPUT REFERENCE SHEET**

1. Document Identifier No./Rev.: MDL-NBS-HS-000007/Rev. 00		Change:	Title: Mountain-Scale Coupled Processes (TH) Models						
Input Document			4. Input Status	5. Section Used in	6. Input Description	7. TBV/TBD Priority	8. TBV Due To		
2. Technical Product Input Source Title and Identifier(s) with Version		3. Section					Unqual.	From Uncontrolled Source	Un-confirmed
2a									
41.	Garg, S.K. and Pritchett, J.W. 1990. "Cold Water Injection Into Single- and Two-Phase Geothermal Reservoirs." <i>Water Resources Research</i> , 26 (2), 331-338. Washington, D.C.: American Geophysical Union. TIC: applied for.	Entire	N/A-Reference only	6.12	N/A	N/A	N/A	N/A	N/A
42.	Hanano, M. 1992. "Reservoir Engineering Studies of the Matsukawa Geothermal Field, Japan." <i>Geothermal Resources Council Transactions</i> , 16 October, 643-650. Davis, California: Geothermal Resources Council. TIC: 247116.	Entire	N/A-Reference only	6.12	N/A	N/A	N/A	N/A	N/A
43.	Haukwa, C.B.; Wu, Y.S.; and Bodvarsson, G.S. 1999. "Thermal Loading Studies Using the Yucca Mountain Unsaturated Zone Model." <i>Journal Of Contaminant Hydrology</i> 38 (1-3), 217-255. Amsterdam, The Netherlands: Elsevier Science Publishers. TIC: 244160.	Entire	N/A-Reference only	6.12	Corroborative Studies	N/A	N/A	N/A	N/A

**OFFICE OF CIVILIAN RADIOACTIVE WASTE MANAGEMENT
DOCUMENT INPUT REFERENCE SHEET**

1. Document Identifier No./Rev.: MDL-NBS-HS-000007/Rev. 00		Change:	Title: Mountain-Scale Coupled Processes (TH) Models						
Input Document		4. Input Status	5. Section Used in	6. Input Description	7. TBV/TBD Priority	8. TBV Due To			
2. Technical Product Input Source Title and Identifier(s) with Version	3. Section					Unqual.	From Uncontrolled Source	Un-confirmed	
2a									
44.	Ho, C.K. and Francis, N.D. 1997. "Correction to Base-Case Thermal Properties for TSPA-VA Modeling." Memo from Ho, C.K. and Francis, N.D. to Distribution, August 7, 1997. Albuquerque, New Mexico: Sandia National Laboratories. ACC: MOL.19980518.0230.	Entire	N/A-Reference only	6.4 6.5	Thermal properties	N/A	N/A	N/A	N/A
45.	Hunt, T.M.; Allis, R.G.; Blakeley, M.R.; and O'Sullivan, M. J. 1990. "Testing Reservoir Simulation Models for the Broadlands Geothermal Field using Precision Gravity Data." <i>Geothermal Resources Council Transactions, 14, Part II August, 1287-1294.</i> Davis, California: Geothermal Resources Council. TIC: 246942.	Entire	N/A-Reference only	6.12	N/A	N/A	N/A	N/A	N/A

**OFFICE OF CIVILIAN RADIOACTIVE WASTE MANAGEMENT
DOCUMENT INPUT REFERENCE SHEET**

1. Document Identifier No./Rev.: MDL-NBS-HS-000007/Rev. 00		Change:	Title: Mountain-Scale Coupled Processes (TH) Models						
Input Document		4. Input Status	5. Section Used in	6. Input Description	7. TBV/TBD Priority	8. TBV Due To			
2. Technical Product Input Source Title and Identifier(s) with Version	3. Section					Unqual.	From Uncontrolled Source	Un-confirmed	
2a									
46.	Ingebritsen, S.E. and Sorey, M.L. 1988. "Vapor-Dominated Zones Within Hydrothermal Systems: Evolution and Natural State." <i>Journal of Geophysical Research</i> , 93 (B11), 13635–13655. Washington, D.C.: American Geophysical Union. TIC: applied for.	Entire	N/A-Reference only	6.12	N/A	N/A	N/A	N/A	N/A
47.	Klavetter, E.A. and Peters, R.R. 1986. <i>Estimation of Hydrologic Properties of an Unsaturated Fractured Rock Mass</i> . Report SAND84-2642. Albuquerque, New Mexico: Sandia National Laboratories. TIC: 202727.	Entire	N/A-Reference only	6.1	N/A	N/A	N/A	N/A	N/A
48.	Lam, S.T.; Hunsbedt, A.; Kruger, P.; and Pruess, K. 1988. "Analysis of the Stanford Geothermal Reservoir Model Experiments Using the LBL Reservoir Simulator." <i>Geothermics</i> , 17 (4), 595–605. Oxford, United Kingdom: Elsevier Science Publishers. TIC: 247098.	Entire	N/A-Reference only	6.12	N/A	N/A	N/A	N/A	N/A

**OFFICE OF CIVILIAN RADIOACTIVE WASTE MANAGEMENT
DOCUMENT INPUT REFERENCE SHEET**

1. Document Identifier No./Rev.: MDL-NBS-HS-000007/Rev. 00		Change:	Title: Mountain-Scale Coupled Processes (TH) Models						
Input Document			4. Input Status	5. Section Used in	6. Input Description	7. TBV/TBD Priority	8. TBV Due To		
2. Technical Product Input Source Title and Identifier(s) with Version		3. Section					Unqual.	From Uncontrolled Source	Un-confirmed
2a									
49.	Liu, H.H.; Doughty, C.; and Bodvarsson, G.S. 1998. "An Active Fracture Model for Unsaturated Flow and Transport in Fractured Rocks." <i>Water Resources Research</i> , 34 (10), 2633–2646. Washington, D.C.: American Geophysical Union. TIC: 243012.	Entire	N/A-Reference only	6.1 6.8 6.9 6.10 6.11	N/A	N/A	N/A	N/A	N/A
50.	Menzies, A.J.; Granados, E.E.; Sanyal, S.K.; Merida-I, L. and Caicedo-A, A. 1991. "Numerical Modeling of the Initial State and Matching of Well Test Data from the Zunil Geothermal Field, Guatemala." <i>Sixteenth Workshop on Geothermal Reservoir Engineering, Stanford University</i> , 193–210. Stanford, California: Stanford University. TIC: applied for.	Entire	N/A-Reference only	6.12	N/A	N/A	N/A	N/A	N/A

**OFFICE OF CIVILIAN RADIOACTIVE WASTE MANAGEMENT
DOCUMENT INPUT REFERENCE SHEET**

1. Document Identifier No./Rev.: MDL-NBS-HS-000007/Rev. 00		Change:	Title: Mountain-Scale Coupled Processes (TH) Models						
Input Document		4. Input Status	5. Section Used in	6. Input Description	7. TBV/TBD Priority	8. TBV Due To			
2. Technical Product Input Source Title and Identifier(s) with Version	3. Section					Unqual.	From Uncontrolled Source	Un-confirmed	
2a									
51.	Montazer, P. and Wilson, W.E. 1984. <i>Conceptual Hydrologic Model of Flow in the Unsaturated Zone, Yucca Mountain, Nevada</i> . Water-Resources Investigations Report 84-4345. Lakewood, Colorado: U.S. Geological Survey. ACC: NNA.19890327.0051.	Entire	N/A-Reference only	6.1 6.8 6.9 6.10 6.11	N/A	N/A	N/A	N/A	N/A
52.	Nitao, J.J. 1988. <i>Numerical Modeling of the Thermal and Hydrological Environment around a Nuclear Waste Package Using the Equivalent Continuum Approximation: Horizontal Emplacement</i> . UCID-21444. Livermore, California: Lawrence Livermore National Laboratory. ACC: NNA.19890317.0021.	Entire	N/A-Reference only	6.12	N/A	N/A	N/A	N/A	N/A

**OFFICE OF CIVILIAN RADIOACTIVE WASTE MANAGEMENT
DOCUMENT INPUT REFERENCE SHEET**

1. Document Identifier No./Rev.: MDL-NBS-HS-000007/Rev. 00		Change:	Title: Mountain-Scale Coupled Processes (TH) Models						
Input Document		4. Input Status	5. Section Used in	6. Input Description	7. TBV/TBD Priority	8. TBV Due To			
2. Technical Product Input Source Title and Identifier(s) with Version	3. Section					Unqual.	From Uncontrolled Source	Un-confirmed	
2a									
53.	O'Sullivan, M. J.; Barnett, B. G.; and Razali, M. Y. 1990. "Numerical Simulation of the Kamojang Geothermal Field, Indonesia." <i>Geothermal Resources Council Transactions</i> , 14, Part II (August), 1317-1324. Davis, California: Geothermal Resources Council. TIC: applied for.	Entire	N/A-Reference only	6.12	N/A	N/A	N/A	N/A	N/A
54.	Pruess, K. 1987. <i>TOUGH User's Guide</i> . Nuclear Regulatory Commission, Report NUREG/CR-4645, Report LBL-20700. Berkeley, California: Lawrence Berkeley National Laboratory. ACC: MOL.19960314.0434.	2-11	N/A-Reference only	6.1 6.8 6.9 6.10 6.11 6.12	N/A	N/A	N/A	N/A	N/A
55.	Pruess, K. 1991. <i>TOUGH2—A General Purpose Numerical Simulator for Multiphase Fluid and Heat Flow</i> . Report LBL-29400, UC-251. Berkeley, California: Lawrence Berkeley National Laboratory. ACC: NNA.19940202.0088.	Entire	N/A-Reference only	5.1 5.2 6.1 6.2 6.4 6.8 6.12	N/A	N/A	N/A	N/A	N/A

**OFFICE OF CIVILIAN RADIOACTIVE WASTE MANAGEMENT
DOCUMENT INPUT REFERENCE SHEET**

1. Document Identifier No./Rev.: MDL-NBS-HS-000007/Rev. 00		Change:	Title: Mountain-Scale Coupled Processes (TH) Models						
Input Document			4. Input Status	5. Section Used in	6. Input Description	7. TBV/TBD Priority	8. TBV Due To		
2. Technical Product Input Source Title and Identifier(s) with Version		3. Section					Unqual.	From Uncontrolled Source	Un-confirmed
2a									
56.	Pruess, K. and Narasimhan, T.N. 1985. "A Practical Method for Modeling Fluid and Heat Flow in Fractured Porous Media." <i>Society of Petroleum Engineers Journal</i> , 25 (1), 14–26. Richardson, Texas: Society of Petroleum Engineers. TIC: 221917.	Entire	N/A-Reference only	6.1 6.12	N/A	N/A	N/A	N/A	N/A
57.	Pruess, K. and Tsang, Y.W. 1994. <i>Thermal Modeling for a Potential High-Level Nuclear Waste Repository at Yucca Mountain, Nevada</i> . Report LBL-35381, UC-600. Berkeley, California: Lawrence Berkeley National Laboratory. ACC: NNA.19940427.0248.	Entire	N/A-Reference only	6.12	N/A	N/A	N/A	N/A	N/A
58.	Pruess, K. and Wang, J.S.Y. 1984. <i>TOUGH—A Numerical Model for Nonisothermal Unsaturated Flow to Study Waste Canister Heating Effects</i> . New York, New York: Elsevier Science Publishers. TIC: 221408.	Entire	N/A-Reference only	6.12	N/A	N/A	N/A	N/A	N/A

**OFFICE OF CIVILIAN RADIOACTIVE WASTE MANAGEMENT
DOCUMENT INPUT REFERENCE SHEET**

1. Document Identifier No./Rev.: MDL-NBS-HS-000007/Rev. 00		Change:	Title: Mountain-Scale Coupled Processes (TH) Models						
Input Document			4. Input Status	5. Section Used in	6. Input Description	7. TBV/TBD Priority	8. TBV Due To		
2. Technical Product Input Source Title and Identifier(s) with Version		3. Section					Unqual.	From Uncontrolled Source	Un-confirmed
2a									
59.	Pruess, K.; Wang, J.S.Y.; and Tsang, Y.W. 1990a. "On Thermohydrologic Conditions near High-Level Nuclear Wastes Emplaced in Partially Saturated Fractured Tuff, Part I. Simulation Studies with Explicit Consideration of Fracture Effects." <i>Water Resources Research</i> , 26 (6), 1235–1248. Washington, D.C.: American Geophysical Union. TIC: 221923.	Entire	N/A-Reference only	5.1 5.2 6.1 6.12	N/A	N/A	N/A	N/A	N/A
60.	Pruess, K.; Wang, J.S.Y.; and Tsang, Y.W. 1990b. "On the Thermohydrologic Conditions near High-Level Nuclear Wastes Emplaced in Partially Saturated Fractured Tuff, Part 2. Effective Continuum Approximation." <i>Water Resources Research</i> , 26 (6), 1249–1261. Washington, D.C.: American Geophysical Union. TIC: 224854.	Entire	N/A-Reference only	5.1 5.2 6.1 6.12	N/A	N/A	N/A	N/A	N/A

**OFFICE OF CIVILIAN RADIOACTIVE WASTE MANAGEMENT
DOCUMENT INPUT REFERENCE SHEET**

1. Document Identifier No./Rev.: MDL-NBS-HS-000007/Rev. 00		Change:	Title: Mountain-Scale Coupled Processes (TH) Models						
Input Document		4. Input Status	5. Section Used in	6. Input Description	7. TBV/TBD Priority	8. TBV Due To			
2. Technical Product Input Source Title and Identifier(s) with Version	3. Section					Unqual.	From Uncontrolled Source	Un-confirmed	
2a									
61.	Ramspott, L.D. 1991. "The Constructive Use of Heat in an Unsaturated Tuff Repository." <i>Proceedings of the Second International Conference on High Level Radioactive Waste Management</i> , 2, 1602-1607. La Grange Park, Illinois: American Nuclear Society. TIC: 204272.	Entire	N/A-Reference only	6.12	N/A	N/A	N/A	N/A	N/A
62.	Tsang, Y.W. and Birkholzer, J.T. 1999. "Predictions and Observations of the Thermal-Hydrological Conditions in the Single Heater Test." <i>Journal of Contaminant Hydrology</i> , 38 (1-3), 385-425. Amsterdam, The Netherlands: Elsevier Science Publishers. TIC: 244160.	Entire	N/A-Reference only	6.12	N/A	N/A	N/A	N/A	N/A

**OFFICE OF CIVILIAN RADIOACTIVE WASTE MANAGEMENT
DOCUMENT INPUT REFERENCE SHEET**

1. Document Identifier No./Rev.: MDL-NBS-HS-000007/Rev. 00		Change:	Title: Mountain-Scale Coupled Processes (TH) Models						
Input Document			4. Input Status	5. Section Used in	6. Input Description	7. TBV/TBD Priority	8. TBV Due To		
2. Technical Product Input Source Title and Identifier(s) with Version		3. Section					Unqual.	From Uncontrolled Source	Un-confirmed
2a									
63.	Tsang, Y.W. and Pruess, K. 1987. "A Study of Thermally Induced Convection near a High-level Nuclear Waste Repository in Partially Saturated Fractured Tuff." <i>Water Resources Research</i> , 23 (10), 1958-1966. Washington, DC: American Geophysical Union. TIC: 240715.	Entire	N/A-Reference only	5.1 5.2 6.2 6.12	N/A	N/A	N/A	N/A	N/A
64.	van Genuchten, M. 1980. "A Closed-Form Equation for Predicting the Hydraulic Conductivity of Unsaturated Soils." <i>Soil Science Society of America Journal</i> , 44 (5), 892-898. Madison, Wisconsin: Soil Science Society of America. TIC: 217327.	Entire	N/A-Reference only	5.1 5.2 6.1	N/A	N/A	N/A	N/A	N/A

**OFFICE OF CIVILIAN RADIOACTIVE WASTE MANAGEMENT
DOCUMENT INPUT REFERENCE SHEET**

1. Document Identifier No./Rev.: MDL-NBS-HS-000007/Rev. 00		Change:	Title: Mountain-Scale Coupled Processes (TH) Models						
Input Document			4. Input Status	5. Section Used in	6. Input Description	7. TBV/TBD Priority	8. TBV Due To		
2. Technical Product Input Source Title and Identifier(s) with Version		3. Section					Unqual.	From Uncontrolled Source	Un-confirmed
2a									
65.	Wemheuer, R.F. 1999. "First Issue of FY00 NEPO QAP-2-0 Activity Evaluations." Interoffice correspondence from R.F. Wemheuer (CRWMS M&O) to R.A. Morgan (CRWMS M&O), October 1, 1999, LV.NEPO.RTPS.TAG.10/99-155, with attachments, Activity Evaluation for Work Package #1401213UM1. ACC: MOL.19991028.0162.	Work Package #1401213UM1.	N/A-Reference only	2	Activity evaluation	N/A	N/A	N/A	N/A
66.	Wu, Y.S. 1996. <i>On the Effective Continuum Method for Modeling Multiphase Flow, Multicomponent Transport and Heat Transfer in Fractured Rock</i> . LBNL-42720. Berkeley, California: Lawrence Berkeley National Laboratory. TIC: 245761.	Entire	N/A-Reference only	6.1 6.12	N/A	N/A	N/A	N/A	N/A

**OFFICE OF CIVILIAN RADIOACTIVE WASTE MANAGEMENT
DOCUMENT INPUT REFERENCE SHEET**

1. Document Identifier No./Rev.: MDL-NBS-HS-000007/Rev. 00		Change:	Title: Mountain-Scale Coupled Processes (TH) Models						
Input Document		4. Input Status	5. Section Used in	6. Input Description	7. TBV/TBD Priority	8. TBV Due To			
2. Technical Product Input Source Title and Identifier(s) with Version	3. Section					Unqual.	From Uncontrolled Source	Un-confirmed	
2a									
67.	Wu, Y.S.; Haukwa, C. and Bodvarsson, G.S. 1999a. "A Site-Scale Model for Fluid and Heat Flow in the Unsaturated Zone of Yucca Mountain, Nevada." <i>Journal Of Contaminant Hydrology</i> 38, (1-3), 185-215. Amsterdam, The Netherlands: Elsevier Science Publishers. TIC: 244160.	Entire	N/A-Reference only	5.1	N/A	N/A	N/A	N/A	N/A
68.	Wu, Y.S.; Ritcey, A.C.; and Bodvarsson, G.S. 1999b. "A Modeling Study of Perched Water Phenomena in the Unsaturated Zone at Yucca Mountain." <i>Journal Of Contaminant Hydrology</i> 38, (1-3), 157-184. Amsterdam, The Netherlands: Elsevier Science Publishers. TIC: 244160.	Entire	N/A-Reference only	5.3	N/A	N/A	N/A	N/A	N/A

**OFFICE OF CIVILIAN RADIOACTIVE WASTE MANAGEMENT
DOCUMENT INPUT REFERENCE SHEET**

1. Document Identifier No./Rev.: MDL-NBS-HS-000007/Rev. 00		Change:	Title: Mountain-Scale Coupled Processes (TH) Models						
Input Document		4. Input Status	5. Section Used in	6. Input Description	7. TBV/TBD Priority	8. TBV Due To			
2. Technical Product Input Source Title and Identifier(s) with Version	3. Section					Unqual.	From Uncontrolled Source	Un-confirmed	
2a									
69.	Software Code: TOUGH2 V 1.4. STN: 10007-1.4-00.	Entire	N/A- Qualified/ Verified/ Confirmed	6.4 6.8 6.9 6.10 6.11 6.12	General Software use	N/A	N/A	N/A	N/A
70.	Software Code: EXT V1.0. STN: 10047-1.0-00.	Entire	N/A- Qualified/ Verified/ Confirmed	6.8 6.9 6.10 6.11 6.12	General software use	N/A	N/A	N/A	N/A
71.	Software code: Inf2grd V 1.6. CSCI: 10077-1.6-00.	Entire	TBV	6.6	General software use	1	✓	N/A	N/A
72.	Software code: WinGridder V 1.0. STN: 10024-1.0-00.	Entire	TBV	6.2	General software use	1	✓	N/A	N/A
73.	Software Routine: thbcgen-v0.f V1.0, STN: 10219-1.0-00	Entire	N/A- Qualified/ Verified/ Confirmed	3	Routine for processing data for TOUGH2 V1.4	N/A	N/A	N/A	N/A

**OFFICE OF CIVILIAN RADIOACTIVE WASTE MANAGEMENT
DOCUMENT INPUT REFERENCE SHEET**

1. Document Identifier No./Rev.: MDL-NBS-HS-000007/Rev. 00		Change:	Title: Mountain-Scale Coupled Processes (TH) Models						
Input Document		4. Input Status	5. Section Used in	6. Input Description	7. TBV/TBD Priority	8. TBV Due To			
2. Technical Product Input Source Title and Identifier(s) with Version						3. Section	Unqual.	From Uncontrolled Source	Un-confirmed
2a									
74.	Software Routine: gen-incon-v0.f V1.0, STN: 10220-1.0-00.	Entire	N/A- Qualified/ Verified/ Confirmed	3	Routine for processing data for TOUGH2 V1.4	N/A	N/A	N/A	N/A
75.	Software Routine: get_a_layer_v0.f V1.0, STN: 10221-1.0-00.	Entire	N/A- Qualified/ Verified/ Confirmed	3	Routine for processing data for TOUGH2 V1.4	N/A	N/A	N/A	N/A
76.	Software Routine: get_temp_v0.f V1.0, STN: 10222-1.0-00.	Entire	N/A- Qualified/ Verified/ Confirmed	3	Routine for processing data for TOUGH2 V1.4	N/A	N/A	N/A	N/A
77.	Software Routine: add_rep_v0.f V1.0, STN: 10223-1.0-00.	Entire	N/A- Qualified/ Verified/ Confirmed	3	Routine for processing data for TOUGH2 V1.4	N/A	N/A	N/A	N/A
78.	Software Routine: toptemp_v0.f V1.0, STN: 10224-1.0-00.	Entire	N/A- Qualified/ Verified/ Confirmed	3	Routine for processing data for TOUGH2 V1.4	N/A	N/A	N/A	N/A
79.	Software Routine: hsource_v0.f V1.0, STN: 10225-1.0-00.	Entire	N/A- Qualified/ Verified/ Confirmed	3	Routine for processing data for TOUGH2 V1.4	N/A	N/A	N/A	N/A

**OFFICE OF CIVILIAN RADIOACTIVE WASTE MANAGEMENT
DOCUMENT INPUT REFERENCE SHEET**

1. Document Identifier No./Rev.: MDL-NBS-HS-000007/Rev. 00		Change:	Title: Mountain-Scale Coupled Processes (TH) Models						
Input Document			4. Input Status	5. Section Used in	6. Input Description	7. TBV/TBD Priority	8. TBV Due To		
2. Technical Product Input Source Title and Identifier(s) with Version		3. Section					Unqual.	From Uncontrolled Source	Un-confirmed
2a									
80.	Software Routine: dk2ecm_mat_v0.f V1.0, STN: 10226-1.0-00.	Entire	N/A- Qualified/ Verified/ Confirmed	3	Routine for processing data for TOUGH2 V1.4	N/A	N/A	N/A	N/A

Attachment II

List of Model Input and Output Files

Model input and output files submitted under DTN: LB991201233129.001 with this AMR.
Folder names identify cases described in Table 6 in Section 6 of this AMR.

FOLDERS	FILES
\3D_Case1, Part 1	INCON_thm_s32.dat
\3D_Case1, Part 1	MESH_rep.V1.gz
\3D_Case1, Part 1	MESH_rep.VF.gz
\3D_Case1, Part 1	thm_s32.dat
\3D_Case1, Part 1	thm_s32.dat_tram.out.gz
\3D_Case1, Part 2	thm_s32.out
\3D_Case2, Part 1	thm_usz.dat
\3D_Case2, Part 1	thm_usz.out_1
\3D_Case2, Part 2	thm_usz.out_2
\3D_Case2, Part 3	thm_usz.out_3
\NS\NS#1_Case1	heat_ns1.dat_v2.gz
\NS\NS#1_Case1	heat_ns1.out2
\NS\NS#1_Case1	MESH_ns.V1_sz.gz
\NS\NS#1_Case1	MESH_ns.VF.gz
\NS\NS#1_Case2	bs_v2.out.gz
\NS\NS#1_Case2	drft_bs_v2.dat
\NS\NS#1_Case2	drft_bs_v2.out.gz
\NS\NS#1_Case2	GASOBS.DAT_rev1.gz
\NS\NS#1_Case2	MESH_REV1.gz
\NS\NS#2_Case1	MESH_2k.sz.gz
\NS\NS#2_Case1\GASOBS	GASOBS.DAT
\NS\NS#2_Case1\GASOBS	GASOBS.DAT_2000y
\NS\NS#2_Case1\GASOBS	GASOBS.DAT_212y.gz
\NS\NS#2_Case1\GASOBS	GASOBS.DAT_2130y
\NS\NS#2_Case1\GASOBS	GASOBS.DAT_221y.gz
\NS\NS#2_Case1\GASOBS	GASOBS.DAT_258y.gz
\NS\NS#2_Case1\GASOBS	GASOBS.DAT_560y.gz
\NS\NS#2_Case1\GASOBS	GASOBS.DAT_600y.gz
\NS\NS#2_Case1\Input	bs_nsr_v2.dat
\NS\NS#2_Case1\NSR_OUT	nsr_1.out.gz
\NS\NS#2_Case1\NSR_OUT	nsr_2.out
\NS\NS#2_Case1\NSR_OUT	nsr_3.out
\NS\NS#2_Case1\NSR_OUT	nsr_4.out
\NS\NS#2_Case1\NSR_OUT	nsr_5.out
\NS\NS#2_Case2\GASOBS	GASOBS.DAT_100ky.gz
\NS\NS#2_Case2\GASOBS	GASOBS.DAT_2000y.gz
\NS\NS#2_Case2\GASOBS	GASOBS.DAT_516y.gz
\NS\NS#2_Case2\GASOBS	GASOBS.DAT_6000y.gz
\NS\NS#2_Case2\GASOBS	GASOBS.DAT_600y.gz
\NS\NS#2_Case2\GASOBS	GASOBS.DAT_815y.gz
\NS\NS#2_Case2\Input	vt_nsr_v2.dat.gz
\NS\NS#2_Case2\NSR_OUT	vt_nsr_1.out.gz
\NS\NS#2_Case2\NSR_OUT	vt_nsr_2.out.gz
\NS\NS#2_Case2\NSR_OUT	vt_nsr_3.out.gz
\NS\NS#2_Case2\NSR_OUT	vt_nsr_4.out.gz